

# THÈSE DE DOCTORAT

PRÉSENTÉE PAR

**HOUSSAM HIJAZI**

---

POUR L'OBTENTION DU GRADE DE

**DOCTEUR DE L'UNIVERSITÉ DE LILLE 1**

ECOLE DOCTORALE : SCIENCES DE LA MATIÈRE, DU RAYONNEMENT ET DE  
L'ENVIRONNEMENT

**RÉACTIVITÉ CHIMIQUE DES AÉROSOLS D'IODE EN CONDITIONS  
ACCIDENTELLES DANS UN RÉACTEUR NUCLÉAIRE**

SOUTENUE LE 16 NOVEMBRE 2017

DEVANT LE JURY COMPOSÉ DE:

Prof. Eric SIMONI	Paris Sud	Rapporteur
Dr. Monica CALATAYUD	Université P. M. Curie	Rapporteur
Prof. Denis PETITPREZ	Université Lille 1	Examineur
Prof. Jean-Sébastien FILHOL	Université de Montpellier	Examineur
Prof. Jean-François PAUL	Université de Lille 1	Directeur de thèse
Dr. Laurent Cantrel (Ingénieur Chercheur)	IRSN	Co-directeur







# *Remerciement*

Dans cette petite page, je voudrais consacrer ce manuscrit à toutes les personnes qui m'ont aidé et soutenu pendant les trois années de mon doctorat.

Je remercie sincèrement M. Laurent Cantrel, directeur de recherche chez IRSN, pour m'avoir confié pour intégrer son domaine de recherche. Je suis très reconnaissant à M. Jean-François Paul, mon directeur de thèse, de m'avoir accueilli dans le laboratoire UCCS. MM. J-F et Laurent, j'ai profité de votre connaissance approfondie du domaine qui a avancé le travail rapidement à côté de votre patience et votre gentillesse, vous avez montré en répondant à mes questions et en résolvant les problèmes auxquels je suis confronté.

Je tiens à remercier l'équipe avec laquelle j'ai travaillé, Dimitri, Mireille, Eric, Siwar et Fatah.

J'aimerais également remercier tous mes collègues de mon bureau au cours de mes trois années, Soraya, Marine, Marie, Ayman, Shreya, Gorge, Camilla, Renata, Carlos, Francisco, Leila et Claudia.

Un merci spécial à ma famille. Je suis très reconnaissant à ma mère Zeinab et à mon père Dib pour leurs sacrifices qu'ils ont faits en mon nom. Aussi, je tiens à remercier mes sœurs Lina, Wafaa et mes frères Youssef, Ali, Khalil, Imad, Hassan, Hussein, Mohamad et Hadi.

Enfin, je tiens à remercier tous mes amis en France et au Liban, Aude, Rachad, Hammoud, Najib, Daoud, Krayem et Ali Deeb en dehors de mon travail qui m'a soutenu et m'a encouragé à accomplir ce travail aussi bien que possible.



# *Acknowledgements*

In this small page, I would like to dedicate this manuscript to all persons who have helped and supported me during the three years of my PhD.

I sincerely thank Mr. Laurent Cantrel, research director at IRSN, for giving me confidence to integrate his research field. I am very grateful to Mr. Jean-François Paul, my thesis director, for welcoming me in the laboratory UCCS. Messrs. J-F and Laurent I have benefited from your deep knowledge of the field which advanced the work fast beside your patience and kindness you showed in answering my questions and solving the problems I faced.

I would like to thank the team I worked with, Dimitri, Mireille, Eric, Siwar and Fatah.

I would like to thank also all my office colleagues during my three years, Soraya, Marine, Marie, Ayman, Shreya, Gorge, Gillium, Camilla, Renata, Carlos, Francisco, Leila and Claudia.

A special thanks to my family. I am very grateful to my mother Zeinab and my father Dib for their sacrifices that they have made on my behalf. Also I would like to thank my sisters Lina, Wafaa, and my brothers Youssef, Ali, Khalil, Imad, Hassan, Hussein, Mohamad and Hadi.

Finally, I want to thank all my friends in France and Lebanon, Aude, Rachad, Hammoud, Najib, Daoud, Krayem and Ali Deeb outside my work who supported and encouraged me to accomplish this work as good as possible.





## *Résumé*

Lors d'un accident nucléaire grave, plusieurs produits de fission peuvent être libérés dans l'environnement si des fissures apparaissent l'enceinte de confinement du réacteur nucléaire. Parmi ces produits, l'iode radioactif ( $^{131}\text{I}$ ) est un des produits les plus dangereux en raison de ses conséquences radiologiques élevées durant les premières semaines suivant l'accident. Cet iode radioactif va principalement former des aérosols ( $\text{CsI}$  et  $\text{AgI}$ ) dans le système de refroidissement du réacteur. Ils pourront ensuite réagir dans une atmosphère oxydante et humide, résultant de la radiolyse de la vapeur d'eau entraînant la formation d'iode moléculaire gazeux  $\text{I}_2$ .

L'objectif de ce travail est d'étudier la réactivité des aérosols d'iodure afin de comprendre et identifier des voies chimiques possibles conduisant à la formation d'espèces d'iode volatiles. Nous avons mené une étude théorique basée sur la théorie fonctionnelle de la densité (DFT), comprenant les corrections de Van Der Waals, pour définir, à l'échelle moléculaire, les mécanismes des réactions chimiques se produisant à la surface des aérosols. Des corrections thermodynamiques ont également été utilisées pour déterminer l'effet de la température et de la pression sur cette réactivité.

Les résultats montrent que l'adsorption de l'eau sur les particules  $\text{CsI}$  et  $\text{AgI}$  n'est possible qu'à basse des températures et pour des taux d'humidité élevées, non représentatives des conditions présentes dans l'enceinte de confinement mais pouvant être rencontrées à l'extérieur de cette même enceinte. Plusieurs voies de réaction conduisant à la formation d'espèces d'iode volatiles ( $\text{I}_2$ ,  $\text{IOH}$  et  $\text{IH}$ ) ont été explorées. Ces travaux montrent que la formation de ces espèces nécessite une double oxydation de la surface pour libérer une espèce volatile. L'oxydant le plus réactif est  $\text{OH}^\circ$ , résultant de la radiolyse à la vapeur. Dans ce cas, l'énergie d'activation pour formation d' $\text{I}_2$  est respectivement de 1,2 eV et 1,0 eV pour  $\text{CsI}$  et du  $\text{AgI}$ .

**Mots clés: Iodure de césium, iodure d'argent, DFT, énergie d'activation, terme source, d'iode, accident nucléaire.**



## *Abstract*

If a nuclear severe accident happens to a nuclear power plant, fission products can be released in the environment by some leakages of the nuclear containment building. Among them radioactive iodine is one of the most dangerous species due to its high radiological consequences during the first weeks after the accident, mainly due to  $^{131}\text{I}$  isotope. Some iodide aerosols, formed in the reactor coolant system, are expected to reach the containment, typically CsI and AgI, and next can react in moist oxidizing atmosphere resulting from steam/oxygen radiolysis to form gaseous molecular iodine,  $\text{I}_2$ .

The aim of this work is to study the reactivity of iodide aerosols, it means understand/identify possible chemical pathways leading to the formation of volatile iodine species. Theoretical study based on density functional theory (DFT) including Van Der Waals corrections were performed to study at the molecular scale the chemical reactivity at the aerosol surfaces. Thermodynamic model was used also to determine the effect of temperature and pressure on the reactivity.

The results show that adsorption of water on the CsI and AgI particles is only possible at low temperatures, not representative of severe accident conditions. Several reaction pathways leading to the formation of volatile iodine species ( $\text{I}_2$ , IOH and IH) were explored. These works show that formation of these species requires the oxidation the surface twice. One type of oxidant were tested which is  $\text{OH}^\circ$ , resulting from steam radiolysis and initially present in the containment after radiolysis of water. The activation energy of  $\text{I}_2$  formation using  $\text{OH}^\circ$  oxidants is respectively 1.2 and 1.0 eV for CsI and AgI oxidation processes.

**Keywords: cesium iodide, silver iodide, DFT, activation energy, iodine source term, nuclear accident.**



# Table of contents

<b>Abstract.....</b>	<b>1</b>
<b>General Introduction.....</b>	<b>9</b>
<b>Chapter I: General Context .....</b>	<b>13</b>
I.1 Severe accident in Pressurized Water Reactor (PWR) and its impacts.....	15
I.2 Severe accident scenario .....	15
I.3 Radiological effects of iodine and cesium .....	17
I.4 Physical properties of CsI .....	18
I.5 Literature review on iodine properties .....	19
I.5.1 General properties of iodine .....	19
I.5.2 Interaction of iodine with cesium.....	19
I.6 Formation of other iodine species .....	20
I.7 Effect of temperature on the formation of iodine species.....	20
I.8 OECD/STEM Project.....	21
I.9 Iodine Aerosol behavior in the containment.....	22
I.10 Chemistry of Iodine .....	23
I.10.1 Aqueous phase chemistry of iodine .....	25
I.10.2 Gas phase chemistry of iodine.....	26
I.11 Chemical reactivity of CsI aerosol .....	28
I.12 Chemistry of NaCl.....	29
I.12.1 Surface energy .....	29
I.12.2 Water adsorption and hygroscopicity .....	30
I.12.3 Formation of Cl-containing compounds.....	31
I.13 Conclusion.....	33
I.14 Bibliography.....	34

I.15	Appendix .....	40
<b>Chapter II: Methodology.....</b>		<b>43</b>
II.1	Theoretical background.....	45
II.1.1	Hamiltonian of many body system .....	45
II.1.2	Born-Oppenheimer approximation .....	48
II.2	Density Functional Theory.....	48
II.2.1	Hohenberg-Kohn theorems .....	49
II.2.2	Kohn-Sham approach.....	50
II.2.3	Approximations to exchange correlation potential .....	52
II.2.4	Van der Waals interactions.....	54
II.3	Bloch's theorem.....	55
II.4	Pseudopotential.....	56
II.5	Molecular dynamics .....	57
II.5.1	Classical MD formalism.....	57
II.5.2	Born-Oppenheimer MD.....	59
II.5.3	Thermostat.....	59
II.6	Nudged Elastic Band (NEB).....	61
II.7	Application in VASP .....	63
II.8	Cutoff Energy.....	65
II.9	Conclusion.....	66
II.10	References .....	66
<b>Chapter III: Reactivity of CsI aerosols.....</b>		<b>69</b>
III.1	Introduction .....	71
III.2	CsI surfaces reactivity: A DFT study (submitted article) .....	72
III.2.1	Introduction .....	72

III.2.2	Theoretical methods.....	74
III.2.3	Results and discussion .....	77
III.2.4	Conclusion .....	90
III.3	Supplementary data corresponding to the paper.....	92
III.3.1	KPOINTS as function of energy .....	92
III.3.2	Lattice constant and bulk volume .....	92
III.3.3	Formation of I <sub>2</sub> starting by optimized and experimental lattice constant.....	93
III.3.4	Formation of I <sub>2</sub> on a doubled cell in two directions.....	94
III.3.5	Adsorption of one monolayer of water using different geometries .....	95
III.3.6	Effect of temperature and pressure on the adsorption of one water monolayer.....	96
III.3.7	Adsorption of more than one water monolayer on (011) CsI surface.....	97
III.4	Reactivity of defected surfaces .....	98
III.4.1	Oxidation by one OH° .....	99
III.4.2	Oxidation by two OH° .....	100
III.5	Conclusion.....	103
III.6	References .....	104
<b>Chapter IV: Chapter 4: Reactivity of Silver Iodide (AgI)</b> .....		<b>109</b>
IV.1	Introduction .....	110
IV.2	Theoretical parameters of AgI .....	111
IV.3	Surface energy.....	112
IV.4	Water adsorption on AgI surfaces. ....	116
IV.4.1	Associative adsorption of one water molecule on AgI surfaces .....	117
IV.4.2	Dissociative adsorption of one water molecule on AgI surfaces.....	118
IV.4.3	Temperature and pressure dependence on the associative adsorption of water on AgI surfaces .....	119

IV.4.4	Half and one monolayer adsorption of water on AgI surfaces.....	120
IV.4.5	Conclusion concerning adsorption of water on AgI surfaces.....	122
IV.5	Reactivity of AgI .....	122
IV.5.1	Reactivity without oxidant.....	122
IV.5.2	Reactivity with oxidants .....	124
IV.6	Conclusion.....	131
IV.7	Bibliography: .....	132
<b>Chapter V: Reactivity in liquid phase.....</b>		<b>135</b>
V.1	Introduction .....	136
V.2	Classical molecular dynamics.....	136
V.3	Implicit solvent model.....	137
V.4	Ab initio molecular dynamics.....	138
V.4.1	Free energy diagram and dynamics evolution.....	140
V.4.2	Pair correlation function and coordination number .....	142
V.4.3	Diffusion coefficient of water .....	145
V.4.4	Iodide reactivity in liquid phase .....	146
V.5	Conclusion.....	146
V.6	References: .....	147
<b>Chapter VI: General conclusion and perspectives .....</b>		<b>149</b>



# **General Introduction**



# General Introduction

**Motivation** Electricity is one of the most important needs in our daily life beside its importance for developing artificial activities. Different sources were used to produce electricity like solar, thermal, chemical, etc. One of the modern methods is to convert nuclear energy to electricity in nuclear power plants by chain reactions. However, controlling the safety of these nuclear plants is of prime importance to prevent any non-controlled outside releases of volatile radioactive compounds. For safety reasons, nuclear power plants are secured by number of safety systems to control the chain reaction and consequently to cool down the fuel. Beside all safety procedures, some LOss of Coolant Accidents (LOCA) leading to severe accident were happened like Three Mile Island in 1979, Tchernobyl in 1986 and more recently Fukushima in 2011 in which an important amount of radioactive contamination were released into the environment.

Number of experimental projects on nuclear safety were launched to understand the physical and chemical processes in the contamination after a severe accident. PHEBUS-FP program took place from 1988 to 2010 with some integral tests. Its purpose was to improve the understanding of the phenomena occurring during a core meltdown accident in a light water reactor and to validate the computational software used to represent these phenomena in reactor safety evaluations. Tests have shown/confirmed that during a severe accident, elements composed of caesium, boron and iodine were released in significant amounts and released in the primary circuit in gas or aerosol form and that which interacts between each other. The radiolytic reactions governs the chemical reactivity after fission products reached the nuclear containment building. Recently, experimental study done in the frame of OECD/STEM project (2011-2015, <https://www.oecd-nea.org/jointproj/stem.html>) examined the release of volatile iodine species from caesium iodide (CsI) aerosols under irradiation for long time (30 hours).

To predict the radiological consequences of a severe accident on population, the French Institute of radioprotection and nuclear safety (IRSN) is developing modelling codes called ASTEC ('Accidental Source Term Evaluation Code) which models the scenario of severe accidents in different types of reactors. This code is composed of many modules which take into account the

phenomena that happen in different parts of pressurized water reactor in each stage of the accident

**Objectives** In our project, we will perform a theoretical study to discover the reactional mechanism leading to the formation of iodine containing species especially  $I_2$  starting by some possible iodide metallic aerosols that may exist in the nuclear containment building after a severe accident like CsI and AgI.

**Approach** This manuscript is composed of five chapters:

Chapter I is constituted by the bibliography and presents wide range of experimental and theoretical data on aerosols and the context of the work carried out in this thesis. We present also the released species after a severe accident and its chemical properties. Later we present the liquid and gas phase chemistry of aerosols and at the end we showed chemistry of NaCl aerosols since its chemistry is quiet similar to that of CsI.

Chapter II presents briefly the methods and techniques used in our calculation. Small description of many body theory is given. Next, we showed density functional theory (DFT) and its approximations and finally we presented briefly the used code (VASP).

Chapter III shows all studies on CsI surface.

Chapter IV shows all studies on AgI surface.

Chapter V is constituted of conclusion and perspectives.

# **Chapter I: General Context**



## I.1 Severe accident in Pressurized Water Reactor (PWR) and its impacts

Nuclear reactor is a facility used to produce electricity basing on fission chain reactions. The heat produced from this reaction is used to heat pressurized water which flow through the fuel rods surrounded by a zirconium alloy cladding. This pressurized water circulates in the reactor coolant system (RCS) and via a heat exchanger (called steam generator) heats the water secondary system which is at saturation. The secondary-side steam is delivered to the turbines to make electricity. The steam is subsequently condensed via cooled water from a tertiary loop and returned to the steam generator to be heated once again (see Figure I-1).

Fission of heavy nucleus like uranium or plutonium, gives new fragments. Generally, at least one of these two daughter nuclei is radioactive, which will still disintegrate until it reaches a stable nucleus. All fission fragments and their daughters present in the fuel are called fission products (FP), which they constitute the major part of the nuclear wastes.

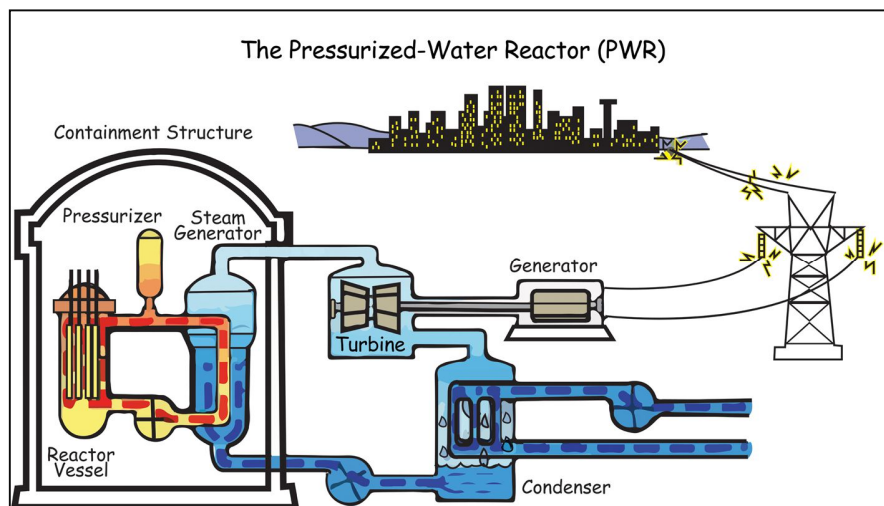


Figure I-1: Schematic presentation of PWR<sup>1</sup>.

## I.2 Severe accident scenario

One of the important issues during the normal functioning is the safety procedures. Three basic functions of nuclear safety must be ensured in all circumstances to have safe reactor:

- Control of the chain reactions, and thus the power produced by the fissions; This control is ensured by control rods and boric acid in the water. Both can capture neutrons.
- Discharge of the energy released by the fuel elements after stopping the chain reaction (residual power). The residual power is evacuated by water cooling of the fuel rods ;
- Confinement of the radioactive fission products.

Confinement of radioactive materials is therefore a key element for the safety of the reactor. To ensure the confinement, the reactor has three containment barriers. The fuel pellets are first placed in sealed sheaths zirconium alloy, which prevents the release of radioactive products in the primary circuit. Next, the RCS as a whole is a sealed circuit which may retain the radioactive products. Finally, the entire primary circuit is placed in a sealed chamber formed of concrete, which can withstand high internal pressure, called the nuclear containment building. Thus, the radioactive products can only be released into the environment if all three containment barriers are broken.

A severe accident can occur when the core is no longer cooled enough. Several scenarios can lead to partial or total loss of cooling systems. The fusion of the core leads to the formation of a complex mixture based on uranium dioxide  $UO_2$  ( $PuO_2$  for MOX fuels) and also consisting of all the materials present in the vessel (Fe and control rod materials for instance), this mixture is called corium. The non-submerged parts of the core undergo significant temperature rise (more than  $1200^\circ C$ ), causing the occurrence of physicochemical phenomena leading core degradation until its merger. Since the beginning of the civilian usage of nuclear energy, three serious accidents industrial nuclear reactors took place. The first, March 28, 1979, on the second nuclear reactor of the Three Mile Island (TMI-2) generating station in the US; the second, April 26, 1986 on the fourth reactor of the Chernobyl plant in Ukraine, and the last one, March 11, 2011, three of the six reactors at the Fukushima Daiichi plant in Japan. Chernobyl and Fukushima accidents were classified on level 7 the INES scale (Figure I-2), the TMI accident was classified at level 5.



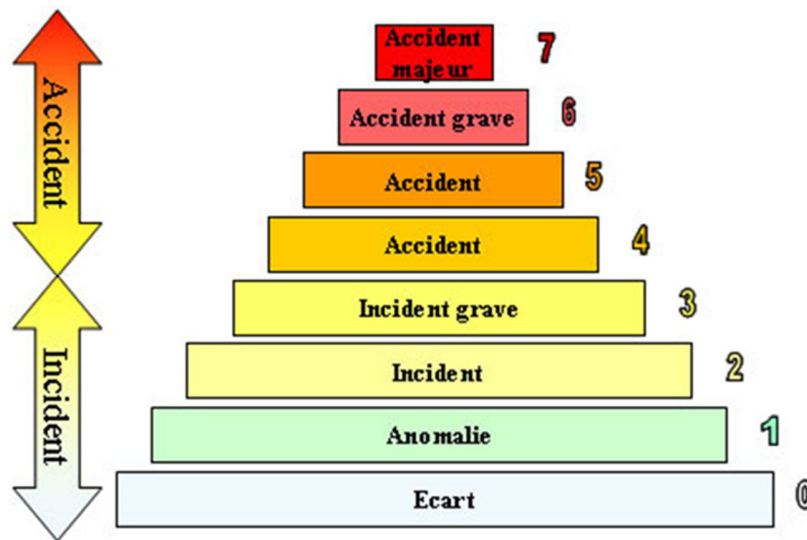


Figure I-2. International Nuclear Events Scale (INES) ([www.irsn.com](http://www.irsn.com)).

Severe nuclear accident can lead to significant radioactive elements and FP release into the environment. The main radiological significant FP are iodine, cesium and tellurium, strontium and to a lesser measurement, ruthenium, barium, molybdenum and the lanthanides. Among them, radioactive airborne iodine is of particular interest since it is produced in important amounts in air/steam in the presence of radiation. In the case of Chernobyl accident, the activity ratio of  $^{131}\text{I}$  relative to  $^{137}\text{Cs}$  in air is 7<sup>2</sup>. However, the activity of  $^{131}\text{I}$  measured on dry soil from Fukushima Daiichi facility during the first 20 days after the accident is between 10 and 629 relative to  $^{137}\text{Cs}$ , and iodine has the highest activity of all other radioactive elements<sup>3</sup>.

### I.3 Radiological effects of iodine and cesium

Radiotoxic parameters of  $^{131}\text{I}$  and  $^{137}\text{Cs}$  presented in **Table I-1**. These two elements were reported to be of high toxicity<sup>4</sup>, also considered as the sources of the most important dose received by the human beings<sup>5</sup>.

**Table I-1: Physical and radiological properties of radionuclide  $^{131}\text{I}$  and  $^{137}\text{Cs}$  <sup>6</sup>. \* Dose Per Unit Intake (radiation)**

<b>Isotope</b>	<b>Emission</b>	<b>Half-life</b>	<b>Mass activity (Bq/g)</b>	<b>DPUI* inhalation (Sv/Bq) (Thyroid)</b>	<b>DPUI ingestion (Sv/Bq) (Thyroid)</b>
$^{131}\text{I}$	$\beta, \gamma$	8.04 days	$4.6 \times 10^{15}$	$2.92 \times 10^{-7}$	$4.76 \times 10^{-7}$
$^{137}\text{Cs}$	$\beta$	30 years	$3.22 \times 10^{12}$	$1.26 \times 10^{-8}$	$7.93 \times 10^{-9}$

The danger of these elements originates from its deposition ability to the lungs and all other body part.  $^{131}\text{I}$  releases in gaseous form which can travel at relatively low altitudes (400 – 1200 m)<sup>7</sup>, in which it will affect more the environment due to higher dispersion and some possibilities to react with the atmospheric species<sup>8</sup>. All these facts give an important motivation to understand deeply chemical and physical properties of concerning CsI particles.

## I.4 Physical properties of CsI

CsI is of interest in our study because of its existence after an accident, also it's volatile and reported to be the source of many iodine-containing volatile species. Some of its properties are presented in Table I-2.

**Table I-2. Physical properties of CsI<sup>9</sup>.**

<b>Melting point</b>	894.15 K
<b>Boiling point</b>	1553.15 K
<b>Density at room T</b>	4.51 g.cm <sup>-3</sup>
<b>Solubility</b>	44 g/100 g H <sub>2</sub> O at 0°C
$\Delta H_f$ at 25°C*	-80.5 kcal/mol
$\Delta H_{\text{disso}}$ *	100.0 kcal/mol
$\Delta H_{\text{vap}}$ (298)C*	46.7 kcal/mol

\*JANAF Thermochemical Tables.

## I.5 Literature review on iodine properties

### I.5.1 General properties of iodine

General properties of iodine element are presented in Table I-3. It's widely used for treating thyroid cancer since it is adsorbed easily by the human organs, also it's used for manufacturing some acids and polymers. The Iodine isotope with mass number 131 (molar masse of 130.906 g.mol<sup>-1</sup>) was discovered in 1938 by Glenn Seaborg and John Livingood <sup>10</sup> and is used mainly for medical purposes. It is one of the major fission products of <sup>235</sup>U and <sup>239</sup>Pu.

**Table I-3. Physical and chemical properties of Iodine element.**

<b>Electron configuration</b>	[ Kr ] 4d <sup>10</sup> 5s <sup>2</sup> 5p <sup>5</sup>
<b>Atomic number</b>	53
<b>Melting point</b>	386.85 K
<b>Boiling point</b>	457.4 K
<b>Density at room T</b>	4.933 g.cm <sup>-3</sup>
<b>Electronegativity (Pauling scale)</b>	2.66
<b>Atomic radius</b>	140 pm
<b>Van der Waals radius</b>	198 pm
<b>Covalent radius</b>	139±3 pm
<b>Triple point</b>	386.65 K, 12.1 kPa
<b>Heat of vaporization (I<sub>2</sub>)</b>	41.57kJ/mol

### I.5.2 Interaction of iodine with cesium

Both aqueous and gas behavior should be studied to follow the evolution of iodine chemical speciation in the containment. Iodine can form some volatile species (organic and inorganic) during a severe accident, it can behave as airborne or it can interact and be deposited on containment surfaces (steels, concrete and paints) while some will be transferred to liquid phase, mainly by settling of the metallic iodide aerosol coming from the RCS. In addition, aqueous iodine forms can be considered after several chemical reactions as a source of gaseous iodine due to molecular iodine (I<sub>2</sub>) formation by radiolytic oxidation of iodides (I).

US studies<sup>11</sup> assumed that, after a severe accident, 95% of the iodine released into the containment from the reactor coolant system are in the form of cesium iodide aerosol (CsI) due to its high thermochemistry stability, while the rest are in the form of vapor species. Formation of bulk CsI is favored even in a steam environment due to the large amount of cesium released comparing to iodine (amount of iodine formed in the fuel during normal operation of power plant is 10 times less than the amount of cesium)<sup>12</sup>. So CsI will be formed by diatomic recombination:



The behavior of Cesium is more complex. experimental studies<sup>13-15</sup> claims that Cs released mainly in the forms of cesium hydroxide which, in a second step, interacts in gas phase with boric acid<sup>15,16</sup> to form cesium borate according to the following equation:



In reductive conditions, Cesium hydroxide can also react with iodine and hydrogen to form CsI<sup>12,17</sup> according to the following reaction:



Understanding the long term evolution of CsI is a major challenge to be able of model correctly the possible outside releases.

## **I.6 Formation of other iodine species**

In addition to formation of CsI aerosols, PHEBUS FP<sup>18</sup> program showed the formation of other iodine species, possible candidates are for instance: silver iodide (AgI), rubidium iodide (RbI), indium iodide (InI<sub>x</sub>) and cadmium iodide (CdI<sub>2</sub>). Some of these chemical species may be formed after the interaction between silver indium cadmium control rod and the fuel.

## **I.7 Effect of temperature on the formation of iodine species**

Several studies<sup>19-21</sup> have showed the effect of fuel properties (temperature, pressure, power, surrounding environment) on the amount and rate of the released fission products. Thermodynamic equilibrium calculations predict that CsI is the most stable iodine species at low temperatures (< 1000K), while volatile forms of iodine such as HI, I<sub>2</sub> and I are important at

higher temperatures. Calculations were done on three-node temperature system for 1500 K, 1000 K and 750 K<sup>22</sup>. The results show a very quick formation of CsI and CsOH at 1500 K and 1000 K (time required to reach equilibrium about 10<sup>-3</sup> sec for high concentrations while it's about 10<sup>-2</sup> sec for lower ones), while at 750 K, the system takes more than 1000 sec to reach equilibrium. Whatever the condition, CsI will be formed in less than 1 hours and may such be in important sources of iodine releases.

## I.8 OECD/STEM Project

Recent experimental study <sup>23</sup> done in the frame of OECD/STEM project (<https://gforge.irsn.fr/gf/project/stem/>) examined volatilization of iodine species released from CsI under irradiation. In this study, the tests were done on three different surfaces which are stainless steel, quartz and EPOXY painted surfaces. The samples consisted in deposited CsI aerosols on the surfaces and next are irradiated for long time (30 hours). Schematic diagram of the setup (EPICUR) used is presented in Figure I-3. EPICUR is a  $\gamma$ -cell with a vessel of about 4.5 L where are deposited the surfaces with CsI.

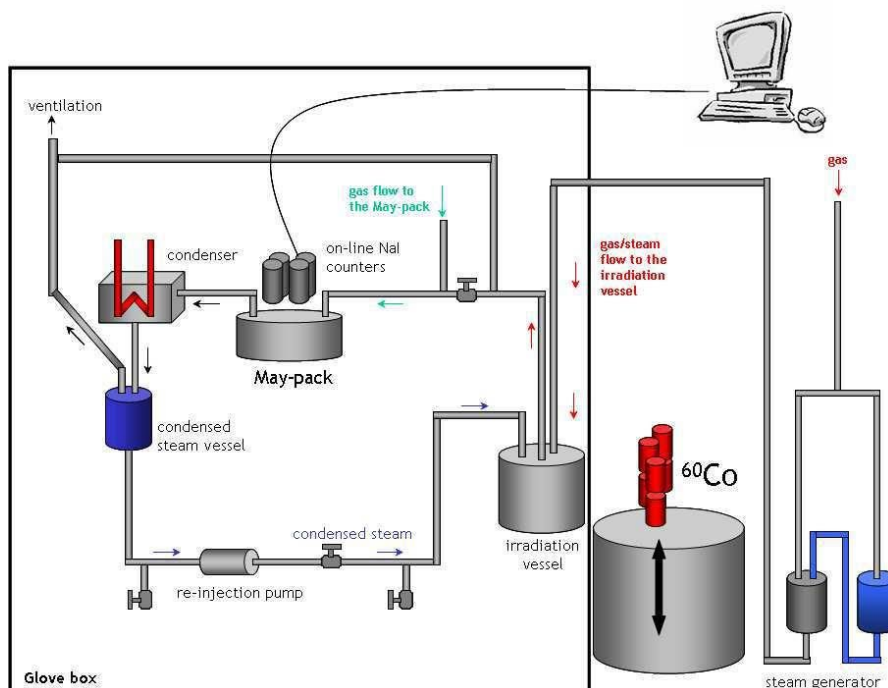


**Figure I-3. Schematic diagram of EPICUR setup.**

Figure I-4 shows the amount of iodine species released from CsI aerosols deposited on stainless steel irradiated at 50% relative humidity. The results shows early and fast release of I<sub>2</sub> (pink

curve) during the first stages of irradiation (between 10 and 15 hours), while the release kinetics is slower after this time. Some other releases under aerosol for (grey curve) and organic iodides (blue curve) are observed but in a smaller extent. Aerosol can be attributed to iodine oxides whereas organic iodides are formed by reaction between  $I_2$  and organic pollutants present. Moreover, at relative humidity close to the deliquescence point of CsI (about 57%), the release of molecular iodine,  $I_2$ , is high. Two tests were made at 80 °C and 120 °C to study the effect of temperature on the kinetics, the results show that effect of the temperature on the quantity of  $I_2$  released is small.

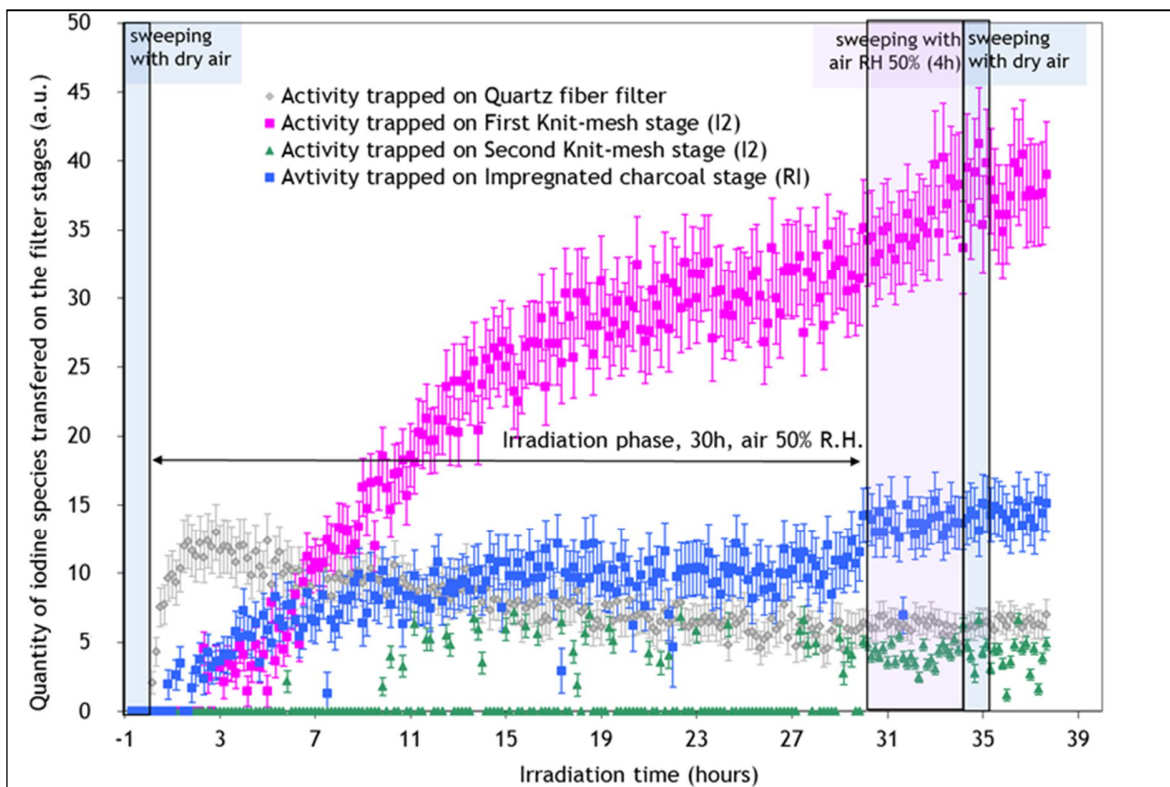


**Figure I-4. Quantity of iodine species transferred from the sample to the gas phase for AER6 test performed at 80°C, a stainless steel coupon and a dose rate of 3.7 kGy/h.**

## I.9 Iodine Aerosol behavior in the containment

Fission products reaching the containment can be characterized in terms of aerosol deposition and agglomeration processes. Reactor safety study (1985-1987)<sup>24</sup> determined important physiochemical processes in the containment, and its effects on the transport of fission products

and aerosols. For the homogenous nucleation of CsI, they claim that aerosol particles will be smaller as temperature of the vapor decreased, also that liquid droplets are formed above 1150K. More recent study<sup>25</sup> have been published on behavior of aerosol particles produced during a severe accident of nuclear reactor. The particle shape appeared to be spherical droplet in the presence of steam condensation, also it has been shown that aerosols in the containment are constituted by primary circuit particles and their agglomerates.

It is worth noticing that Adachi et al.<sup>26</sup> reported the release of radioactive Cs-bearing particles at early stages of the Fukushima nuclear accident. The aerosol composition is made in addition of Cs of Fe, Zn and other possible elements. The aerosols diameter are approximately 2 $\mu$ m and aerosols are insoluble in water.

## **I.10 Chemistry of Iodine**

Wren et al.<sup>27</sup> and Bosland et al.<sup>28</sup> reviewed the literature on iodine chemistry in containment and showed its chemical reaction pathways (Figure I-5). Volatile molecular iodine I<sub>2</sub> formed from oxidation by radiolysis of nonvolatile iodine I<sup>-</sup> under severe accident conditions, may oxidized again to form iodine oxides or reduced to return back to nonvolatile iodine I<sup>-</sup>. Presence of silver in aqueous allows the trapping of iodine under non soluble form AgI. Molecular iodine could also interact with some organic compounds either in the liquid phase or in the gas phase to form volatile organic iodides, noted RI. In the following section we will present aqueous and gas phase chemistry of iodine.

Molecular iodine is also adsorbed by painted inner wall and iodine adsorbed can be partially released under RI(g) form.

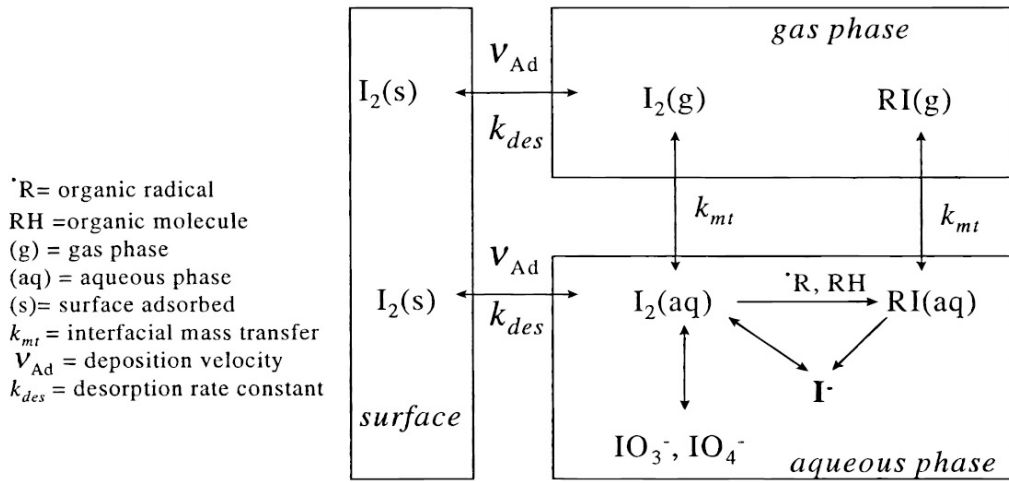


Figure I-5. Simplified chemical reaction pathways for iodine in containment (Wren et al.)



## I.10.1 Aqueous phase chemistry of iodine

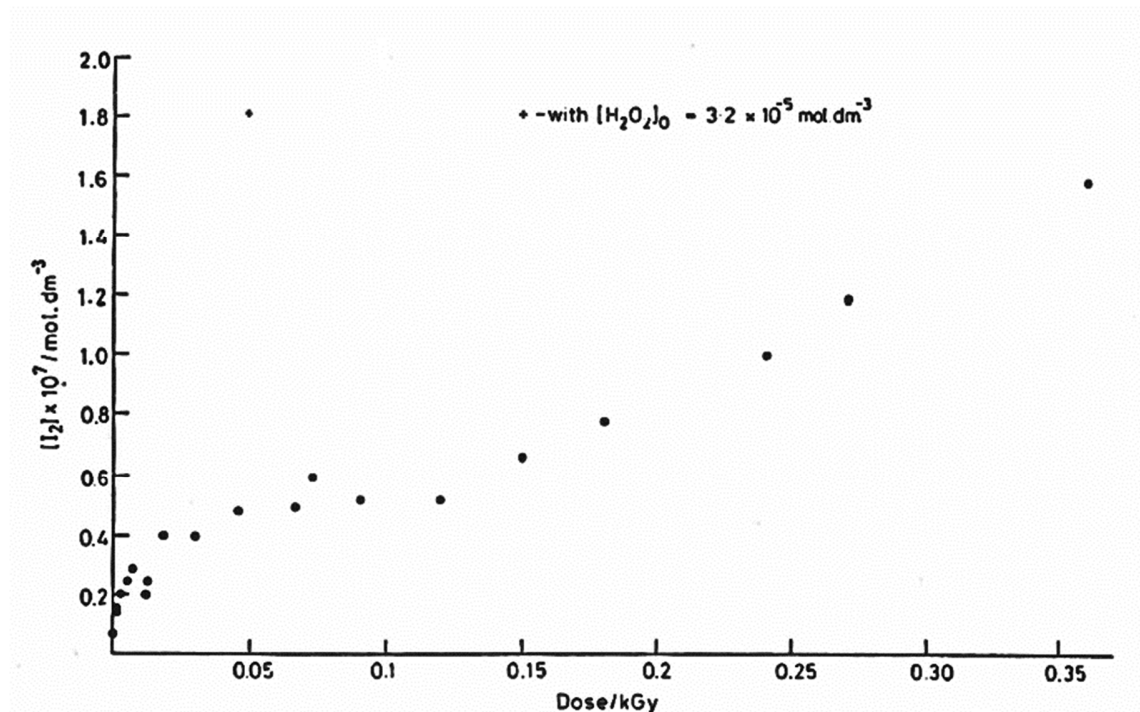
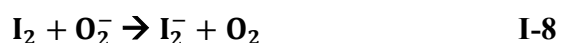
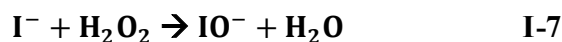
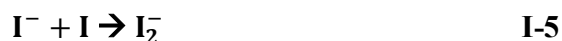
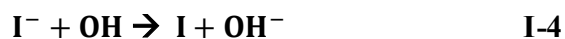


Figure I-6: Formation of iodine at low doses (Burns et al. 1990).

CsI is hygroscopic, so it will be easily dissolved in water droplets. In saturated steam atmosphere, this will lead to condensation droplets and forming  $\text{Cs}^+$  and  $\text{I}^-$  in solutions. For that, large number of studies, iodine is supposed to be initially present in the containment as  $\text{I}^-$ , after metallic iodide aerosols settling, and after to be oxidized to form to  $\text{I}_{2(\text{aq})}$ . Some experiments (Program PHEBUS FP) have shown that a part of iodine coming from the RCS can be under volatile formed, probably  $\text{I}_2(\text{g})$  due to some kinetic limitations.

Number of studies have been performed on the effect water radiolysis of iodine chemistry<sup>30-32</sup>. Burns et al.<sup>32</sup> measured experimentally yields of the radiolysis  $\text{I}_2$  and  $\text{IO}_3^-$  production, starting by solutions of CsI and  $\text{CsIO}_3$  irradiated under varying factors like temperature, concentration and pH. In the Burns's works, many tests were performed to investigate the molecular iodine formation as a function of experimental parameters. For instance, the results obtained for dose parameter with a initial iodide concentration fixed at  $10^{-4} \text{ mol} \cdot \text{l}^{-1}$ , are presented in Figure I-6. It shows initial formation of  $\text{I}_2$  till it stays in steady state between dose about 50 and 100 Gy value

which is referred by the authors to the following oxidizing (rxn. 4-7) and reducing (rxn. 8) reactions:



with the complementary reactions:



The concentration of  $\text{H}_2\text{O}_2$  is enhanced by the radiolysis of water, this leads to the formation of large quantities of OH according to the following equation:

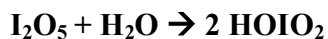


Then it proportionally decreases the amount of  $\text{e}^-$  and increases the amount of oxidation of I to  $\text{I}_2$ .

Temperature dependent investigations are also performed in this study, the conclusion drawn is that the initial rate of formation of  $\text{I}_2$  is independent on temperature, while the final steady state does. With respect to the pH effect on the iodine yield, it has been showed that iodine formation will decrease greatly as the pH increases slightly.

## **I.10.2 Gas phase chemistry of iodine**

Beside liquid chemistry of iodine, gas phase chemistry was also studied widely for atmospheric and nuclear safety topics. Canneaux et al.<sup>33</sup> presented reaction rate and transition state geometries of gas phase reactions of iodine atoms with  $\text{H}_2$ ,  $\text{H}_2\text{O}$ , HI and OH using wide number of theoretical chemistry levels. Kanniche et al.<sup>34</sup> reported theoretical study of iodine oxides chemistry where they concentrated on the gas phase reaction between pentoxide iodine and water vapor:



I-14

Transition state of this reaction was discovered (Figure I-7b) in which we have water molecule dissociation into one OH and one Hydrogen, each one connected to different iodine atom as displayed in Figure I-7.

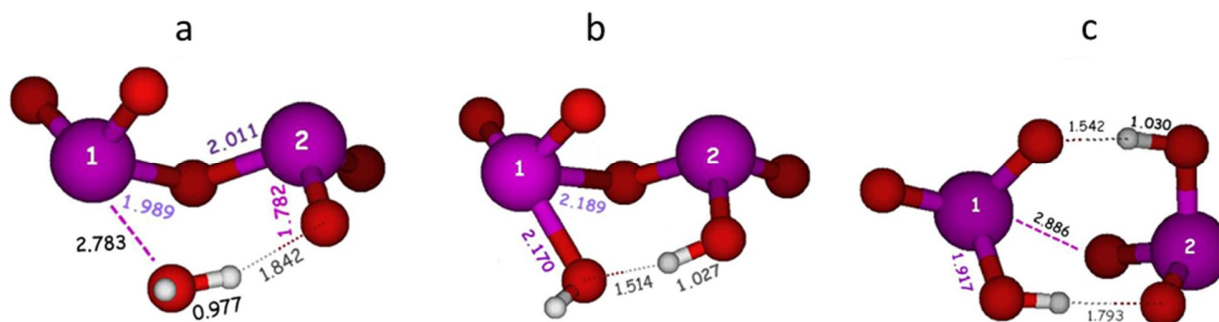


**Figure I-7. Molecular complex structures of the reactant(a), transition state(b) and product(c)(distances in Å)** <sup>34</sup>

By transition state theory, forward and reverse rate constants were measured as function of T to be respectively:

$3.61 \times 10^{-22} \times T^{2.05} \exp(-32.3 \text{ (kJ mol}^{-1}\text{)}/RT)$  and  $6.73 \times 10^{-27} \times T^{2.90} \exp(-24.5 \text{ (kJ mol}^{-1}\text{)}/RT)$ , respectively, k in  $\text{cm}^3 \text{ molecule}^{-1} \text{ s}^{-1}$ .

Very recent publication for the same authors<sup>35</sup> reported chemical properties of HIO<sub>3</sub> isomers and claimed that iodic acid isomer (HOIO<sub>2</sub>) is the most stable one. Mono and di-hydration of HOIO<sub>2</sub> also were studied in details including lots of isomers/geometries. Iodine monoxide (IO) is also of great interest since it is produced after reaction between iodine atoms and ozone<sup>35-38</sup>. Reaction of IO with HO<sub>2</sub> has been studied by many references experimentally. Major product of this reaction is HIO as mentioned by<sup>39-41</sup>. Then the studied reaction is



I-15

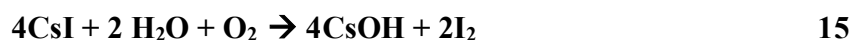
Methods used, temperatures, references and the rate constants are sum-up in Table I-4. Moreover, temperature dependence rate constant was obtained by experiments done by Cronkhite et al.<sup>42</sup>, it was established that  $k(274\text{-}373 \text{ K}) = 9.3 \times 10^{-12} \exp(680/T)$  in  $\text{cm}^3 \text{ molecule}^{-1} \text{ s}^{-1}$ . Other possible products may exist for this reaction such as OIO + OH and HOIO<sub>2</sub>.

Reactant	method	T (K)	Rate constant K ( $\text{cm}^3 \text{ molecule}^{-1} \text{ s}^{-1}$ )	reference
IO + HO <sub>2</sub>	molecular modulation technique/UV-visible spectroscopy	298	$(6.4 \pm 0.7) \times 10^{-11}$	39
	discharge flow/mass spectrometry	298	$(1.03 \pm 0.13) \times 10^{-10}$	41
	discharged-flow tube/resonance fluorescence and chemiluminescence	296	$(7.1 \pm 1.6) \times 10^{-11}$	40
	flash photolysis/Vis-UV absorption	298	$(9.7 \pm 2.9) \times 10^{-11}$	42
	discharge-flow/mass spectrometry	298	$8.42 \times 10^{-11}$	43

**Table I-4. Kinetic parameters for the (IO + HO<sub>2</sub>) reactant**

## I.11 Chemical reactivity of CsI aerosol

Behavior of CsI aerosols in water vapor-gas phase was studied by<sup>44</sup>. The CsI aerosols particles were produced by sublimation process from metallic surface and exposed to different gas mixture argon, air and water vapor-air mixture at 900-1570 K. Oxidative hydrolysis reaction of CsI were proposed in the presence of H<sub>2</sub>O and O<sub>2</sub>:



This reaction is promoted by high temperature. The results show formation of large amounts of CsOH and I<sub>2</sub> after vaporization in air. However, the ratio of Cs/I species formed in water vapor-air mixture is greater by ~25% from that formed in air. This increase in ratio was attributed to the hydrolysis of CsI in water which forms CsOH aerosols.

Moreover, recent works by nks<sup>45</sup> aimed to study the reactivity of iodine containing aerosols (CsI and IOx). These aerosols were deposited on different surface materials (paint films and metal surfaces such as Cu, Zn, Al and SS) and analysis with various methods. The aerosols were revaporized from the surfaces in the presence of humidity, with and without irradiation but irradiation increases the oxidative kinetics. XPS analysis shows that the deposited IOx particles were in the form of HIO<sub>3</sub> on metallic and painted surfaces. However, CsI solid particles were observed on the metallic surfaces while nothing is observed on the painted ones which seems that they are dissolved in presence of moist atmosphere. Revaporisation process seems to be affected by the heat and irradiation. The painted surfaces reacts more with the iodine from CsI than that of the IOx.

On the other hand, Lin et al<sup>46</sup> investigated the effect of gamma radiation on the potassium iodine (KI) aerosols. They have shown that some iodine species like I<sub>2</sub>, HIO and organic additives can be produced after oxidization of iodide ions (I<sup>-</sup>) present in aerosols.

## I.12 Chemistry of NaCl

Since literature about chemistry surface of CsI is scarce, it is relevant to look for other types of aerosols which they have similar chemistry like NaCl. Atmospheric aerosols are composed of chemical mixture with a great amount of salt<sup>47</sup>. For example, marine aerosols containing important amounts of chlorides and bromides<sup>48</sup> interact with NO<sub>2</sub> and NO<sub>3</sub>. NaCl aerosol has been widely studied experimentally and theoretically since it is the major component of sea salt<sup>49,50</sup>, can be a good system to compare it with CsI since their chemistry will be quite similar.

### I.12.1 Surface energy

Sodium chloride is formed after interaction between sodium and chlorine atoms according to the following formula:



NaCl solid has a simple cubic structure<sup>51</sup> with lattice parameter around 5.64 Å<sup>52</sup> at room temperature, such that each chlorine atom has one type of neighbors which is sodium and vice versa. Bruno et al.<sup>51,52</sup> studied surface energy and relaxation of (100), (110) and (111) planes of

NaCl. The two first are nonpolar surfaces which terminate with  $\text{Na}^+$  and  $\text{Cl}^-$  ions, while the last is polar that ends up with only one type of ions. Among all low indices planes of NaCl, (100) plane seems to be the most stable one. The surface energies (calculated at  $T=0$  K) is  $160 \text{ mJ/m}^2$ . The (100) surface is formed of neutral layers each one contains alternating  $\text{Na}^+$  and  $\text{Cl}^-$  ions. Surface energies were also calculated at  $T > 0$ , the calculations show that only (100) plane forms the equilibrium shape of crystal.

## **I.12.2 Water adsorption and hygroscopicity**

*Ab initio* calculation were done by Yong et al.<sup>53</sup> to study water adsorption on NaCl (100) surface. They mentioned that adsorption of water molecules is due to two kinds of interaction, covalent and electrostatic. For the most favorable adsorption geometry, the oxygen located near  $\text{Na}^+$  while the hydrogen near  $\text{Cl}^-$  such that O- $\text{Na}^+$  interaction is dominant one (O- $\text{Na}^+ \approx 2.4 \text{ \AA}$ , H- $\text{Cl}^- \approx 2.2 \text{ \AA}$  and  $E_{\text{ads}} = 0.37 \text{ eV}$ ), in contrast to Meyer et al.<sup>54</sup> which found that the most important contribution to adsorption energy is H- $\text{Cl}^-$  interaction. ( $E_{\text{ads}}=0.44 \text{ eV}$ )

For the adsorption of more than one water molecule, other factors play a role in determining the favorable adsorption geometries which are inter molecules adsorption/repulsion and the attraction between molecules and the underlying substrate. Water molecules try to displace in a way to reduce water-water repulsion between neighboring molecules and to create hydrogen bonds. Pepa et al.<sup>55</sup> studied adsorption of one monolayer water coverage over NaCl (100) substrate. Adsorption energy per molecule for the most stable geometry was calculated to be  $0.41 \text{ eV}$  with H-H bond about  $3.1 \text{ \AA}$ . They concluded that once we increase H-H bond distance between neighbor molecules, adsorption energy will be higher due to the decrease in water-water repulsion. Repulsion between adsorbed water molecules reduced by directing the hydrogen atom of one water toward the oxygen of the neighbor one, while the water surface attraction optimized when O is near Na and H pointed toward Cl on the surface<sup>54</sup>. After one monolayer adsorption, water molecules become close to each other resulting in hydrogen bonds thus the intermolecular interaction becomes more important than interaction with surface<sup>53</sup>.

One of the interesting properties for aerosols is hygroscopic behavior after exposure to humidity. Deliquescence is a main property of aerosols since it calls for the solid-liquid phase transition once the relative humidity overcomes a threshold value which is proper for each salt [15], [16],<sup>29</sup>. Hygroscopicity is larger for lower deliquescence relative humidity values [14]. Ewing et al.<sup>56-58</sup>

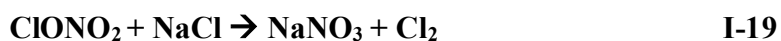
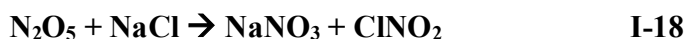
expressed adsorption of water on NaCl single crystal face considering different coverage regions; for low coverage case (less than half monolayer) they noticed formation of isolated islands of water on the surface interacting by hydrogen bonds, while in the transition region (between half and 2.5 monolayers) they reported the formation of isolated islands and multilayer thin films. Further at the high coverage (between 2.5 and 3.5 monolayers), multilayers thin-film formed little by little, while at very high coverage, we got NaCl salt solution. These results agree with many references<sup>56,59-61</sup> which say that deliquescence takes place at ~75% relative humidity. This relative humidity corresponds to an adsorption of 3 monolayers of water.

On the other hand, polycrystalline NaCl contains defects such as edges, corners, and steps which may be active sites and more sensitive to water adsorption<sup>62</sup>. Adsorption of water on NaCl polycrystalline at 298K was investigated by Barraclough and Hall[30], they reported that solution of NaCl was obtained only after adsorption of two monolayers of water.

### **I.12.3 Formation of Cl-containing compounds**

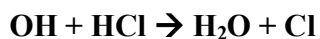
Furthermore, Cabrera-Sanfelix et al.<sup>64</sup> have studied possible release of Cl<sup>-</sup> from NaCl (100) crystal at low humidity (less than 40%). Chlorine anion supposed to move 2.4Å perpendicularly from the surface to a water monolayer that already exists on the surface. The dissolution of one chlorine is athermic and implies 0.12 eV which is almost negligible; same reaction on dry NaCl (100) is very endothermic and requires ~1.75 eV, it reflects the important role of water monolayer in the process (they refer this low energetic cost to the screening provided by the highly polarized water monolayer).

Wide number of studies<sup>65-98</sup> demonstrated heterogeneous reactions of NaCl for atmospheric chemistry interest. Some of these reactions produce chlorine containing compounds like:



Sea salt aerosols show chlorine deficits<sup>99-105</sup> which has been referred to the interaction with strong acids. Reaction  $\text{HNO}_3 + \text{NaCl} \rightarrow \text{NaNO}_3 + \text{HCl}$  I-17 seems to be very important due to the large amounts of HCl formed<sup>73,74,78,92,106</sup>.

HCl produces atomic chlorine after interaction with OH radicals according to the following reaction:



I-20

Reaction of HNO<sub>3</sub> has been studied with NaCl single crystals and with NaCl powders, it is much faster in the latter case than the former one. This difference results from water which is more favorably adsorbed in defects and steps more present in powders, their amounts control the reaction extent<sup>49</sup>. Moreover, Rachel<sup>107</sup> has proposed a mechanism for reaction of HNO<sub>3</sub> with NaCl crystal at two different sites, one on dry terrace while second one on water associated edge as shown in Figure I-8. HNO<sub>3</sub> adsorbed beside edges forms HCl while NO<sub>3</sub><sup>-</sup> crystallizes to form NaNO<sub>3</sub>, so a new NaCl step is formed (see Figure I-8b). This reaction goes on and the surface will not be saturated since new steps are formed. However, on flat terrace HNO<sub>3</sub> adsorbed leads to formation of HCl while chloride anion is replaced by NO<sub>3</sub><sup>-</sup>, this reaction doesn't form NaNO<sub>3</sub> since NO<sub>3</sub><sup>-</sup> takes place of the released Cl anion (Figure I-8c). Terrace surface will be saturated as soon as all chlorine ions are released then the reaction will stop after that.



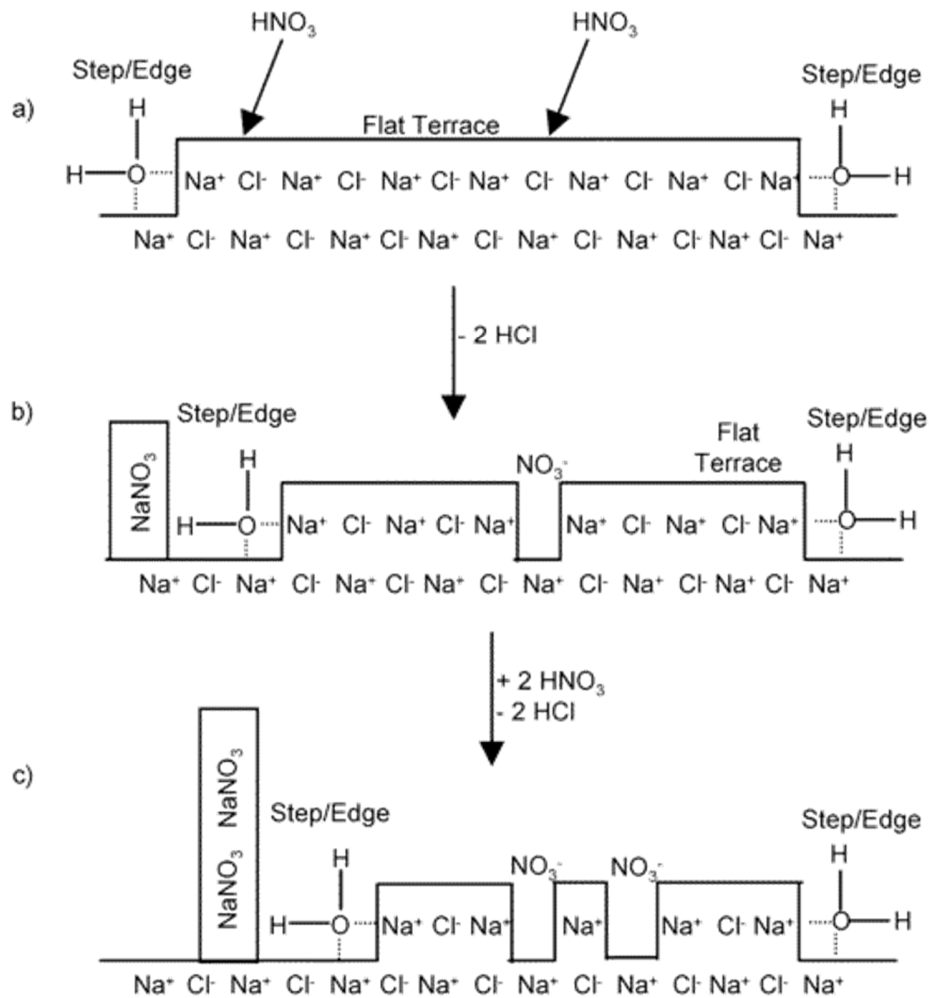


Figure I-8. Schematic diagram for reaction of HNO<sub>3</sub> and NaCl crystal<sup>107</sup>

## I.13 Conclusion

As detailed in this short literature review, metallic iodide aerosols (CsI, AgI etc) are important contamination products that may be released inside the nuclear containment building in case of severe accident and next potentially in the environment via containment leakages with high radiological consequences due to iodine and cesium radioactive isotopes. Before being released outside, these aerosols can chemically react in the containment, leading to gaseous iodine as recently shown by IRSN and NKS experiments. Few studies in the literature are available concerning the reactivity of iodine aerosols. It is therefore essential to study the reactivity of

these aerosols to first understand potential mechanism of oxidation and next be able to extrapolate experimental results to a wide range of boundary conditions as well as to extend the results to other iodide metallic aerosols. In this PhD, we will study potential oxidation mechanism by theoretical chemistry, it means at the molecular scale and we will focus on their behavior after interacting with the existing chemical species in gas phase, mainly steam and radicals coming from steam radiolysis. However, some of these aerosols (CsI) are well known to be hygroscopic in the presence of water. In order to ensure this, we will extend the study to the behavior of CsI in liquid phase.

## I.14 Bibliography

- (1) art-students-reactors-1-lg.gif (2680×1512) <https://www.nrc.gov/admin/img/art-students-reactors-1-lg.gif> (accessed Apr 10, 2017).
- (2) DENSCHLAG, H. O.; DIEL, A.; GLÄSEL, K.-H.; HEIMANN, R.; KAFFRELL, N.; KNITZ, U.; MENKE, H.; TRAUTMANN, N.; WEBER, M.; HERRMANN, G. Fallout in the Mainz Area from the Chernobyl Reactor Accident. *Radiochim. Acta* **1987**, *41* (4), 163–172.
- (3) Schwantes, J. M.; Orton, C. R.; Clark, R. A. Analysis of a Nuclear Accident: Fission and Activation Product Releases from the Fukushima Daiichi Nuclear Facility as Remote Indicators of Source Identification, Extent of Release, and State of Damaged Spent Nuclear Fuel. *Environ. Sci. Technol.* **2012**, *46* (16), 8621–8627.
- (4) Clefs CEA n°48 [http://www.lyc-hoche-versailles.ac-versailles.fr/wwwmanuel/physique/Revues/ClefsCEA/Clefs48/Clefs48\\_sommaire.html](http://www.lyc-hoche-versailles.ac-versailles.fr/wwwmanuel/physique/Revues/ClefsCEA/Clefs48/Clefs48_sommaire.html) (accessed Apr 11, 2017).
- (5) Saenko, V.; Ivanov, V.; Tsyb, A.; Bogdanova, T.; Tronko, M.; Demidchik, Y.; Yamashita, S. The Chernobyl Accident and Its Consequences. *Clin. Oncol.* **2011**, *23* (4), 234–243.
- (6) US EPA, O. Federal Guidance Report No. 11: Limiting Values Of Radionuclide Intake And Air Concentration And Dose Conversion Factors For Inhalation, Submersion, And Ingestion <https://www.epa.gov/radiation/federal-guidance-report-no-11-limiting-values-radionuclide-intake-and-air-concentration> (accessed Apr 11, 2017).
- (7) Pöllänen, R.; Valkama, I.; Toivonen, H. Transport of Radioactive Particles from the Chernobyl Accident. *Atmos. Environ.* **1997**, *31* (21), 3575–3590.
- (8) Julien Trincal. Mosélisation du comportement de l'iode dans l'atmosphère, Lille 1, 2015.
- (9) R. A. Lorenz; M. F. Osborne; J. L. Collins; S. R. Manning; A. P. Malinauskas; R. A. Lorenz. *Behavior of Iodine, Methyl Iodide, Cesium Oxide, and Cesium Iodide in Steam and Argon*; ORNL/NUREG/TM-25 NRC-3; Oak ridge national laboratory, 1976.
- (10) Livingood, J. J.; Seaborg, G. T. Radioactive Iodine Isotopes. *Phys. Rev.* **1938**, *53* (12), 1015–1015.

- (11) Soffer, L.; Burson, S. B.; Ferrell, C. M.; Lee, R. Y.; Ridgely, J. N. Accident Source Terms for Light-Water Nuclear Power Plants. *NUREG-1465* **1995**, 6.
- (12) OECD NEA/CSNI/R. State-of the Art Report on Iodine Chemistry. 2007.
- (13) Lemire, R. J.; Paquette, J.; Torgerson, D. F.; Wren, D. J.; Fletcher, J. W. *Assessment of Iodine Behaviour in Reactor Containment Buildings from a Chemical Perspective*; AECL--6812; Atomic Energy of Canada Ltd., 1981.
- (14) Garisto, F. *Thermodynamics of Iodine, Cesium and Tellurium in the Primary Heat-Transport System under Accident Conditions*; AECL--7782; Atomic Energy of Canada Ltd., 1982.
- (15) Bowsher, B. R. Fission-Product Chemistry and Aerosol Behaviour in the Primary Circuit of a Pressurized Water Reactor under Severe Accident Conditions. *Prog. Nucl. Energy* **1987**, 20 (3), 199–233.
- (16) Mellor, J. W. *A Comprehensive Treatise on Inorganic and Theoretical Chemistry: Vol. 5, Supplement. Boron. Boron - Oxygen Compounds*; Longmans, 1980.
- (17) Elrick, R. M.; Sallach, R. A.; Ouellette, A. L.; Douglas, S. C. *Reaction Between Some Cesium-Iodine Compounds and the Reactor Materials 304 Stainless Steel, Inconel 600 and Silver. Volume 1: Cesium Hydroxide Reactions*; NUREG/CR-3197-Vol.1; SAND-83-0395-Vol.1; Sandia National Labs., Albuquerque, NM (USA), 1984.
- (18) Clément, B.; Hanniet-Girault, N.; Repetto, G.; Jacquemain, D.; Jones, A. V.; Kissane, M. P.; von der Hardt, P. LWR Severe Accident Simulation: Synthesis of the Results and Interpretation of the First Phebus FP Experiment FPT0. *Nucl. Eng. Des.* **2003**, 226 (1), 5–82.
- (19) Burns, P. C.; Ewing, R. C.; Navrotsky, A. Nuclear Fuel in a Reactor Accident. *Science* **2012**, 335 (6073), 1184–1188.
- (20) Badawi, M.; Xerri, B.; Canneaux, S.; Cantrel, L.; Louis, F. Molecular Structures and Thermodynamic Properties of 12 Gaseous Cesium-Containing Species of Nuclear Safety Interest: Cs<sub>2</sub>, CsH, CsO, Cs<sub>2</sub>O, CsX, and Cs<sub>2</sub>X<sub>2</sub> (X=OH, Cl, Br, and I). *J. Nucl. Mater.* **2012**, 420 (1–3), 452–462.
- (21) Paquette, J.; Torgerson, D. F.; Wren, J. C.; Wren, D. J. Volatility of Fission Products during Reactor Accidents. *J. Nucl. Mater.* **1985**, 130, 129–138.
- (22) Wren D.J. *KINETICS OF IODINE AND CESIUM REACTIONS IN THE CANDU REACTOR PRIMARY HEAT TRANSPORT SYSTEM UNDER ACCIDENT CONDITIONS*; Report AECL-7781; Atomic Energy of Canada Ltd, 1983.
- (23) J.Colombani, C.Pascal, L.Martinet, C.Duffieux, O.Leroy. AER-CsI STEM/EPICUR Tests Synthesis Report. Juillet 2015.
- (24) Beard, A. M.; Commission of the European Communities; Joint Research Centre; Ispra Establishment. *Fission Product and Aerosol Behaviour within the Containment.*; Commission of the European Communities, 1990.
- (25) Kissane, M. P. On the Nature of Aerosols Produced during a Severe Accident of a Water-Cooled Nuclear Reactor. *Nucl. Eng. Des.* **2008**, 238 (10), 2792–2800.
- (26) Adachi, K.; Kajino, M.; Zaizen, Y.; Igarashi, Y. Emission of Spherical Cesium-Bearing Particles from an Early Stage of the Fukushima Nuclear Accident. *Sci. Rep.* **2013**, 3.
- (27) Wren, J. C.; Ball, J. M.; Glowa, G. A. The Chemistry of Iodine in Containment. *Nucl. Technol.* **2000**, 129 (3), 297–325.
- (28) Bosland, L.; Cantrel, L.; Girault, N.; Clement, B. Modeling of Iodine Radiochemistry in the ASTEC Severe Accident Code: Description and Application to FPT-2 Phébus Test. *Nucl. Technol.* **2010**, 171 (1), 88–107.

- (29) Dutton, L. M. C.; Grindon, E.; Handy, B. J.; Sutherland, L.; Burns, W. G.; Dickinson, S.; Sims, H. E.; Hueber, C.; Jacquemain, D. Iodine Behaviour in Severe Accidents. In *WORKSHOP ON THE CHEMISTRY OF IODINE IN REACTOR SAFETY*; 1996; p 615.
- (30) Sellers, R. M. *Reaction Kinetics of Iodine Compounds in Aqueous Solution*; CEGB-TPRD/B--0688/R85; Central Electricity Generating Board, 1985.
- (31) Sawai, T.; Shinozaki, Y.; Meshitsuka, G. The Radiolysis of Aqueous Solutions of Potassium Iodide. *Bull. Chem. Soc. Jpn.* **1966**, *39* (5), 951–955.
- (32) W G Burns, M C Kent, W R Marsh and H E Sims. The Radiolysis of Aqueous Solutions of Caesium Iodide and Caesium Iodate. March 1990.
- (33) Canneaux, S.; Xerri, B.; Louis, F.; Cantrel, L. Theoretical Study of the Gas-Phase Reactions of Iodine Atoms ( $^2P_{3/2}$ ) with  $H_2$ ,  $H_2O$ , HI, and OH. *J. Phys. Chem. A* **2010**, *114* (34), 9270–9288.
- (34) Khanniche, S.; Louis, F.; Cantrel, L.; Černušák, I. Computational Study of the  $I_2O_5 + H_2O = 2 HOIO_2$  Gas-Phase Reaction. *Chem. Phys. Lett.* **2016**, *662*, 114–119.
- (35) Khanniche, S.; Louis, F.; Cantrel, L.; Černušák, I. A Theoretical Study of the Microhydration of Iodic Acid ( $HOIO_2$ ). *Comput. Theor. Chem.* **2016**, *1094*, 98–107.
- (36) Aliche, B.; Hebestreit, K.; Stutz, J.; Platt, U. Iodine Oxide in the Marine Boundary Layer. *Nature* **1999**, *397* (6720), 572–573.
- (37) Allan, B. J.; McFiggans, G.; Plane, J. M. C.; Coe, H. Observations of Iodine Monoxide in the Remote Marine Boundary Layer. *J. Geophys. Res. Atmospheres* **2000**, *105* (D11), 14363–14369.
- (38) Whalley, L. K.; Furneaux, K. L.; Gravestock, T.; Atkinson, H. M.; Bale, C. S. E.; Ingham, T.; Bloss, W. J.; Heard, D. E. Detection of Iodine Monoxide Radicals in the Marine Boundary Layer Using Laser Induced Fluorescence Spectroscopy. *J. Atmospheric Chem.* **2007**, *58* (1), 19–39.
- (39) Jenkin, M. E.; Cox, R. A.; Hayman, G. D. Kinetics of the Reaction of IO Radicals with  $HO_2$  Radicals at 298 K. *Chem. Phys. Lett.* **1991**, *177* (3), 272–278.
- (40) Canosa-mas, C. E.; Flugge, M. L.; Shah, D.; Vipond, A.; Wayne, R. P. Kinetics of the Reactions of IO with  $HO_2$  and  $O(3P)$ . *J. Atmospheric Chem.* *34* (1), 153–162.
- (41) Maguin, F.; Laverdet, G.; Le Bras, G.; Poulet, G. Kinetic Study of the Reactions Iodine Monoxide + Hydroperoxo and Iodine Monoxide + Nitrogen Dioxide at 298 K. *J. Phys. Chem.* **1992**, *96* (4), 1775–1780.
- (42) Cronkhite, J. M.; Stickel, R. E.; Nicovich, J. M.; Wine, P. H. Laser Flash Photolysis Studies of Radical–Radical Reaction Kinetics: The  $HO_2 + IO$  Reaction. *J. Phys. Chem. A* **1999**, *103* (17), 3228–3236.
- (43) Knight, G. P.; Crowley, J. N. The Reactions of IO with  $HO_2$ , NO and  $CH_3SCH_3$ : Flow Tube Studies of Kinetics and Product Formation. *Phys. Chem. Chem. Phys.* **2001**, *3* (3), 393–401.
- (44) Kulyukhin, S. A.; Mikheev, N. B.; Kamenskaya, A. N.; Rumer, I. A.; Konovalova, N. A.; Novichenko, V. L. Oxidative Hydrolysis in Water Vapor-Air Phase of CsI Radioaerosols Produced by CsI Sublimation from Metallic Surface. *Radiochemistry* **2004**, *46* (1), 63–66.
- (45) Tietze, S.; Foreman, M.; Ekberg, C.; Kaerkelae, T.; Auvinen, A.; Tapper, U.; Jokiniemi, J. *Adsorption and Revaporisation Studies of Thin Iodine Oxide and CsI Aerosol Deposits from Containment Surface Materials in LWRs*; Nordisk Kernesikkerhedsforskning, 2013.
- (46) Lin, C. C.; Wang, C. F.; Sun, Y. C.; Chao, J. H.; Tseng, C. L. Radiation Effects on Gaseous Iodine at Very Low Concentrations. *J. Radioanal. Nucl. Chem.* **2006**, *268* (2), 419–424.

- (47) Buseck, P. R.; POsfai, Miha. Airborne Minerals and Related Aerosol Particles: Effects on Climate and the Environment. *Proc. Natl. Acad. Sci.* **1999**, *96* (7), 3372–3379.
- (48) Chemistry of the Natural Atmosphere (International Geophysics, Vol 41) by P. Warneck: Academic Press Inc 9780127356303 - Anybook Ltd. <http://www.abebooks.com/servlet/BookDetailsPL?bi=17026454242&searchurl=isbn%3D0127356304%26sortby%3D17> (accessed Oct 20, 2016).
- (49) Rossi, M. J. Heterogeneous Reactions on Salts. *Chem. Rev.* **2003**, *103* (12), 4823–4882.
- (50) Finlayson-Pitts, B. J. The Tropospheric Chemistry of Sea Salt: A Molecular-Level View of the Chemistry of NaCl and NaBr. *Chem. Rev.* **2003**, *103* (12), 4801–4822.
- (51) Bruno, M.; Aquilano, D.; Pastero, L.; Prencipe, M. Structures and Surface Energies of (100) and Octopolar (111) Faces of Halite (NaCl): An Ab Initio Quantum-Mechanical and Thermodynamical Study. *Cryst. Growth Des.* **2008**, *8* (7), 2163–2170.
- (52) Bruno, M.; Aquilano, D.; Prencipe, M. Quantum-Mechanical and Thermodynamical Study on the (110) and Reconstructed (111) Faces of NaCl Crystals. *Cryst. Growth Des.* **2009**, *9* (4), 1912–1916.
- (53) Yang, Y.; Meng, S.; Wang, E. G. Water Adsorption on a NaCl (001) Surface: A Density Functional Theory Study. *Phys. Rev. B* **2006**, *74* (24).
- (54) Meyer, H.; Entel, P.; Hafner, J. Physisorption of Water on Salt Surfaces. *Surf. Sci.* **2001**, *488* (1–2), 177–192.
- (55) Cabrera-Sanfelix, P.; Holloway, S.; Darling, G. R. Monolayer Adsorption of Water on NaCl(100). *Appl. Surf. Sci.* **2007**, *254* (1), 87–91.
- (56) Foster, M. C.; Ewing, G. E. Adsorption of Water on the NaCl(001) Surface. II. An Infrared Study at Ambient Temperatures. *J. Chem. Phys.* **2000**, *112* (15), 6817–6826.
- (57) Peters, S. J.; Ewing, G. E. Thin Film Water on NaCl (100) under Ambient Conditions: An Infrared Study. *Langmuir* **1997**, *13* (24), 6345–6348.
- (58) Cantrell, W.; McCrory, C.; Ewing, G. E. Nucleated Deliquescence of Salt. *J. Chem. Phys.* **2002**, *116* (5), 2116–2120.
- (59) National Research Council (U.S.); Washburn, E. W.; West, C. J. *International Critical Tables of Numerical Data, Physics, Chemistry and Technology*; Pub. for the National research council by the McGraw-Hill Book Company, Inc.: New York, 1926.
- (60) Peters, S. J.; Ewing, G. E. Water on Salt: An Infrared Study of Adsorbed H<sub>2</sub>O on NaCl(100) under Ambient Conditions. *J. Phys. Chem. B* **1997**, *101* (50), 10880–10886.
- (61) Xu, L.; Lio, A.; Hu, J.; Ogletree, D. F.; Salmeron, M. Wetting and Capillary Phenomena of Water on Mica. *J. Phys. Chem. B* **1998**, *102* (3), 540–548.
- (62) Somorjai, G. A.; Mujumdar, A. S. Introduction to Surface Chemistry and Catalysis. *Dry. Technol.* **1995**, *13* (1–2), 507–508.
- (63) Barraclough, P. B.; Hall, P. G. The Adsorption of Water Vapour by Lithium Fluoride, Sodium Fluoride and Sodium Chloride. *Surf. Sci.* **1974**, *46* (2), 393–417.
- (64) Cabrera-Sanfelix, P.; Sanchez Portal, D.; Verdaguer, A.; Darling, G. R.; Salmeron, M.; Arnau, A. Spontaneous Emergence of Cl<sup>-</sup> Anions from NaCl(100) at Low Relative Humidity. *J. Phys. Chem. C* **2007**, *111* (22), 8000–8004.
- (65) Behnke, W.; Scheer, V.; Zetzsch, C. 16 O 04 Formation of ClNO<sub>2</sub> and HNO<sub>3</sub> in the Presence of N<sub>2</sub>O<sub>5</sub> and Wet Pure NaCl- and Wet Mixed NaCl/Na<sub>2</sub>SO<sub>4</sub>- Aerosol. *J. Aerosol Sci.* **1993**, *24*, S115–S116.
- (66) Vogt, R.; Finlayson-Pitts, B. J. A Diffuse Reflectance Infrared Fourier Transform Spectroscopic (DRIFTS) Study of the Surface Reaction of NaCl with Gaseous NO<sub>2</sub> and

- HNO<sub>3</sub>. [Erratum to Document Cited in CA120:228408]. *J. Phys. Chem.* **1995**, *99* (34), 13052–13052.
- (67) Vogt, R.; Finlayson-Pitts, B. J. A Diffuse Reflectance Infrared Fourier Transform Spectroscopic Study of the Surface Reaction of NaCl with Gaseous NO<sub>2</sub> and HNO<sub>3</sub>. *J. Phys. Chem.* **1994**, *98* (14), 3747–3755.
- (68) Koch, T. G.; Bergh, H. van den; Rossi, M. J. A Molecular Diffusion Tube Study of N<sub>2</sub>O<sub>5</sub> and HONO<sub>2</sub> Interacting with NaCl and KBr at Ambient Temperature. *Phys. Chem. Chem. Phys.* **1999**, *1* (11), 2687–2694.
- (69) Andreae, M. O.; Crutzen, P. J. Atmospheric Aerosols: Biogeochemical Sources and Role in Atmospheric Chemistry. *Science* **1997**, *276* (5315), 1052–1058.
- (70) Msibi, I. M.; Li, Y.; Shi, J. P.; Harrison, R. M. Determination of Heterogeneous Reaction Probability Using Deposition Profile Measurement in an Annular Reactor: Application to the N<sub>2</sub>O<sub>5</sub>/H<sub>2</sub>O Reaction. *J. Atmospheric Chem.* *18* (3), 291–300.
- (71) Ghosal, S.; Hemminger, J. C. Effect of Water on the HNO<sub>3</sub> Pressure Dependence of the Reaction between Gas-Phase HNO<sub>3</sub> and NaCl Surfaces. *J. Phys. Chem. A* **1999**, *103* (25), 4777–4781.
- (72) Behnke, W.; Krüger, H.-U.; Scheer, V.; Zetzsch, C. Formation of Atomic Cl from Sea Spray via Photolysis of Nitryl Chloride: Determination of the Sticking Coefficient of N<sub>2</sub>O<sub>5</sub> on NaCl Aerosol. *J. Aerosol Sci.* **1991**, *22*, S609–S612.
- (73) Finlayson-Pitts, B. J.; Ezell, M. J.; Pitts, J. N. Formation of Chemically Active Chlorine Compounds by Reactions of Atmospheric NaCl Particles with Gaseous N<sub>2</sub>O<sub>5</sub> and ClONO<sub>2</sub>. *Nature* **1989**, *337* (6204), 241–244.
- (74) Ravishankara, A. R. Heterogeneous and Multiphase Chemistry in the Troposphere. *Science* **1997**, *276* (5315), 1058–1065.
- (75) Hemminger, J. C. Heterogeneous Chemistry in the Troposphere: A Modern Surface Chemistry Approach to the Study of Fundamental Processes. *Int. Rev. Phys. Chem.* **1999**, *18* (3), 387–417.
- (76) Abbatt, J. P. D.; Waschewsky, G. C. G. Heterogeneous Interactions of HOBr, HNO<sub>3</sub>, O<sub>3</sub>, and NO<sub>2</sub> with Deliquescent NaCl Aerosols at Room Temperature. *J. Phys. Chem. A* **1998**, *102* (21), 3719–3725.
- (77) Fenter, F. F.; Caloz, F.; Rossi, M. J. Heterogeneous Kinetics of N<sub>2</sub>O<sub>5</sub> Uptake on Salt, with a Systematic Study of the Role of Surface Presentation (for N<sub>2</sub>O<sub>5</sub> and HNO<sub>3</sub>). *J. Phys. Chem.* **1996**, *100* (3), 1008–1019.
- (78) Behnke, W.; Zetzsch, C. Heterogeneous Photochemical Formation of Cl Atoms from NaCl Aerosol, NO<sub>x</sub> and Ozone. *J. Aerosol Sci.* **1990**, *21*, S229–S232.
- (79) Timonen, R. S.; Chu, L. T.; Leu, M.-T.; Keyser, L. F. Heterogeneous Reaction of ClONO<sub>2</sub>(g) + NaCl(s) → Cl<sub>2</sub>(g) + NaNO<sub>3</sub>(s). *J. Phys. Chem.* **1994**, *98* (38), 9509–9517.
- (80) Leu, M.-T.; Timonen, R. S.; Keyser, L. F.; Yung, Y. L. Heterogeneous Reactions of HNO<sub>3</sub>(g) + NaCl(s) → HCl(g) + NaNO<sub>3</sub>(s) and N<sub>2</sub>O<sub>5</sub>(g) + NaCl(s) → ClONO<sub>2</sub>(g) + NaNO<sub>3</sub>(s). *J. Phys. Chem.* **1995**, *99* (35), 13203–13212.
- (81) Sporleder, D.; Ewing, G. E. Infrared Spectroscopic Investigation of the Heterogeneous Reaction of HNO<sub>3</sub> and NaCl(100). *J. Phys. Chem. A* **2001**, *105* (10), 1838–1846.
- (82) Fenter, F. F.; Caloz, F.; Rossi, M. J. Kinetics of Nitric Acid Uptake by Salt. *J. Phys. Chem.* **1994**, *98* (39), 9801–9810.
- (83) Davies, J. A.; Cox, R. A. Kinetics of the Heterogeneous Reaction of HNO<sub>3</sub> with NaCl: Effect of Water Vapor. *J. Phys. Chem. A* **1998**, *102* (39), 7631–7642.

- (84) Hoffman, R. C.; Gebel, M. E.; Fox, B. S.; Finlayson-Pitts, B. J. Knudsen Cell Studies of the Reactions of N<sub>2</sub>O<sub>5</sub> and ClONO<sub>2</sub> with NaCl: Development and Application of a Model for Estimating Available Surface Areas and Corrected Uptake Coefficients. *Phys. Chem. Chem. Phys.* **2003**, *5* (9), 1780–1789.
- (85) Beichert, P.; Finlayson-Pitts, B. J. Knudsen Cell Studies of the Uptake of Gaseous HNO<sub>3</sub> and Other Oxides of Nitrogen on Solid NaCl: The Role of Surface-Adsorbed Water. *J. Phys. Chem.* **1996**, *100* (37), 15218–15228.
- (86) Schweitzer, F.; Mirabel, P.; George, C. Multiphase Chemistry of N<sub>2</sub>O<sub>5</sub>, ClONO<sub>2</sub>, and BrNO<sub>2</sub>. *J. Phys. Chem. A* **1998**, *102* (22), 3942–3952.
- (87) Fenter, F. F.; Caloz, F.; Rossi, M. J. Paper II: Simulation of Flow Conditions in Low-Pressure Flow Reactors (Knudsen Cells) Using a Monte Carlo Technique. *Rev. Sci. Instrum.* **1997**, *68* (8), 3180–3186.
- (88) Brink, H. T.; Waijers-Ijpelaan, A.; Slanina, S. Performance of an Automated Thermodenuder for Ammonium Nitrate Measurements. *J. Aerosol Sci.* **1998**, *29*, S633–S634.
- (89) Finlayson-Pitts, B. J.; Hemminger, J. C. Physical Chemistry of Airborne Sea Salt Particles and Their Components. *J. Phys. Chem. A* **2000**, *104* (49), 11463–11477.
- (90) Behnke, W.; George, C.; Scheer, V.; Zetzsch, C. Production and Decay of ClONO<sub>2</sub> from the Reaction of Gaseous N<sub>2</sub>O<sub>5</sub> with NaCl Solution: Bulk and Aerosol Experiments. *J. Geophys. Res. Atmospheres* **1997**, *102* (D3), 3795–3804.
- (91) Zangmeister, C. D.; Pemberton, J. E. Raman Spectroscopy of the Reaction of Sodium Chloride with Nitric Acid: Sodium Nitrate Growth and Effect of Water Exposure. *J. Phys. Chem. A* **2001**, *105* (15), 3788–3795.
- (92) Finlayson-Pitts, B. J. Reaction of NO<sub>2</sub> with NaCl and Atmospheric Implications of NOCl Formation. *Nature* **1983**, *306* (5944), 676–677.
- (93) George, C.; Ponche, J. L.; Mirabel, P.; Behnke, W.; Scheer, V.; Zetzsch, C. Study of the Uptake of N<sub>2</sub>O<sub>5</sub> by Water and NaCl Solutions. *J. Phys. Chem.* **1994**, *98* (35), 8780–8784.
- (94) Livingston, F. E.; Finlayson-Pitts, B. J. The Reaction of Gaseous N<sub>2</sub>O<sub>5</sub> with Solid NaCl at 298 K: Estimated Lower Limit to the Reaction Probability and Its Potential Role in Tropospheric and Stratospheric Chemistry. *Geophys. Res. Lett.* **1991**, *18* (1), 17–20.
- (95) Finlayson-Pitts, B. J.; Pitts, J. N. Tropospheric Air Pollution: Ozone, Airborne Toxics, Polycyclic Aromatic Hydrocarbons, and Particles. *Science* **1997**, *276* (5315), 1045–1051.
- (96) Vogt, R.; Finlayson-Pitts, B. J. Tropospheric HONO and Reactions of Oxides of Nitrogen with NaCl. *Geophys. Res. Lett.* **1994**, *21* (21), 2291–2294.
- (97) Guimbaud, C.; Arens, F.; Gutzwiller, L.; Gäggeler, H. W.; Ammann, M. Uptake of HNO<sub>3</sub> to Deliquescent Sea-Salt Particles: A Study Using the Short-Lived Radioactive Isotope Tracer <sup>13</sup>N. *Atmos Chem Phys* **2002**, *2* (4), 249–257.
- (98) Laux, J. M.; Hemminger, J. C.; Finlayson-Pitts, B. J. X-Ray Photoelectron Spectroscopic Studies of the Heterogenous Reaction of Gaseous Nitric Acid with Sodium Chloride: Kinetics and Contribution to the Chemistry of the Marine Troposphere. *Geophys. Res. Lett.* **1994**, *21* (15), 1623–1626.
- (99) Pszenny, A. A. P.; Keene, W. C.; Jacob, D. J.; Fan, S.; Maben, J. R.; Zetwo, M. P.; Springer-Young, M.; Galloway, J. N. Evidence of Inorganic Chlorine Gases Other than Hydrogen Chloride in Marine Surface Air. *Geophys. Res. Lett.* **1993**, *20* (8), 699–702.
- (100) Wingenter, O. W.; Kubo, M. K.; Blake, N. J.; Smith, T. W.; Blake, D. R.; Rowland, F. S. Hydrocarbon and Halocarbon Measurements as Photochemical and Dynamical Indicators

- of Atmospheric Hydroxyl, Atomic Chlorine, and Vertical Mixing Obtained during Lagrangian Flights. *J. Geophys. Res. Atmospheres* **1996**, *101* (D2), 4331–4340.
- (101) H. B. Singh, G. L. Gregory, B. Anderson, E. Browell, G. W. Sachse, D. D. Davis, J. Crawford, J. D. Bradshaw, R. Talbot, D. R. Blake, D. Thornton, R. Newell, J. Merrill. Low Ozone in the Marine Boundary Layer of the Tropical Pacific Ocean: Photochemical Ozone, Chlorine Atoms, and Entrainment. *JOURNAL OF GEOPHYSICAL RESEARCH*. 1996, pp 1907–191.
- (102) Junge, C. E. Recent Investigations in Air Chemistry. *Tellus* **1956**, *8* (2), 127–139.
- (103) Moyers, J. L.; Duce, R. A. Gaseous and Particulate Iodine in the Marine Atmosphere. *J. Geophys. Res.* **1972**, *77* (27), 5229–5238.
- (104) Martens, C. S.; Wesolowski, J. J.; Harriss, R. C.; Kaifer, R. Chlorine Loss from Puerto Rican and San Francisco Bay Area Marine Aerosols. *J. Geophys. Res.* **1973**, *78* (36), 8778–8792.
- (105) Mouri, H.; Okada, K. Shattering and Modification of Sea-Salt Particles in the Marine Atmosphere. *Geophys. Res. Lett.* **1993**, *20* (1), 49–52.
- (106) Karlsson, R.; Ljungström, E. A Laboratory Study of the Interaction of NH<sub>3</sub> and NO<sub>2</sub> with Sea Salt Particles. *Water, Air, Soil Pollut.* **103** (1–4), 55–70.
- (107) Hoffman, R. C.; Kaleuati, M. A.; Finlayson-Pitts, B. J. Knudsen Cell Studies of the Reaction of Gaseous HNO<sub>3</sub> with NaCl Using Less than a Single Layer of Particles at 298 K: A Modified Mechanism. *J. Phys. Chem. A* **2003**, *107* (39), 7818–7826.

## I.15 Appendix

### STEM experimental data about behavior of CsI under irradiation

In this part we will show the two tables taken from the STEM/EPICUR tests synthesis report, which summarizes the experimental conditions used for these tests (Table I-5), while the second one shows the corresponding post-test results (Table I-6).



**Table I-5: Experimental conditions used for the tests.**

	AER-1	AER-2b	AER-3	AER-4	AER-5	AER-6	AER-11
<b>24.6</b>							
Coupon surface (cm <sup>2</sup> )							
Nature of the coupon	Quartz	Quartz	Epoxy paint	Epoxy paint	Epoxy paint	Stainless steel	Stainless steel
Initial iodine concentration ( $=[Cs]_i$ ) on the coupon (mol.m <sup>-2</sup> )	$(6.1 \pm 0.2) \times 10^{-3}$	$(3.9 \pm 0.2) \times 10^{-3}$	$(6.6 \pm 0.7) \times 10^{-3}$	$(5.3 \pm 0.3) \times 10^{-3}$	$(2.2 \pm 0.1) \times 10^{-4}$	$(7.4 \pm 0.2) \times 10^{-5}$	$(2.1 \pm 0.1) \times 10^{-4}$
<b>Pre-irradiation phase</b>							
Temperature (°C)	80	80	80	80	80	80	120
R.H. of Air (%)	Air-20%R.H.	Air-50%R.H.	Air-50%R.H.	Air-50%R.H.	Air-50%R.H.	Air-50%R.H.	Dry air
Duration (h)	30	30	30	30	30	30	1
Coupon Dose rate (kGy.h <sup>-1</sup> )	1.2 ± 0.1	1.1 ± 0.1	1.1 ± 0.1	3.9 ± 0.4	3.9 ± 0.4	3.7 ± 0.4	3.5 ± 0.4
<b>Post-irradiation phase</b>							
Temperature (°C)	Step 1 80	Step 1 80	Step 1 80	Step 1 80	Step 1 80	Step 1 80	Step 1 80
R.H. of Air (%)	Air-20%R.H. Dry Air	Air-50%R.H. Dry Air	Air-50%R.H. Dry Air	Air-50%R.H. Dry Air	Air-50%R.H. Dry Air	Air-50%R.H. Dry Air	Air-50%R.H. Dry Air
Duration (h)	4 1	4 1	4 1	4 1	4 1	4 1	3.5* 1
<b>Specific objective</b>	R.H. effect	R.H. effect	Nature of the coupon surface effect	Dose rate effect	[I] effect (= [Cs])	Nature of the coupon surface effect	Temperature effect
<p>* The irradiation phase and the post-irradiation phase had to be shortened for this test because of a sensor defect during the preliminary heating phase which required the replacement of the sensor and led to a delayed start of the test.</p>							

Table I-6: Post-test measurements.

Nature of the coupon	AER-1	AER-2b	AER-3	AER-4	AER-5	AER-6	AER-11
	Quartz		Epoxy paint			Stainless steel	
Initial iodine concentration ( $=[CsI]$ ) on the coupon ( $\text{mol.m}^{-2}$ )	$(6.1 \pm 0.2) \times 10^{-3}$	$(3.9 \pm 0.2) \times 10^{-3}$	$(6.6 \pm 0.7) \times 10^{-3}$	$(5.3 \pm 0.3) \times 10^{-3}$	$(2.2 \pm 0.1) \times 10^{-4}$	$(7.4 \pm 0.2) \times 10^{-5}$	$(2.1 \pm 0.1) \times 10^{-4}$
Dose rate at the coupon level ( $\text{kGy.h}^{-1}$ )	$1.2 \pm 0.1$	$1.1 \pm 0.1$	$1.1 \pm 0.1$	$3.9 \pm 0.4$	$3.9 \pm 0.4$	$3.7 \pm 0.4$	$3.5 \pm 0.4$
Relative Humidity (%)	50						
Temperature (°C)	80						
Initial activity loaded on the coupon (Bq)	$(2.01 \pm 0.07) \times 10^5$	$(1.3 \pm 0.06) \times 10^5$	$(3.32 \pm 0.04) \times 10^5$	$(1.67 \pm 0.09) \times 10^5$	$(1.31 \pm 0.05) \times 10^5$	$(5.92 \pm 0.01) \times 10^4$	$(9.82 \pm 0.07) \times 10^4$
Final activity on the coupon after irradiation (%)	$47.2 \pm 1.1$	$1.03 \pm 0.03$	$85.3 \pm 1.4$	$22.5 \pm 1.0$	$75.1 \pm 1.3$	$0.53 \pm 0.04$	$0.43 \pm 0.01$
Activity on the quartz fiber filter (%): *Aerosols release (%)	$14.5 \pm 0.3$	$11.5 \pm 0.2$	$1.40 \pm 0.03$	$21.7 \pm 1.6$	$0.25 \pm 0.02$	$6.1 \pm 0.4$	$0.73 \pm 0.05$
Activity on the knit-mesh filters (%)	$19.3 \pm 1.7$	$41.5 \pm 4.0$	$5.3 \pm 0.4$	$26.9 \pm 2.4$	$2.4 \pm 0.1$	$42.8 \pm 2.8$	$23.0 \pm 1.7$
Corrected I <sub>2</sub> release (%)	$23.6 \pm 2.5$	$64.4 \pm 4.9$	$11.7 \pm 1.5$	$41.3 \pm 3.3$	$15.8 \pm 1.3$	$56.0 \pm 3.2$	$56.0 \pm 2.1$
Activity on the charcoal filters (%): RI release (%)	$1.6 \pm 0.2$	$2.8 \pm 0.2$	$0.41 \pm 0.05$	$6.0 \pm 0.2$	$2.2 \pm 0.2$	$13.7 \pm 0.3$	$10.2 \pm 0.9$
Activity in the rinsing solution of the irradiation vessel (%)	$9.6 \pm 0.5$	$18.3 \pm 0.3$	$0.91 \pm 0.01$	$4.57 \pm 0.01$	$1.74 \pm 0.01$	$13.4 \pm 0.1$	$2.4 \pm 0.3$
Activity in the rinsing solutions of the experimental loop and May-pack (%)	$3.4 \pm 0.5$	$2.0 \pm 0.1$	$0.23 \pm 0.01$	$3.98 \pm 0.02$	$4.8 \pm 0.1$	$10.4 \pm 0.1$	$30.3 \pm 0.4$
Iodine activity balance (%)	$95.7 \pm 1.9$	$77.1 \pm 2.9$	$93.6 \pm 1.4$	$85.6 \pm 2.2$	$86.6 \pm 1.3$	$86.8 \pm 1.5$	$67.0 \pm 1.3$
Missing activity balance (%)	$4.3 \pm 1.9$	$22.9 \pm 2.9$	$6.4 \pm 1.4$	$14.4 \pm 2.2$	$13.4 \pm 1.3$	$13.2 \pm 1.5$	$33.0 \pm 1.3$
Global release (%)	$52.8 \pm 1.1$	$98.9 \pm 0.03$	$14.6 \pm 1.4$	$77.6 \pm 1.0$	$24.9 \pm 1.3$	$99.47 \pm 0.04$	$99.57 \pm 0.01$

## **Chapter II: Methodology**



## II.1 Theoretical background

This chapter contains theoretical background that set up the framework in which our work in this thesis has been done and will be presented in the coming chapters. Our purpose from this part is to present the fundamental concepts necessary for a good understanding of theoretical Chemistry work.

### II.1.1 Hamiltonian of many body system

Einstein and Planck presented photons as quanta of energy (i.e. "light particles") in their work on the nature of light which leads to the well-known concept of wave-particle duality of light, where De Broglie wondered if this duality exist for all particles<sup>1</sup>. In this case, the electrons and nucleons obey the law of propagation of waves. Based on this assumption, Schrödinger built his equation<sup>2</sup> that governs the position and movement of these particles:

$$i\hbar \frac{\partial \Psi(\mathbf{r}, t)}{\partial t} = -\frac{\hbar^2}{2m} \Delta \Psi(\mathbf{r}, t) + V(\mathbf{r})\Psi(\mathbf{r}, t) \quad \text{II-1}$$

Where  $t$  is the time,  $\mathbf{r}$  is position of the particle considered in Cartesian coordinate basis,  $\Psi$  its wave function,  $m$  its mass,  $V$  the potential energy of the particle,  $\Delta$  the Laplace space operator,  $\hbar$  the reduced Planck constant, and  $i$  such that  $i^2 = -1$ . This linear partial differential equation is valid for nonrelativistic system. If the particle moves in a potential independent of time, its potential energy becomes independent of time. In this context, Schrödinger tried to find solutions of equation (

$$i\hbar \frac{\partial \Psi(\mathbf{r}, t)}{\partial t} = -\frac{\hbar^2}{2m} \Delta \Psi(\mathbf{r}, t) + V(\mathbf{r})\Psi(\mathbf{r}, t)$$

II-1II-1) in the form of standing waves, for which  $\Psi$  can be written into a separated product of spatial and time components:

$$\Psi(\mathbf{r}, t) = \psi(\mathbf{r})\varphi(t)$$

Substituting in equation (II-1) and dividing the whole equation by  $\psi(\mathbf{r})\varphi(t)$ , we get:

$$i\hbar \frac{\frac{\partial \varphi(t)}{\partial t}}{\varphi(t)} = -\frac{\hbar^2}{2m} \frac{\Delta \psi(\mathbf{r})}{\psi(\mathbf{r})} + V(\mathbf{r})$$

The two sides of the equation are related to independent variables, and such must be constant. This constant denoted by  $\epsilon$  and it's related to the energy of the considered particle. Then we obtain:

$$-\frac{\hbar^2}{2m} \frac{\Delta\psi(\mathbf{r})}{\psi(\mathbf{r})} + V(\mathbf{r}) = \epsilon$$

Which can be rewritten as:

$$-\frac{\hbar^2}{2m} \Delta\psi(\mathbf{r}) + V(\mathbf{r})\psi(\mathbf{r}) = \epsilon\psi(\mathbf{r}) \quad \text{II-2}$$

We call Hamiltonian  $\hat{H}$  the operator involving the Laplace operator and the potential:

$$\hat{H} = -\frac{\hbar^2}{2m} \Delta + V$$

Equation (II-2) is an eigenvalue equation, which can be solved if we specify the boundary conditions of the system. Solving such equation gives us the eigenvalues and the corresponding eigenvectors.

The energy of an object is an intuitive concept present in classical physics, but it is interesting to specify how to interpret  $\psi$  which is purely quantum object. One postulate of quantum mechanics says that  $\psi$  contains all available information about the state of the considered particle, but this cannot be considered as great help for better understanding of its nature. However, from homogeneity considerations, it is also postulated that square modulus of the wave function represents the probability density. The value taken from  $\psi$  therefore gives an idea about the probability of the particle that considered to be present in an area of space.  $|\psi|^2$  is the probability density, the value of its integration over all the space should be 1, in this case we say  $\psi$  is normalized.

Schrödinger equation (II-2) describes the behavior of any particle subject to an electric field. Then it is obvious and very interesting to obtain solution(s) to this equation. However, the expression of Hamiltonian as defined above depends on the considered system and the conditions in which the system operates.

In quantum chemistry, the interesting system will be generally a molecule or a solid, which means a set of  $N_e$  electrons labeled by  $i = 1, 2, \dots, N_e$  (negatively charged) and  $N_n$  atomic nuclei labeled by  $k = 1, 2, \dots, N_n$  (positively charged).

The Hamiltonian of such a global system is the sum of individual operators of each system of particles.

$$\hat{H} = \hat{T} + \hat{V}$$

The Laplace operator corresponding to the general case is here the kinetic energy operator  $\hat{T}$ , which decomposed into an operator applied to  $N_n$  cores (noted  $\hat{T}_n$ ) and other one applied to  $N_e$  electrons (noted  $\hat{T}_e$ ):

$$\begin{aligned}\hat{T} &= \hat{T}_e + \hat{T}_n \\ \hat{T}_e &= - \sum_{i=1}^{N_e} \frac{\hbar^2}{2m_e} \Delta_i \\ \hat{T}_n &= - \sum_{k=1}^{N_n} \frac{\hbar^2}{2M_k} \Delta_k\end{aligned}$$

The index  $i$  labels the electrons of the system and  $k$  for the nuclei,  $m_e$  and  $M_k$  being respectively the mass of an electron and the mass of the  $k$ -th core.

Similarly, in the simplest cases, the corresponding operator of potential energy  $\hat{V}$  consists of the sum of several electrostatic terms which are attractive or repulsive depending on the sign of charges on the involved particles.

$$\hat{V} = \hat{V}_{ee} + \hat{V}_{nn} + \hat{V}_{en}$$

Then  $V$  contains two repulsive terms:

$$\hat{V}_{nn} = \sum_{k=1}^{N_n} \sum_{l>k}^{N_n} \frac{e^2 Z_k Z_l}{R_{kl}} \quad \text{and} \quad \hat{V}_{ee} = \sum_{i=1}^{N_e} \sum_{j>i}^{N_e} \frac{e^2}{r_{ij}}$$

Operator  $\hat{V}_{nn}$  applied between core pairs and  $\hat{V}_{ee}$  between electron pairs where  $i$  is another indication pass through all the electrons and  $l$  another index through all the cores.

At these repulsive terms we add an attractive one noted  $\hat{V}_{en}$  that applies to electron-core interaction:

$$\widehat{V}_{en} = - \sum_{i=1}^{N_e} \sum_{k=1}^{N_n} \frac{e^2 Z_k}{r_{ik}}$$

Then the overall Hamiltonian of the system is the sum of all these terms:

$$\widehat{H} = - \sum_{i=1}^{N_e} \frac{\hbar^2}{2m_e} \Delta_i - \sum_{k=1}^{N_n} \frac{\hbar^2}{2M_k} \Delta_k + \sum_{k=1}^{N_n} \sum_{l>k}^{N_n} \frac{e^2 Z_k Z_l}{R_{kl}} + \sum_{i=1}^{N_e} \sum_{j>i}^{N_e} \frac{e^2}{r_{ij}} - \sum_{i=1}^{N_e} \sum_{k=1}^{N_n} \frac{e^2 Z_k}{r_{ik}}$$

## II.1.2 Born-Oppenheimer approximation

For a medium size molecule, the number of nuclei can be estimated to several tens and for electrons to several hundreds. Equation (II-2) applied on such systems is impossible to solve analytically and very complex to solve numerically. Approximations will then be done to solve it. The so-called Born-Oppenheimer<sup>3</sup> approximation states that nuclei move much slower than electrons because of the large difference in masses between each other, and offers to consider fixed nuclei for calculating the electronic energy.

In practice, this allows to simplify equation (II-2): the operator  $\widehat{T}_n$  becomes zero and the operator  $\widehat{V}_{nn}$  becomes a constant.

Equation (II-2) then takes the form:

$$- \sum_{i=1}^{N_e} \frac{\hbar^2}{2m_e} \Delta_i \psi + \sum_{i=1}^{N_e} \sum_{j>i}^{N_e} \frac{e^2}{r_{ij}} \psi - \sum_{i=1}^{N_e} \sum_{k=1}^{N_n} \frac{e^2 Z_k}{r_{ik}} \psi = E \psi$$

Or

$$\widehat{H}_e \psi = E \psi \quad \text{II-3}$$

The equation is simpler compared to equation (II-2), but it's still complicated for large systems due to the electron-electron interactions.

## II.2 Density Functional Theory

Density Functional Theory (DFT) is based on solving the Schrödinger equation from the knowledge of the total electron density of the system, denoted by  $\rho$ . This quantity represents the



quantity of electrons present per unit volume and it is easier to handle than wave function presentation. The first property of the electron density is that its integration over all space is equal to the total number of electrons of the system:

$$\int \rho(\mathbf{r})d\mathbf{r} = N_e$$

We first present the basic principles of the DFT and the theoretical foundations on which it rests, then we will show and explain different types of available functional.

## II.2.1 Hohenberg-Kohn theorems

Hohenberg and Kohn (H-K) theorems<sup>4</sup> were established to allow using electron density for solving Schrödinger equation. The first H-K theorem states that for a system for interacting particles in a given external potential, the electron density is uniquely determined, which means that the total energy and then any electronic property is a density functional. To prove this, they assumed that a given electron density  $\rho$  associates two external potentials  $V$  and  $V'$ .  $\hat{H}$  and  $\hat{H}'$  are the Hamiltonians corresponding to  $V$  and  $V'$  respectively, also  $\Psi$  and  $\Psi'$  are the normalized eigenvectors of the ground state of each Hamiltonian respectively.

According to that, we have:

$$E' < \langle \Psi | \hat{H}' | \Psi \rangle$$

Because  $\Psi$  is not eigenvector of  $\hat{H}'$ . We can mathematically decompose  $\hat{H}'$  in the following form:

$$\langle \Psi | \hat{H}' | \Psi \rangle = \langle \Psi | \hat{H} | \Psi \rangle + \langle \Psi | \hat{H}' - \hat{H} | \Psi \rangle = E + \int \rho(\mathbf{r})[V'(\mathbf{r}) - V(\mathbf{r})]d\mathbf{r}$$

Also we can do the same thing for  $E$  instead of  $E'$ :

$$E < \langle \Psi' | \hat{H} | \Psi' \rangle = \langle \Psi' | \hat{H}' | \Psi' \rangle + \langle \Psi' | \hat{H} - \hat{H}' | \Psi' \rangle = E' + \int \rho(\mathbf{r})[V(\mathbf{r}) - V'(\mathbf{r})]d\mathbf{r}$$

Adding the two previous inequalities, we get:

$$E' + E < E + E'$$

Which is impossible!

This means that our postulate was wrong, and that we have unique external potential associated with the ground state electron density.

A Second H-K theorem states the existence of a variational principle for calculating the ground state energy using electron density.

## II.2.2 Kohn-Sham approach

DFT attempts to calculate the energy of interacting particles as functional of the density, but is limited by the lack of accurate kinetic energy functional for example. Kohn and Sham proposed to replace the system of interacting particles (mainly electrons) by a *fictitious* non-interacting one in a way that its **density is the same as that of the interacting particles**. The problem now is to find the fictitious system of non-interacting particles which has the same density and the same energy as the interacting particles instead of finding the universal H-K functional. Following this approach, the expression of kinetic energy of non-interacting particles is known which allows us to build more accurate DFT calculations.

For  $N$  non-interacting electrons moving in an external potential  $V_s$  (its fictitious external potential in which non-interacting particles move called Kohn-Sham potential), the Hamiltonian is sum of all one-electron Hamiltonian:

$$\widehat{H}_s = -\frac{1}{2} \sum_{i=1}^N \nabla^2(\mathbf{i}) + \sum_{i=1}^N V_s(\mathbf{i})$$

The density is constructed as function of Kohn-Sham orbital  $\varphi_i(\mathbf{r})$ :

$$\rho(\mathbf{r}) = \sum_{i=1}^N |\varphi_i(\mathbf{r})|^2$$

Where  $i$  passes over the occupied orbitals.

We can write the Kohn-Sham total energy of the system as a functional of charge density:

$$E_{KS} = T_s[\rho] + E_{ext}[\rho] + E_H[\rho] + E_{XC}[\rho] \quad \text{II-4}$$

$T_s$  is the Kohn-Shan kinetic energy that can be expressed in terms of the Kohn-Sham orbitals:

$$T_s[\rho] = \sum_{i=1}^N \int d\mathbf{r} \varphi_i^*(\mathbf{r}) \left( -\frac{\hbar^2}{2m} \nabla^2 \right) \varphi_i(\mathbf{r})$$

The second term of the K-S energy arises from the fictitious potential  $V_s$ :

$$E_{ext}[\rho] = \int V_s(\mathbf{r}) \rho(\mathbf{r}) d\mathbf{r}$$

$E_H$  is the Hartree energy which represents the electrostatic repulsion energy between pair electrons:

$$E_H[\rho] = \frac{e^2}{2} \int d\mathbf{r} \int d\mathbf{r}' \frac{\rho(\mathbf{r})\rho(\mathbf{r}')}{|\mathbf{r} - \mathbf{r}'|}$$

$E_{XC}$  is the exchange correlation terms which is the only one unknown terms in the Kohn-Sham energy equation (II-4), it will be explicated in the coming paragraph.

To have accurate and efficient solution, Kohn-Sham equations must be solved numerically using an iterative process. The following diagram shows the different steps of the iteration process.

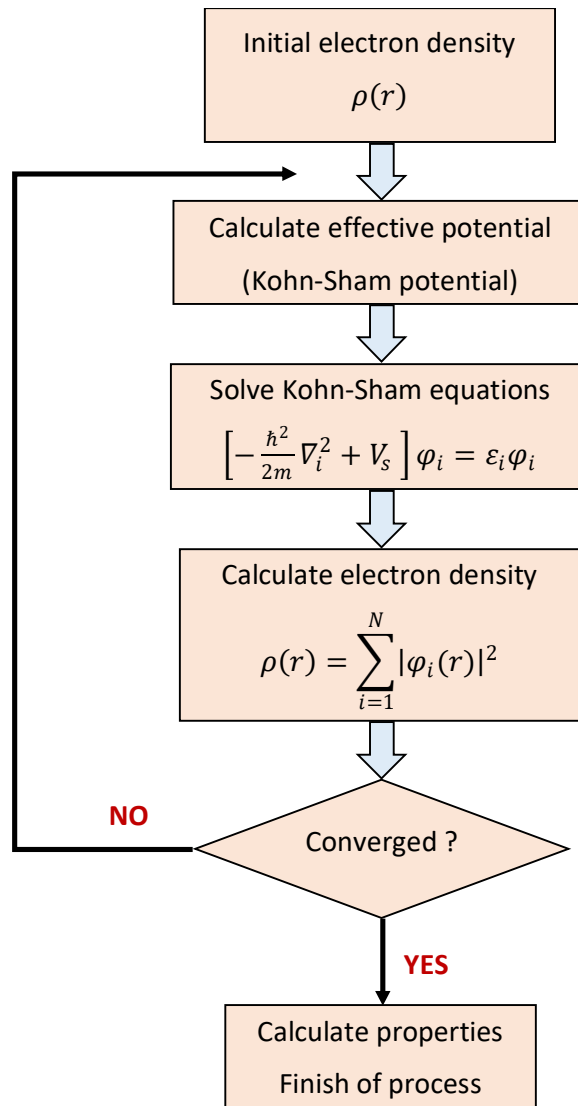


**Figure II-1. Iterative solution to Kohn-Sham equations**

### II.2.3 Approximations to exchange correlation potential

The problem is to build the exchange-correlation energy  $E_{xc}$ . In particular, the dependence of  $E_{xc}$  on  $\rho$  can be expressed as follows:

$$E_{xc}[\rho(\mathbf{r})] = \int \rho(\mathbf{r}) \varepsilon_{xc}[\rho(\mathbf{r})] d\mathbf{r}$$

Where  $\varepsilon_{xc}$  is the exchange-correlation energy density, it represents the energy per electron depending also on  $\rho$ .

In the following paragraphs, we will present different expressions of the energy density  $\varepsilon_{xc}$  using different methods developed in order to perform DFT calculations.

### II.2.3.1 Local Density Approximation (LDA)

The simplest approximation is considering  $\varepsilon_{xc}$  to depend locally on density, it means that the value of  $\varepsilon_{xc}$  depends only on the value of electron density at the coordinate where the functional is evaluated, this approach is known by Local Density Approximation (LDA) which has been introduced originally by Kohn and Sham<sup>5</sup>. It can be used in systems where the density doesn't vary much (slow variation) for homogenous electron gas, such that we can treat it like uniform electron gas (UEG).

In this context the LDA exchange correlation energy can be written in the following way:

$$E_{xc}^{LDA}[\rho(\mathbf{r})] = \int \rho(\mathbf{r}) \varepsilon_{xc}^{UEG}[\rho(\mathbf{r})] d\mathbf{r}$$

Now  $\varepsilon_{xc}^{UEG}$  is the exchange correlation energy density of a uniform electron gas of density  $\rho$ .

The problem is now simplified in knowing the exchange energy per particle for uniform electron gas of density  $\rho$ . It is useful to separate  $\varepsilon_{xc}^{UEG}$  into correlation  $\varepsilon_c^{UEG}$  and exchange  $\varepsilon_x^{UEG}$  potentials. The exchange energy is determined by Slater<sup>6</sup> and Dirac<sup>7</sup>:

$$\varepsilon_x^{UEG}[\rho(\mathbf{r})] = -\frac{3}{4} \left( \frac{3\rho(\mathbf{r})}{\pi} \right)^{1/3}$$

For the correlation part, an exact expression is not determined. Analytical expressions for  $\varepsilon_c^{UEG}$  obtained by quantum Monte-Carlo calculations<sup>8</sup>. The most famous approximation for  $\varepsilon_c^{UEG}$  is done by Wang and Perdew<sup>9</sup>.

Local spin density approximation (LSDA) is an extended version of LDA which takes into account the spin of electrons. Then the electron density is splitted into spin up and spin down density:

$$\rho(\mathbf{r}) = \rho(\mathbf{r}, \uparrow) + \rho(\mathbf{r}, \downarrow)$$

And the exchange-correlations energy in this context is:

$$E_{xc}^{LSDA}[\rho^\uparrow, \rho^\downarrow] = \int \rho(\mathbf{r}) \varepsilon_{xc}[\rho(\mathbf{r}, \uparrow), \rho(\mathbf{r}, \downarrow)] d\mathbf{r}$$

### II.2.3.2 Generalized Gradient Approximation (GGA)

LDA functional type does not lead to accurate results for the description of gaseous molecules and solids since considering the electron density as uniform electron gas for such systems is a rough approximation. To consider the inhomogeneity of the electronic density in the calculation of exchange and correlation energy, it is convenient to introduce the dependence of  $\varepsilon_{xc}$  on the gradient of the density.

Generalized gradient approximation is an improved version of LDA (second order correction) to have a better description of systems that can't be described as uniform electron gas like in solids and molecules.

In this context, the expression of  $\varepsilon_{xc}$  will depend also on the gradient of the density at the point of calculation, so we write the exchange correlation energy in the following way:

$$E_{xc}^{GGA}[\rho(\mathbf{r})] = \int d^3\mathbf{r} \rho(\mathbf{r}) \varepsilon_{xc}[\rho(\mathbf{r}), \nabla\rho(\mathbf{r})] d\mathbf{r}$$

The results given by the functional GGA are generally much better than those given by LSDA functional. However, to improve the accuracy, functionals including Laplace of the electronic density (third order correction) have been also developed which are called "meta-GGA."

## II.2.4 Van der Waals interactions

Density functional theory is a successful method for computing electronic structure in condensed matter and quantum chemistry<sup>10-12</sup>. Several works have been developed recently to improve and parametrize the functions used in order to take into account other physical aspects and to investigate more complex systems. This approximation cannot adequately describe long-range non-local interactions which are originated from the weak forces of Van der Waals (VdW). However, the absence of Van der Waals interactions may lead to badly describe systems including adsorption of molecules on surfaces.

Grimme <sup>13</sup> proposed a semi-empirical approach in adding a dispersion term to the total energy:

$$E_{disp} = -S_6 \sum_{i \neq j}^{N_{at}} \frac{C_6^{ij}}{R_{ij}^6} f_{dmp}(R_{ij}),$$

Where  $N_{at}$  refers to the number of atoms in the system,  $C_6^{ij}$  is the dispersion coefficient for pair of atoms  $i$  and  $j$ ,  $R_{ij}$  is the distance between atoms,  $f_{dmp}$  is a damping factor and  $S_6$  is an empirical scaling factor.

However, Tkatchenko and Scheffler <sup>14</sup> (DFT-TS) proposed a method for calculating the dispersion coefficients ( $C_6$ ) between interacting atoms. This approach allows to express these coefficients in terms of an effective volume of atoms in molecule or solid:

$$C_{6ii} = v_i^2 C_{6ii}^{free}$$

Where the dispersion coefficients  $C_{6ii}$  and  $C_{6ii}^{free}$  are related to the atom in its environment and isolated, respectively. TS is based on the atomic polarizability to calculate the  $C_6$  coefficients of the isolated atoms. ( $C_{6ii}$  coefficients are calculated starting by individual  $C_{6i}$  ones)

This method is improved recently by Bucko et al. <sup>15,16</sup> to describe better the energy of ionic solids, in which they proposed appropriate partitioning based on Hirshfeld algorithm. This method denoted (DFT-TS/Hi) will be used in this PhD.

## II.3 Bloch's theorem

The eigenstates of the Schrödinger equation for an independent particle, in a system where the electrons are moving in an effective potential  $V_{eff}(r)$  as in Kohn and Sham approach, satisfy the eigenvalue equations:

$$\hat{H}_{eff}(\mathbf{r})\psi_i(\mathbf{r}) = \left[ -\frac{\hbar^2}{2m_e} \nabla^2 + V_{eff}(\mathbf{r}) \right] \psi_i(\mathbf{r}) = \epsilon_i \psi_i(\mathbf{r}) \quad \text{II-5}$$

In the periodic systems like in crystals, the effective potential of the periodicity of the crystal can be expressed using Fourier series:

$$V_{eff}(\mathbf{r}) = \sum_m V_{eff}(\mathbf{G}_m) e^{i\mathbf{G}_m \cdot \mathbf{r}},$$

Where  $\mathbf{G}_m$  are the reciprocal lattice vectors, then:

$$V_{eff}(\mathbf{G}) = \frac{1}{\Omega} \int_{\Omega} V_{eff}(\mathbf{r}) e^{-i\mathbf{G} \cdot \mathbf{r}} d\mathbf{r}$$

Where  $\Omega$  is the volume of the primitive cell.

If we have translational symmetry in the system, the states are orthogonal and governed by the boundary conditions of the crystal (infinite volume). In this case, the K-S eigenfunctions are governed by Bloch theorem<sup>17</sup>: they have two quantum numbers; the wave Vector  $\mathbf{k}$  in the Brillouin zone (BZ) and the band index  $i$  (plus spin in case of magnetic material), and thus they can be expressed as product of a plane wave  $e^{i\mathbf{k} \cdot \mathbf{r}}$  and a periodic function:

$$\psi_i(\mathbf{r}) = e^{i\mathbf{k} \cdot \mathbf{r}} u_{i,\mathbf{k}}(\mathbf{r})$$

$u_{i,\mathbf{k}}(\mathbf{r})$  is the periodic function which has the periodicity of the lattice with  $u_{i,\mathbf{k}}(\mathbf{r}) = u_{i,\mathbf{k}}(\mathbf{r} + \vec{R})$  and  $\mathbf{R}$  represents the translational vector in the lattice.

The Bloch wave function is in general solution to the stationary Schrodinger equation including a periodic potential  $V(\mathbf{r} + \mathbf{L}) = V(\mathbf{r})$ , while  $\mathbf{L}$  is any translation vector of the lattice under consideration. Within Bloch theorem, the problem is simpler by calculating finite number of electronic wave functions instead of infinite ones.

## II.4 Pseudopotential

The useful chemical and physical properties of a crystal are determined generally by valence electrons which contribute to the chemical bonds, while other electrons, located in the core, are not involved in the chemical bonds. From this point, we do an approximation by taking only the valence electrons into account in the *ab initio* calculations to optimize the computation cost.



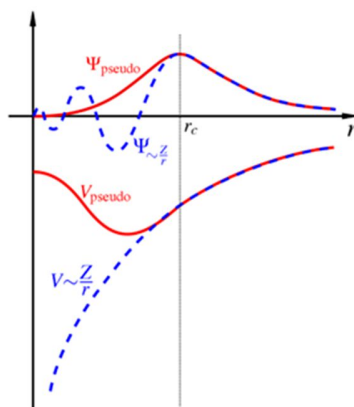


**Figure II-2. Comparison between original potentials (blue) and pseudopotentials (red).**

The core electrons are considered as in frozen states in their fundamental states during the calculation. Near the core, the coulomb potential  $V$  (in Figure II-2 the blue dashed line) is then replaced by a pseudopotential  $V_{\text{pseudo}}$  (red line) which is identical after a certain radius  $r_c$  (cutoff radius). The pseudopotential generates a pseudo wave function  $\Psi_{\text{pseudo}}$  which is also the same as the real one after  $r_c$ , which is smoother near the core and it requires less plane waves to describe it.

## II.5 Molecular dynamics

Molecular dynamics (MD) is used to model systems at the atomic level. It is an efficient method for modeling solvent effects and studying physical parameter, noticeably temperature. Newton's equation of motion is integrated to determine the atomic positions depending on the forces applied on each atom.

### II.5.1 Classical MD formalism

The time evolution of a system of  $N$  particles described by momentum ( $p_i$ ) and coordinates ( $q_i$ ) is given by the following equations<sup>18,19</sup>:

$$\begin{cases} \dot{p} = -\frac{\partial H}{\partial q} \\ \dot{q} = +\frac{\partial H}{\partial p} \end{cases} \quad \text{II-6}$$

Then we can write the Hamiltonian as the sum of kinetic and potential energies which depends on coordinates and momentum:

$$H = K(\mathbf{p}) + U(\mathbf{q}) \quad \text{II-7}$$

In which the kinetic term is expressed as follows:

$$K(\mathbf{p}) = \frac{\mathbf{p}^2}{2m} \quad \text{II-8}$$

Substituting equations II-7 and II-8 in II-6, we get

$$\begin{cases} \dot{\mathbf{p}} = -\frac{\partial U}{\partial \mathbf{q}}, \\ \dot{\mathbf{q}} = \frac{\mathbf{p}}{m} \end{cases} \quad \text{II-9}$$

Which gives

$$m\ddot{\mathbf{r}} = -\frac{\partial U}{\partial \mathbf{q}} \quad \text{II-10}$$

Which is Newton's second equation of motion with the force expressed as the negative gradient of the potential.

Molecular dynamics works by solving this Newton's equation numerically for all the atoms in the system. Then we can write the equation for atom  $i$  as:

$$\mathbf{a}_i = \ddot{\mathbf{r}}_i = \frac{\mathbf{F}_i}{m_i} \quad \text{II-11}$$

Verlet algorithm is used to integrate this equation numerically over a time step  $\Delta t$ . the atomic positions and velocities can be computed in the following way:

$$\mathbf{F}_i(\mathbf{t}) = -\nabla V(\mathbf{R}_i(\mathbf{t})) \quad \text{II-12}$$

$$\mathbf{R}_i(\mathbf{t} + \Delta \mathbf{t}) = \mathbf{R}_i(\mathbf{t}) + \mathbf{v}_i(\mathbf{t})\Delta \mathbf{t} + \frac{1}{2m_i} \mathbf{F}_i(\mathbf{t})\Delta \mathbf{t}^2 \quad \text{II-13}$$

$$\mathbf{F}_i(\mathbf{t} + \Delta \mathbf{t}) = -\nabla V(\mathbf{R}_i(\mathbf{t} + \Delta \mathbf{t})) \quad \text{II-14}$$

$$\mathbf{v}_i(\mathbf{t} + \Delta \mathbf{t}) = \mathbf{v}_i(\mathbf{t}) + \frac{1}{2m_i} [\mathbf{F}_i(\mathbf{t}) + \mathbf{F}_i(\mathbf{t} + \Delta \mathbf{t})]\Delta \mathbf{t} \quad \text{II-15}$$

Where  $V(\mathbf{r})$  is the potential containing all the interactions between atoms in the system. For this algorithm; the input is the initial positions of the atoms and the potentials to calculate forces between atoms.

## II.5.2 Born-Oppenheimer MD

Practically, several approaches are applied to combine electronic structure calculations with MD. The main are: Ehrenfest, Born-Oppenheimer and Car-Parrinello molecular dynamics.

For our concern, the Born-Oppenheimer (BO) approach will be used since it is implemented in our simulation tool, the VASP software. In BO approach, the nuclear positions evolve in the manner of classical molecular dynamics while the electronic structure is obtained by solving time independent Schrödinger equation. The time dependence of the electronic structure becomes a result of the nuclear motion which is not intrinsic as in the case of Ehrenfest. So, we define the following relations according to the Hellmann-Feynman theorem:

$$M_I \ddot{\mathbf{R}}_I = -\nabla_I \min_{\psi_0} \{\langle \psi_0 | H_e | \psi_0 \rangle\}$$

$$H_e \psi_0 = \epsilon_0 \psi_0$$

Where  $\psi_0$  is the fundamental state and  $H_e$  the electronic Hamiltonian.

## II.5.3 Thermostat

In many molecular dynamic calculations, it is essential to impose boundary conditions to compute thermodynamic parameters. Therefore, it is necessary to force the trajectory to be compatible with some chosen statistical ensembles. Each ensemble is defined by the conserved quantities such as: the number of atoms  $N$ , volume  $V$ , pressure  $P$  and temperature  $T$ . In molecular dynamic simulations, three main canonical ensembles are defined:

- Microcanonical ensemble: NVE in which the energy is fixed constant.
- Canonical ensemble: NVT in which the temperature is fixed constant.

- Isothermal–isobaric ensemble: NPT in which the pressure and temperature are fixed constant.

Sophisticated methods are used normally to impose the conditions of the ensembles, such as thermostat to fix the temperature, barostat to fix the pressure, etc... Only the thermostats have been used in our molecular dynamics.

The temperature is a parameter which used to measure the instantaneous kinetic energy of a molecular system. It can be written in the following formula:

$$T = \frac{\sum_{i=1}^N m_i v_i^2}{3NK_B}$$

While  $m_i$  and  $v_i$  are the mass and velocity of the particle  $i$ , respectively,  $K_B$  is the Boltzmann constant. The thermostat is a device used to maintain the temperature constant in a molecular system. In our molecular system, we have used Nose-Hoover thermostat which will be detailed hereafter.

The Nose-Hoover thermostat introduced by Nose (1984)<sup>20</sup> and improved by Hoover (1985)<sup>21</sup> is a deterministic thermostat which characterizes well the canonical ensembles.

In practice, equations of motion were modified by a new term:

$$\frac{d\vec{r}_i}{dt} = \frac{\vec{p}_i}{m_i}$$

$$\frac{d\vec{p}_i}{dt} = \vec{F}_i - \epsilon * \vec{p}_i$$

$$\dot{\epsilon} = \frac{1}{Q} \left[ \sum_{i=1}^N \frac{p_i^2}{m_i} - D_f k_B T_0 \right]$$

While  $\vec{p}_i$  is the momentum of the atom  $i$ ,  $m_i$  the mass of the atom  $i$ ,  $D_f$  in the number of degrees of freedom,  $T_0$  is the temperature of the thermostat and  $Q$  is an adjustable parameter called virtual mass. Note that the parameter  $\epsilon$  is identical for all the particles in the system. When the temperature of the system is higher than  $T_0$ ,  $\epsilon$  increases and subtracts a positive value. However,

when the instantaneous temperature of the system is lower than  $T_0$ ,  $\varepsilon$  decreases and becomes negative value, so that the energy will increase.

The parameter  $Q$  fixes the oscillation frequency of the temperature. If the  $Q$ -value is very high, the fluctuations of temperature are very large, on the other hand, if the  $Q$ -value is very low, the temperature converges correctly, but the sampling of the micro-states are insufficient and the canonical ensemble is not correct anymore.

## II.6 Nudged Elastic Band (NEB)

Studying the reactivity of the surface requires discovering the minima on the free energy surface and also the transition state (TS) of surface reactions. Nudged elastic band<sup>22,23</sup> is a method for determining the Minimum Energy Path (MEP) between two minima i.e. reactants and products. This method is very effective to find the transition state of a chemical reaction, or the diffusion of molecule or atom on a metallic surface.

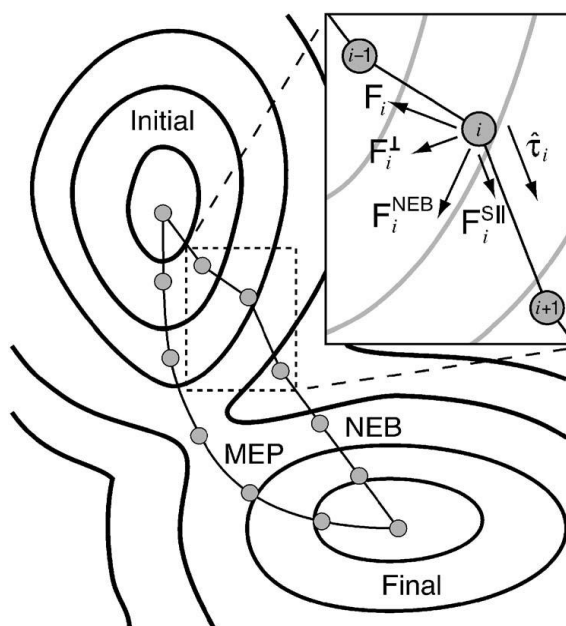


Figure II-3. Schematic diagram of the nudged elastic band theory [16].

The idea of NEB is to take number of images (around 10) between the initial and final states as displayed in Figure II-3. A spring interaction is added between neighboring images to prevent it from falling down toward initial and final states during the simultaneous geometry optimization of the images to define the MEP.

Consider an elastic band of N+1 images, labeled  $R_0, R_1, R_2, \dots, R_N$ , where the extreme points,  $R_0$  and  $R_N$  are fixed and correspond to initial and final states. The N-1 intermediate states are determined by linear interpolation between initial and final states.

To find MEP by the NEB method, the relaxation of the images is done by force projection; the potential forces applied perpendicular to the band while the spring elastic forces are applied along the band (tangent to the path  $\hat{\tau}_i$  on the Figure II-3).  $\hat{\tau}_i$  seems to be the tangent at image i given in ref.<sup>22</sup>:

$$\hat{\tau}_i = \frac{\mathbf{R}_i - \mathbf{R}_{i-1}}{|\mathbf{R}_i - \mathbf{R}_{i-1}|} + \frac{\mathbf{R}_{i+1} - \mathbf{R}_i}{|\mathbf{R}_{i+1} - \mathbf{R}_i|}$$

According to ref.<sup>23</sup>, the NEB force acting on some image i is the addition of the parallel and perpendicular forces:

$$\mathbf{F}_i^{NEB} = \mathbf{F}_i^\perp + \mathbf{F}_i^{S\parallel},$$

where  $F_i^\perp$  acts perpendicular to the band due to the potential:

$$\mathbf{F}_i^\perp = -\nabla(R_i) + \nabla(R_i) \cdot \hat{\tau}_i \hat{\tau}_i,$$

and  $F_i^{S\parallel}$  due to spring forces:

$$\mathbf{F}_i^{S\parallel} = k[(\mathbf{R}_{i+1} - \mathbf{R}_i) - (\mathbf{R}_i - \mathbf{R}_{i-1})] \cdot \hat{\tau}_i \hat{\tau}_i.$$

k is the spring constant and  $R_i$  refers to the position of image i.

The NEB method developed firstly according to the above equation for  $F_i^{NEB}$  and  $\hat{\tau}_i$ , can form kinks along the path for a 2-D LEPS potential<sup>22</sup>.

## II.7 Application in VASP

Vienna Ab-initio simulation package (VASP.5.4) is a quantum chemistry periodic code which uses DFT and plane waves bases to define the solid state properties. VASP uses pseudo-potential and Projector Augmented Wave (PAW)<sup>24</sup> to describe electrons. Different iterative algorithms are implemented in VASP to optimize the wave functions such as conjugate gradient<sup>25</sup>, Davidson diagonalization<sup>26</sup> method and the RMM-DIIS method<sup>27</sup>. After each electronic cycle, we check if the convergence of energy is attained. The algorithm is self-consistent which is shown briefly in the diagram of Figure II-4. The choice of the number of points in reciprocal space plays important role in the resolution of the sampling. The number of points used impact the resolution, and it is necessary to get sufficient points to better describe the energy bands as well as compute the total energy. However, the convergence will slow down by increasing the number of matrix elements. On the other hand, if the sampling point is too low, the band structure will not be described correctly leading to a bad estimation of the total energy. We must test the correct number of points, usually we start from 1 (mesh  $1 \times 1 \times 1$ ) up to 1000 points (mesh  $10 \times 10 \times 10$ ) and sometimes more if we found the energy still changing after increasing the size.

Other important parameter is the cutoff energy, which is used to fix the number of plane waves around our basis set. Normally default value is specified in the VASP (in POTCAR file). Some tests calculations on the bulk are recommended and performed to check if the default value is true.

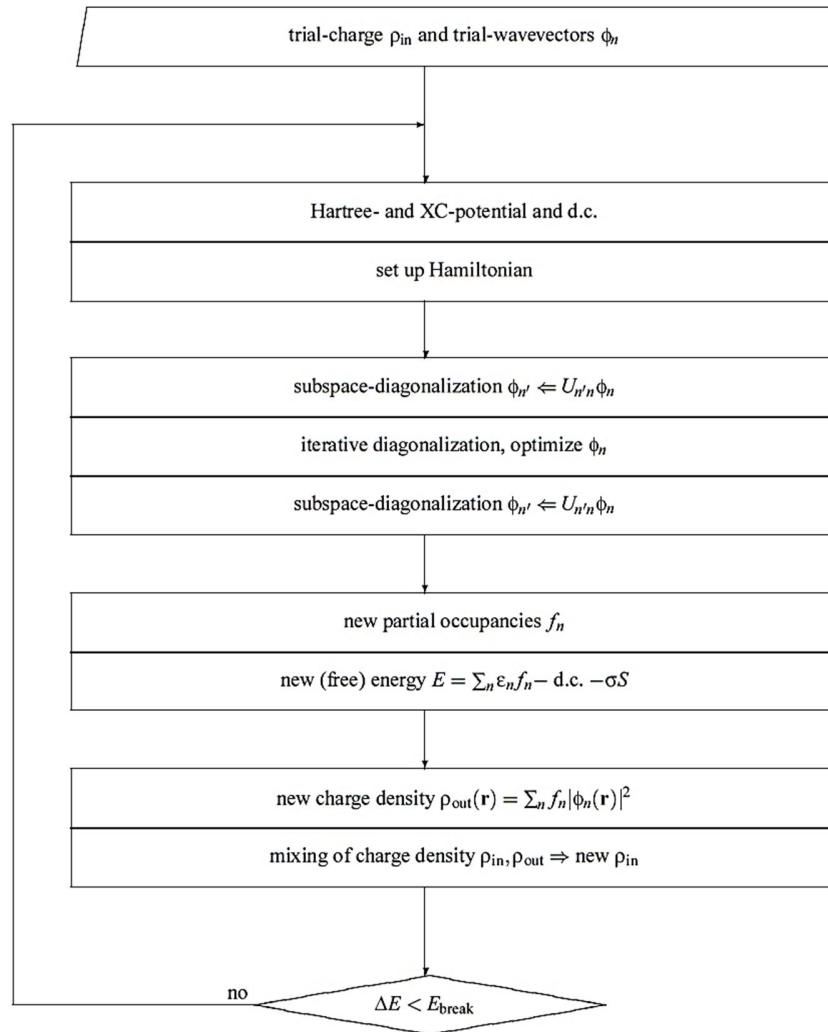


**Figure II-4. Brief preview of the VASP algorithm. [21]**

Four input files were required to perform calculation in VASP which are INCAR, POSCAR, KPOINTS and POTCAR.

- INCAR: it contains input parameters to make calculations and methods (type of pseudopotentials, number of steps, type of the algorithm, speed of calculation, spin-polarization specification, converging criteria and others). Also, it contains calculation parameters concerning the system like cutoff energy.
- POSCAR: it contains the size of the cell and position of atoms. In this file we specify which atoms have to be relaxed, the others being fixed.



- KPOINTS: number of k points used.
- POTCAR: this file contains pseudopotentials of atoms listed in same way as in POSCAR file.

The main output files:

- OUTCAR: it prints all the information during the computation.
- CONTCAR: this file contains the last geometry of the system after optimization.
- OSZICAR: in this file, we find all data about energies from the beginning to the end of the simulation.

Other output file may exist depending on the type of calculation we are performing like DOSCAR, PROCAR and others.

## II.8 Cutoff Energy

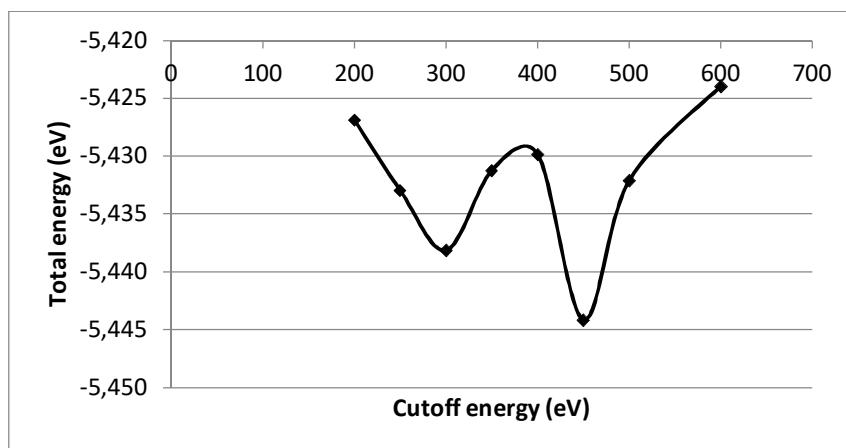


**Figure II-5. Total energy as function of cutoff energy (eV).**

The wave function is developed as a set of plane waves. Calculations were done by varying energy cutoff from 200 to 600 eV to find the energy convergence (Figure II-5). From this evaluation, all the bulk and surface calculations were performed with cutoff energy 450 eV for the plane waves describing the valence electrons. The total energy converges more rapidly for iodine and cesium atoms or ions but this value is needed to correctly describe oxygen atoms.

## II.9 Conclusion

In our work, density functional theory (DFT) were implemented to perform our calculations. This method is well known in computational chemistry science which can be considered as accurate method in describing systems at the atomic level. The calculations were carried out with VASP (Vienna Ab initio Simulation Package). The wave function is developed as a set of plane waves and the electron-ion interactions are described using the method PAW. Atomic positions were optimized using GGA where atomic forces and total energy are minimized. Self-consistent solving of the Kohn–Sham equations until the energy difference between two successive ionic steps is lower than  $10^{-5}$  eV and the atomic positions were optimized with a convergence criterion for the forces less than 0.03 eV/Å. Bulk and surface calculations were performed with cutoff energy 450 eV for the plane waves basis set describing the valence electrons. The k-points mesh were chosen according to the system size, varying from  $3 \times 3 \times 3$  for bulk and  $3 \times 3 \times 1$  for surface calculations.

## II.10 References

- (1) De Broglie, L. Recherches Sur La Théorie Des Quanta, Migration-université en cours d'affectation, 1924.
- (2) E. Schrödinger. Schrodinger.pdf. *Physical Review*. 1926, p 1049.
- (3) M. Born, R. Oppenheimer. Annalen Der Physik. 1927, p 457.
- (4) P. Hohenberg, W. Kohn,. Hohenberg-Kohn.pdf. *Physical Review*. 1964, p B 864.
- (5) W. Kohn and L. J. Sham. Self-Consistent Equations Including Exchange and Correlation Effects. *Physical Review*. 1965, p A1133.
- (6) Slater, J. C. A Simplification of the Hartree-Fock Method. *Phys. Rev.* **1951**, 81 (3), 385.
- (7) P. A. M. Dirac. *Mathematical Proceedings of the Cambridge Philosophical Society*. 1930, pp 367–385.
- (8) Ceperley, D. M.; Alder, B. J. Ground State of the Electron Gas by a Stochastic Method. *Phys. Rev. Lett.* **1980**, 45 (7), 566.
- (9) J. P. Perdew and Y. Wang. Accurate and Simple Analytic Representation of the Electron-Gas Correlation Energy. *Physical Review B*. 1992, pp 13244–13249.
- (10) Hafner, J. *Ab-Initio Simulations of Materials Using VASP: Density-Functional Theory and beyond*. *J. Comput. Chem.* **2008**, 29 (13), 2044–2078.

- (11) Segall, M. D.; Lindan, P. J. D.; Probert, M. J.; Pickard, C. J.; Hasnip, P. J.; Clark, S. J.; Payne, M. C. First-Principles Simulation: Ideas, Illustrations and the CASTEP Code. *J. Phys. Condens. Matter* **2002**, *14* (11), 2717.
- (12) Soler, J. M.; Artacho, E.; Gale, J. D.; García, A.; Junquera, J.; Ordejón, P.; Daniel Sánchez-Portal. The SIESTA Method for Ab Initio Order- N Materials Simulation. *J. Phys. Condens. Matter* **2002**, *14* (11), 2745.
- (13) Grimme, S. Semiempirical GGA-Type Density Functional Constructed with a Long-Range Dispersion Correction. *J. Comput. Chem.* **2006**, *27* (15), 1787–1799.
- (14) Tkatchenko, A.; Scheffler, M. Accurate Molecular Van Der Waals Interactions from Ground-State Electron Density and Free-Atom Reference Data. *Phys. Rev. Lett.* **2009**, *102* (7), 073005.
- (15) Bučko, T.; Lebègue, S.; Hafner, J.; Ángyán, J. G. Improved Density Dependent Correction for the Description of London Dispersion Forces. *J. Chem. Theory Comput.* **2013**, *9* (10), 4293–4299.
- (16) Bučko, T.; Lebègue, S.; Ángyán, J. G.; Hafner, J. Extending the Applicability of the Tkatchenko-Scheffler Dispersion Correction via Iterative Hirshfeld Partitioning. *J. Chem. Phys.* **2014**, *141* (3), 034114.
- (17) Charles Kittel. *Introduction to Solid State Physics*; 1996.
- (18) Hamilton, W. R. Second Essay on a General Method in Dynamics. *Philos. Trans. R. Soc. Lond.* **1835**, *125*, 95–144.
- (19) Hamilton, W. R. On a General Method in Dynamics; by Which the Study of the Motions of All Free Systems of Attracting or Repelling Points Is Reduced to the Search and Differentiation of One Central Relation, or Characteristic Function. *Philos. Trans. R. Soc. Lond.* **1834**, *124*, 247–308.
- (20) A Unified Formulation of the Constant Temperature Molecular Dynamics Methods. *J. Chem. Phys.* **1984**, *81* (1), 511–519.
- (21) Hoover, W. G. Canonical Dynamics: Equilibrium Phase-Space Distributions. *Phys. Rev. A* **1985**, *31* (3), 1695–1697.
- (22) Henkelman, G.; Jónsson, H. Improved Tangent Estimate in the Nudged Elastic Band Method for Finding Minimum Energy Paths and Saddle Points. *J. Chem. Phys.* **2000**, *113* (22), 9978–9985.
- (23) Sheppard, D.; Terrell, R.; Henkelman, G. Optimization Methods for Finding Minimum Energy Paths. *J. Chem. Phys.* **2008**, *128* (13), 134106.
- (24) Kresse, G.; Joubert, D. From Ultrasoft Pseudopotentials to the Projector Augmented-Wave Method. *Phys. Rev. B* **1999**, *59* (3), 1758.
- (25) Teter, M. P.; Payne, M. C.; Allan, D. C. Solution of Schrödinger's Equation for Large Systems. *Phys. Rev. B* **1989**, *40* (18), 12255–12263.

(26) *Methods in Computational Molecular Physics: [Proceedings of a NATO Advanced Study Institute on Methods in Computational Molecular Physics, Held July 22 - August 2, 1991, in Bad Windsheim, Germany]*; Wilson, S., Diercksen, G. H. F., Advanced Study Institute on Methods in Computational Molecular Physics, Eds.; NATO ASI series Series B, Physics; Springer Science+Business Media: New York, NY, 1992.

(27) Wood, D. M.; Zunger, A. A New Method for Diagonalising Large Matrices. *J. Phys. Math. Gen.* **1985**, *18* (9), 1343.

## **Chapter III: Reactivity of CsI aerosols**



## III.1 Introduction

As experimentally observed and theoretically established, iodine can be transported in a large amount as CsI aerosols inside the RCS in severe accident conditions<sup>1</sup>. These aerosols can react with oxidants in gas phase, like OH produced by steam radiolysis, O<sub>2</sub>, O<sub>3</sub>, leading first to the formation of molecular iodine and next iodine oxides<sup>2,3</sup>. However, these aerosols may also be deposited onto inner walls (like painted surfaces, stainless steel and others) after reaching the nuclear containment leading to possible oxidation to formed volatile iodine. The chemical reactivity under radiolysis of CsI deposited aerosols were investigated in the frame of STEM/EPICUR<sup>4</sup>; results are discussed in the first chapter. However, the chemical ageing of CsI aerosols in the gas phase is still poorly understood. Therefore, the purpose of this work is to study/understand the chemical pathways of these metallic iodide aerosols under irradiation.

In this chapter, theoretical study is performed in order to understand the chemical process leading to the formation of molecular iodine (I<sub>2</sub>) coming from CsI aerosol oxidation. The first part is a submitted paper under title: “CsI surfaces reactivity: A DFT study”, in which four main issues were addressed: 1- general properties of CsI aerosols, 2- most stable surfaces of CsI crystal, 3- interaction of CsI with water in gas phase, and 4-formation of iodine species after interaction between CsI and radiolysis products.

However, in reality all surfaces contain some defects. This point is taken into account in the second part of this chapter in order to compare the reactivity on defect surfaces with flat surfaces (ideal surfaces).

## III.2 CsI surfaces reactivity: A DFT study

### (submitted article)

In the present study, we investigate CsI surface stability by periodic DFT (PBE) calculations including van der Waals corrections (TS-HI). Based on these calculations, the (011) surface is the more stable and the only one exposed on small aerosols in the gas phase. Even if CsI is considered as a hygroscopic compound, its interaction with water is weak (between 0.51 eV and 0.72 eV per molecule depending on the coverage) and no water will be adsorbed at room temperature (RT) if the humidity is low. The I<sub>2</sub> gaseous release from the surface is only possible if a strong oxidizing molecule is involved in the reaction. For example, the reaction with OH° that may be produced by water radiolysis is exothermic. The I<sub>2</sub> formation activation energy is 1.2 eV. The oxidation rate will be controlled either by OH° formation or by OH° diffusion into the interface boundary layers.

**Keywords:** CsI, DFT surfaces, reactivity, water adsorption.

### III.2.1 Introduction

Iodine and Cesium arising from fission reactions are released in significant amounts into the nuclear containment building in the case of severe accident. These compounds are of particular interest since they contribute to radiological consequences at short and middle terms (few weeks after the accident for iodine and few years for cesium). Both have serious impact on health and ecosystems. Cesium Iodide (CsI) is the most likely iodine aerosol species that may be formed. It was considered that iodine entering the containment was at least 95% CsI, as documented in NUREG/CR-5732<sup>5</sup>. These particles may lead to the formation of gaseous iodine (I<sub>2</sub>) after chemical reactions on their surfaces or after dissolving in aqueous phase and such may be an important source of radioactive contamination<sup>6-10</sup>. Both theoretical and experimental work<sup>11-13</sup> has been carried out to identify and understand chemical processes involving iodine reactivity in the frame of nuclear accidents. Detailed knowledge of CsI reactivity is essential to develop predicting models of iodine release into the environment and to have a clear understanding of its behavior in presence of oxidative steam atmosphere.



Release of iodine after a severe accident from nuclear fuel was mainly studied experimentally in the 80's and 90's<sup>14</sup>. The total amount of iodine released in the nuclear containment building can reach up to 70% of the reactor iodine core inventory depending on the type of nuclear accident<sup>15</sup>. Formation of bulk CsI is favored in the reactor coolant system at high temperature (~1300 K) due to the high thermochemical stability of this compound<sup>9</sup> and the large amount of cesium released when compared to iodine (amount of iodine formed in the fuel during normal operations of power plant is 10 times less than the amount of cesium)<sup>15</sup>.

Recently, Sudolská et al.<sup>16</sup> performed theoretical studies on the structure and the thermodynamic properties (standard enthalpies of formation and Gibbs free energies) of gaseous cesium species of nuclear safety interest (Cs, CsOH, CsI and its dimer Cs<sub>2</sub>I<sub>2</sub>) in order to refine thermodynamic data that are implemented in simulation tools<sup>17</sup> used to predict radiological consequences in case of a severe accident occurring in a pressurized water reactor (PWR). They have shown that CsOH is the most stable cesium compound followed by CsI and that CsI and CsOH can co-exist in steam atmosphere in the Reactor Cooling System (RCS). Earlier Badawi et al.<sup>9</sup> also computed a thermodynamic data study on 12 gaseous cesium-containing species: Cs<sub>2</sub>, CsH, CsO, Cs<sub>2</sub>O, CsX, and Cs<sub>2</sub>X<sub>2</sub> (X = OH, Cl, Br, and I) while Šulková et al.<sup>18</sup> computed gas phase rate constants for a network of iodine and cesium reactions. Both studies demonstrated that CsI(g) is stable in presence of water. Iodide in aqueous solution is rapidly oxidized by OH<sup>•</sup> (formed by radiolysis) to lead to iodine radical. Recent experimental works<sup>1,19,20</sup> show that CsI particles oxidized by  $\gamma$ -irradiation formed gaseous molecular iodine. As already mentioned CsI particles are a possible source of volatile iodine but the nature of the reaction occurring on their surfaces is still poorly understood. The knowledge of the chemical processes of I<sub>2</sub> formation is fundamental to be able to evaluate with confidence the kinetic of iodine released in severe accident conditions. Some data may be extrapolated from systems with similar chemical properties such as NaCl aerosols that have been studied to evaluate the chlorine production near the seas<sup>21</sup>. On NaCl surfaces, two types of reactions may happen: i) the reaction of the chloride with a strong acid produces HCl that may be released in the gas phase. ii) The reaction of chloride with strong oxidizing agent such as nitric acid will produce Cl<sub>2</sub>(g) via indirect processes involving chlorine oxides. The interaction of water with the perfect NaCl surfaces have been studied<sup>22</sup>. These Density Functional Theory (DFT) calculations concluded that the adsorption is molecular and that the water molecules form a hydrogen bond network above the solid surface. In this project, theoretical

calculations have been carried out to investigate the mechanism of iodine formation from CsI surfaces. In the first part, we studied the stability of the surface in dry atmosphere and determined the shape of the aerosol nanoparticles. In a second part, we first studied the role of water and next, mechanisms that may be responsible for the release of iodine in gaseous phase, taking into account the possible role of oxidizing agent formed under radiation.

## **III.2.2 Theoretical methods**

### **III.2.2.1 Computational parameters**

All DFT calculations were carried out with VASP (Vienna Ab initio Simulation Package)<sup>23,24</sup>. The wave function is developed on a set of plane waves and the electron-ion interactions were described using the PAW method (Projector Augmented Wave)<sup>25</sup>. The energy is calculated using generalized gradient approximation as parameterized by Perdew et al.,<sup>26</sup> and PBE functional was employed with a 0.1 eV gaussian<sup>27</sup> smearing. PBE have been shown to give good results on ionic systems if the Van der Walls corrections are taken into account<sup>28</sup>. In this study, as the iodine oxidation state will change during reactions, the Van der Walls corrections are calculated according to the iterative Tkatchenko Scheffler model<sup>29</sup> which is also well adapted to ionic systems<sup>30,31</sup>. The self-consistent solving of the Kohn–Sham equations is performed until the energy difference between two successive electronic steps is lower than  $10^{-5}$  eV. The atomic positions were optimized until the forces being less than 0.03 eV/Å. The electron configurations [Xe] 6s<sup>1</sup>, [Kr] 4d<sup>10</sup> 5s<sup>2</sup> 5p<sup>5</sup>, [He] 2s<sup>2</sup> 2p<sup>4</sup> and 1s<sup>1</sup> were used for cesium, iodine, oxygen and hydrogen respectively. Test Calculations were done by varying cut-off energy from 200 to 600 eV and the k-points mesh from  $1 \times 1 \times 1$  to  $11 \times 11 \times 11$  following Monkhorst-Pack<sup>32</sup> schemes to define calculation parameters (cf SI). From these evaluations, all the bulk and surface calculations were performed with a 450 eV cut-off energy, a  $3 \times 3 \times 3$  kpoint mesh for bulk calculations, and  $3 \times 3 \times 1$  one for all surface calculations.

CsI crystal has a simple cubic structure which belongs to the Pm3m group, with two atoms in the unit cell, Cesium at (0, 0, 0) and iodine at (a/2) (1, 1, 1) while ‘a’ being the lattice constant (456.67 pm)<sup>33</sup> kept fixed in the calculation at the experimental value. This constraint has only a very small effect on the reaction energy (cf SI)

A supercell composed of eight CsI layers was used for all surfaces (Figure III-1). The four outermost layers were allowed to relax to take into account the surface formation, while the rest layers were kept fixed to mimic bulk constraints. We added 15 Å of vacuum between two consecutive slabs to avoid interactions between them. The following non-equivalent low index surfaces: (001), (011), (111), (210) and (211) were optimized.

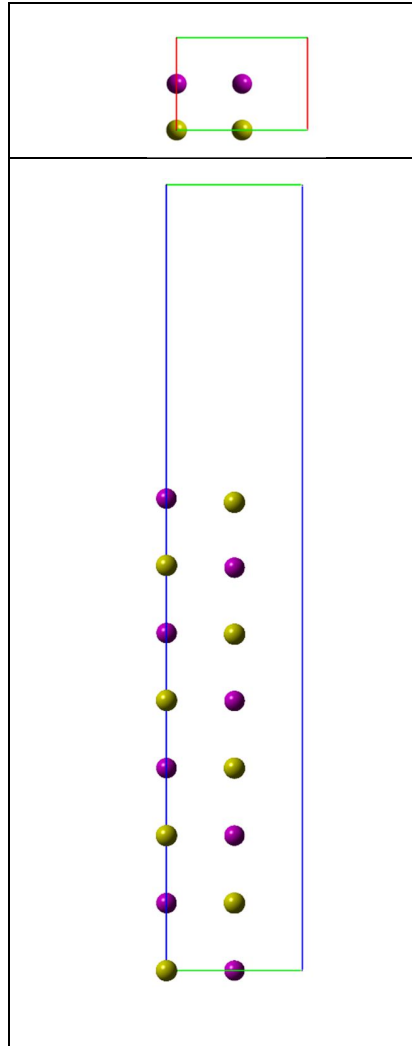


**Figure III-1: Top and side view of the used unit cell for the 011 surface..**

Surface energies for symmetric surfaces were calculated as

$$\gamma = (E_{slab} - nE_{bulk})/2A \quad \text{III-1}$$

where  $E_{slab}$  is the slab energy,  $nE_{bulk}$  denotes the energy of  $n$  unit cells of CsI ( $n$  represents the number of unit cells in the given slab), and  $A$  is the area of the considered surface unit cell. The

relaxation energy was added to the average surface energy to include surface relaxation in the calculations. In order to describe low adsorption coverage to investigate the reactivity of the stable surfaces, larger cells (1x2 or 2x2) were used. Tests calculations on (3x3) and (4x4) surface cells were performed to confirm that reaction energies do not depend on the surface cell size (cf SI).

The adsorption energy is defined by the following formula (III-2):

$$E_{\text{ads}} = E_{\text{CsI}} + n \cdot E_{(\text{H}_2\text{O})_{\text{gas}}} - E_{(\text{CsI} + n\text{H}_2\text{O})} \quad \text{III-2}$$

Where  $E_{\text{CsI}}$ ,  $E_{(\text{H}_2\text{O})_{\text{gas}}}$ ,  $E_{(\text{CsI} + n\text{H}_2\text{O})}$  are, respectively, the energies of the relaxed CsI substrate, the energy of one water molecule in gas phase and the energy of the total system, 'n' being the number of water molecules in adsorbed on the surface, per cell. Using this definition, a positive adsorption energy is related to an exothermic adsorption.

### III.2.2.2 Thermodynamics model

Atomistic thermodynamic models were used to describe water adsorption on the CsI surfaces at defined pressure and temperature. Gas phase presents the reservoir in equilibrium with the surface and the adsorbed molecules. Then we define Gibbs free energy of the adsorption reaction (reaction (R1)) ( $\Delta_r G$ ) as a function of temperature, pressure and the gas phase chemical potential using the following expression (III-3):



$$\Delta_r G = [\Delta E_0 + \Delta E_{\text{zpe}} - n \sum \Delta \mu(\text{T}, \text{p})] \quad \text{III-3}$$

Where  $\Delta E_0$  is the adsorption energy obtained from DFT energies,  $\sum \Delta \mu(\text{T}, \text{p})$  is the chemical potential difference between the gas phase and adsorbed molecules, while  $\Delta E_{\text{zpe}}$  is the zero point energy difference. Temperature and pressure dependent chemical potential of the water molecule can be expressed as following (III-4):

$$\Delta \mu(\text{T}, \text{p}) = \Delta \mu^0(\text{T}) + RT \ln [\text{P}/\text{P}^0] \quad \text{III-4}$$

Where  $\Delta \mu^0(\text{T}) = \Delta [E_{\text{vib}} + E_{\text{rot}} + E_{\text{trans}}] + RT - T \cdot (S_{\text{vib}} + S_{\text{rot}} + S_{\text{trans}})$ . This expression includes thermal contributions of the change in vibrational, rotational and translational degrees of freedom<sup>34,35</sup> and is evaluated using perfect gas partition functions.

### III.2.2.3 Transition state calculations

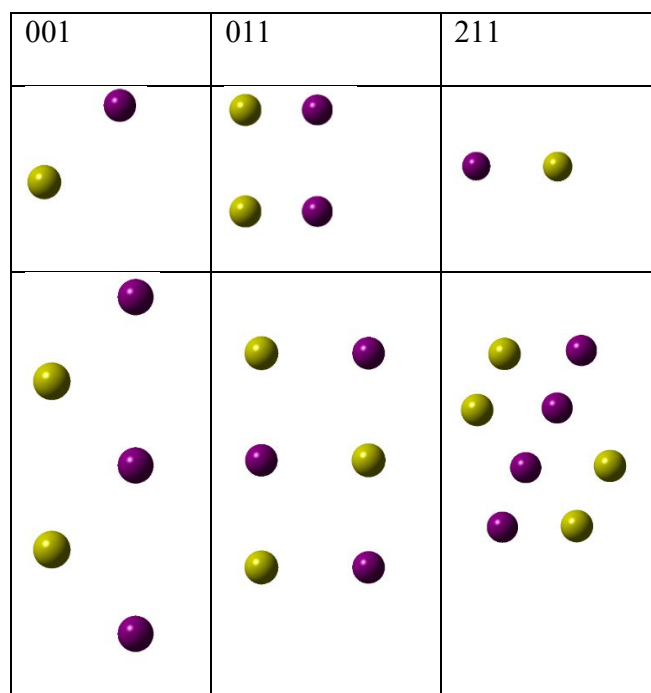
Using Climbing Image Nudged Elastic Band (CI-NEB)<sup>36,37</sup>, we determine the minimum energy path (MEP) between two minima i.e. reactants and products. In our case, 8 images, located between the reactants and the products of elementary reactions defined the reaction path. The highest point on the reaction path is optimized to be saddle point. After optimization the saddle point is characterized by vibrational frequency analysis to know if it is a transition state (TS).

### III.2.3 Results and discussion

In order to study the surface reactivity of CsI particles, we will determine in a first step the most stable surface that will be exposed on gas phase and define its shape. The water adsorption will be considered in a second part while the reactivity will be discussed in the third one.

#### III.2.3.1 Exposed Surface

Low index surfaces are shown in Figure III-2. Before relaxation, surfaces (111) and (001) are polar i.e. they end up with only one type of atoms, either Cs or I, while others ((011), (210) and (211)) are non-polar. In order to cancel this surface polarity, we considered the classical 2x1 reconstruction, by displacing half layer from the bottom to the top of the slab.



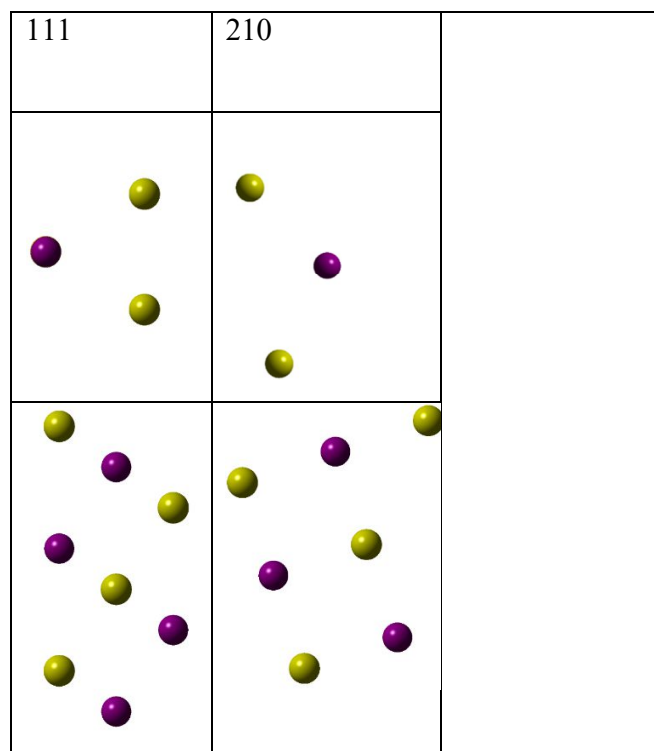


**Figure III-2. Top and side view of different CsI surfaces. (I: purple spheres, Cs : yellow spheres)**

Both the surface energies of the relaxed and rigid planes increase in the following order:  $(011) \ll (210) < (211) < (111) < (001)$  (see Table III-1). The  $(011)$  surface optimization does not lead to significant relaxation. A similar result is obtained for the other surfaces, even if they are stepped. According to the Wulff model<sup>38</sup>, it is possible to define the shape of the particle based on the relaxed surface energies. Since there is a large difference between the surface energy of  $(011)$  plane and the others (surface energy is doubled), the  $(011)$  planes will be the only one exposed on CsI particle. The particle will be rhombic dodecahedron as represented in Figure III-3. The  $(011)$  surfaces are composed of alternated line of I and Cs ions that may favor  $I_2$  formation since there are no caesium between two neighboring iodine.

**Table III-1: Surface energy of the exposed planes.**

Exposed plane	(011)	(111)	(210)	(211)	(001)
$\gamma$ (mJ/m <sup>2</sup> ) rigid surface	200	540	435	520	650
$\gamma$ (mJ/m <sup>2</sup> ) relaxed surface	193	520	365	417	615
Relative relaxation Energy (%)	4	4	16	20	5

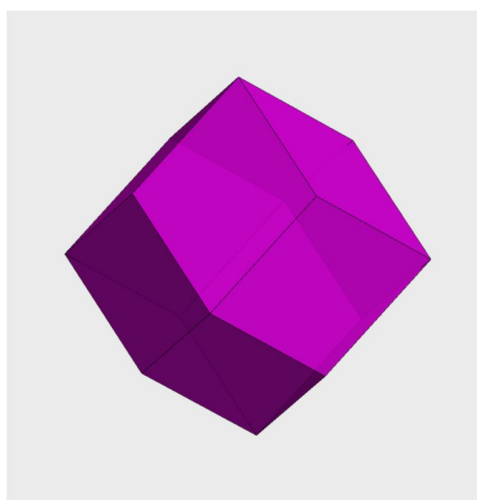


**Figure III-3. Calculated Wulff shape of the CsI particle <sup>39</sup>.**

### **III.2.3.2 Water adsorption**

#### **III.2.3.2.1 First water molecule adsorption**

Water adsorption process was studied by adding successive water molecules on the surface until one monolayer was reached. Dissociative and molecular adsorptions of water molecule were studied to define the most probable adsorption mode. Figure III-4 shows both mentioned cases: the molecular ones 'A<sub>1,2</sub>' in which a water molecule adsorbs on the surface, while in 'B' we dissociated the water molecule into one OH group on the top of Cs and H atom interacting with I.

In the molecular case, we tested two possible orientations for the water molecule on the surface. First the main interaction is the electrostatic one between oxygen atom and the Cs cation. The water molecule lays flat, 3 Å above and is almost parallel to the surface (A<sub>1</sub>). In second, hydrogen bond is formed between the hydrogen atom and the iodide. The water molecule is perpendicular to the surface (A<sub>2</sub>) with H atom pointing toward I anion such that the oxygen atom minimized its distance with the Cs cation. The Cs-O and H-I distances are respectively 3.16 and 2.45 Å. In both cases the geometry of the water molecule is similar to the gas phase one, the H-O-H angle is 105° and O-H bond lengths are 0.99 Å. These geometries are characteristic of weak interaction with the surface. The top layer of CsI does not relax, as almost no change in the positions of atoms was induced by the water adsorption. Adsorption energies are respectively 0.31 and 0.51 eV for the two configurations (flat and hydrogen bond).

Calculation of the electronic density difference corresponding to the electronic transfer between the molecule and the surface is very weak. The main interaction is due to hydrogen bond formation. The strength of H-I hydrogen bonding is two times larger than the O-Cs<sup>+</sup> bonding. This result is in agreement with previous study on NaCl surfaces<sup>40</sup>. In this study the authors assume same type of adsorption for NaCl. Pepa et al.<sup>41</sup> calculated 0.40 eV for the molecular water adsorption parallel mode to the surface, on top of the Na<sup>+</sup> cation on the NaCl (100) surface.

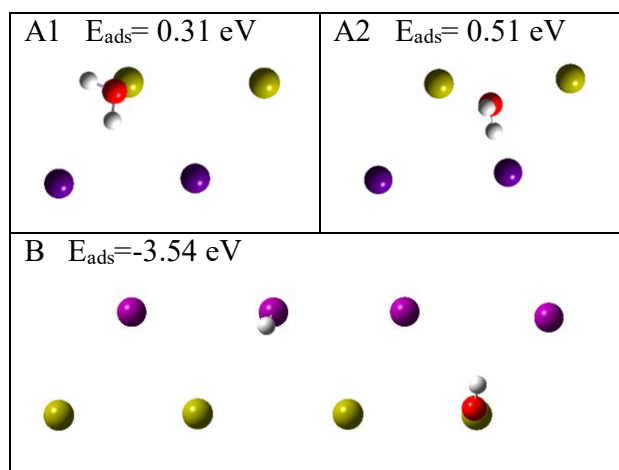


**Figure III-4: molecular and dissociative adsorptions of water molecule on CsI surface geometries and energies (eV). (I: Purple, Cs : Yellow, O: red, H; white)**



We also investigated the dissociative adsorption mode on CsI (011) surface. After optimization, the OH group is located at 2.87 Å above the Cs<sup>+</sup> cation in top position and the proton is placed on the top of an I anion with a I-H distance equal to 1.77 Å. This distance is larger than the distance in the HI gaseous molecule (1.75 Å). The adsorption energy for this case is -3.54 eV associated to a very endothermic adsorption. Furthermore, when the proton is adsorbed on the iodide neighboring the cesium on which the OH group is placed, H moves toward the OH group to form the water molecule without any activation barrier. The H<sup>+</sup> and the OH<sup>-</sup> must be adsorbed on non-neighboring atoms to avoid the spontaneous water formation. This result means that no spontaneous dissociation of an adsorbed water molecule can happen on CsI and thus the formation of IH molecule on the surface is not possible. This result is important since it enlightens that release of iodine as HI acid from CsI surfaces is not probable since its formation on the surface is not possible in the absence of strong acid in the gaseous phase.

In order to take into account the temperature effect, Gibbs free energy plots (see Figure III-5) at different temperatures and pressures were obtained starting from the adsorption energy of one water molecule on CsI surface. The plots show that water can only be adsorbed at low temperatures (i.e. 200 K) even at low pressure and that at room temperature, partial pressure larger than 0.01 bar is needed to stabilize the water on the surface, due to the weak interaction between the molecule and the surface. This value is close to the water saturation vapor pressure (0.03 bar at 298 K) and explains that humidity of 80% is needed to observe the CsI deliquescence<sup>4,42</sup>. Similar results have been observed on NaCl<sup>43-45</sup>.

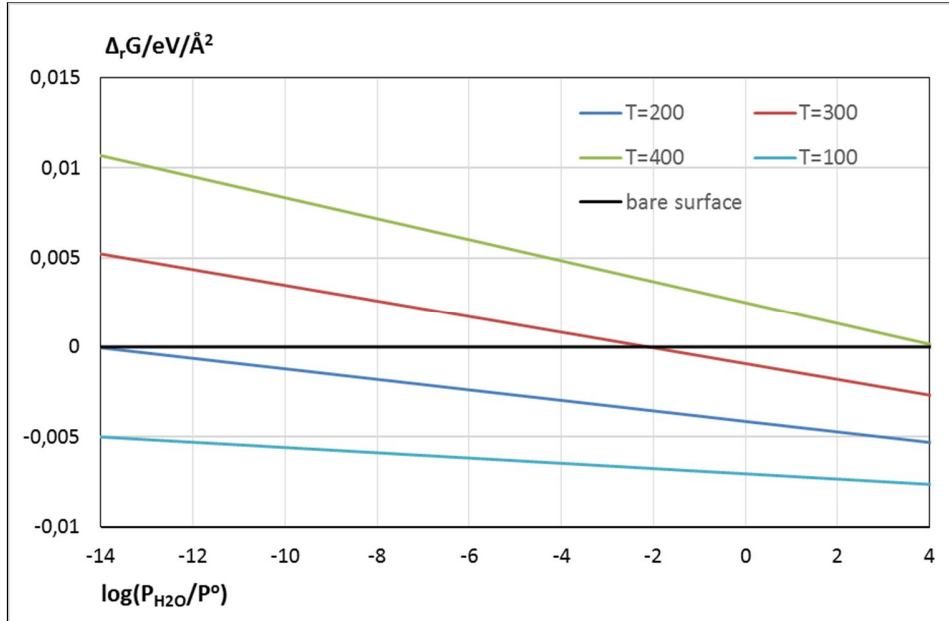


**Figure III-5. Gibbs free energy plots for associative adsorption of H<sub>2</sub>O on CsI surface at different temperatures.**

### III.2.3.2.2 Adsorption of H<sub>2</sub>O molecules layer on (1x2) unit cell of CsI (011) surface

In order to estimate the water coverage effect on the adsorption, water molecules were added to (1x2) CsI (011) surface successively until one monolayer is achieved. Figure III-6 shows the geometry of half and one monolayer of H<sub>2</sub>O adsorbed on the surface (011).

A systematic study of possible adsorption geometries has been performed, adding water molecule on top of Cs and on top of I to determine the most stable geometries depending on the coverage extent. When more than one water molecule is adsorbed on the surface, two types of interaction compete to define the most stable configuration: water-surface ( $E_{w-s}$ ) and water-water ( $E_{w-w}$ ) interactions.

These interactions energies were computed according to the following formulas (III-5, III-6):

$$E_{w-w} = E_{\text{water-polymer}} - nxE_{(\text{H}_2\text{O})\text{gas}} \quad \text{III-6}$$

$$E_{w-s} = E_{\text{ads}} - E_{w-w} \quad \text{III-7}$$

$E_{\text{water-polymer}}$  is the energy of water molecules in the geometry of the adsorbed ones but without solid substrate. Due to the large number of degrees of freedom when eight water molecules are adsorbed on the surface, we performed *ab-initio* molecular dynamic to scan the potential energy surface at 350 K. We fully optimized the energetic minima to compute the adsorption energy.

**Table III-2. Adsorption energy at different coverages for associative mode**

	1 ML (8 H <sub>2</sub> O)	0.5 ML (4 H <sub>2</sub> O)	0.125 ML (1 H <sub>2</sub> O)
$E_{\text{ads}}(\text{eV})$	5.89	2.19	0.51
$E_{\text{w-w}}(\text{eV})$	3.18	0.59	-
$E_{\text{w-s}}(\text{eV})$	2.71	1.60	0.51

In Table III-2 we present adsorption and interaction energies for the investigated cases. Starting with the case of half monolayer (ML) of water (Figure III-6A), the distances between the water molecules on the surface are small leading to water-water interaction. These hydrogen bonds are strong enough to favor the clustering of the water molecule on one side of the surface cell and the formation of a water chain.

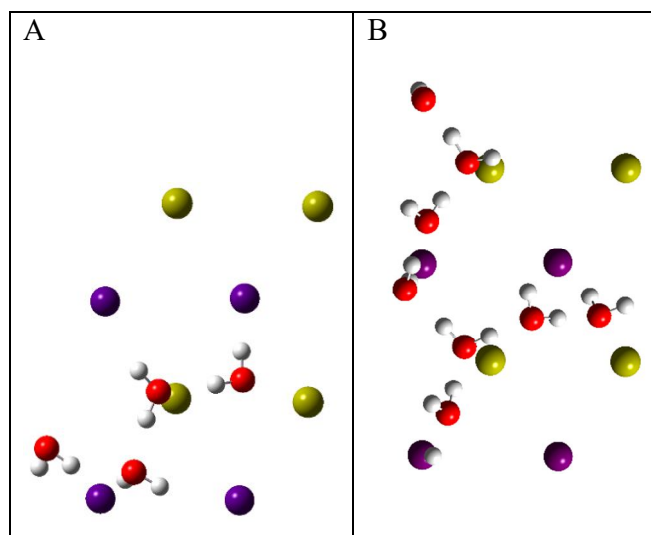


**Figure III-6. Adsorption of half (A) and one monolayer of water (B) on (2x1) CsI (011) surface. (I: Purple, Cs: Yellow, O: red, H: white)**

Furthermore, we notice that only half of the water molecules are interacting directly with the surface and in this case, with one proton only, one molecule is on top of a Cs cation while the last

water molecules are forming only water-water hydrogen bonds. The distance between neighbor water molecules is about 2.8 Å from each other which is in the range of the typical distance for an interacting water dimer<sup>46</sup>. Adsorption energy of this configuration is 2.19 eV in which the water-surface part is 1.60 eV. The water-surface interaction is only multiplied by three compared to the single molecule adsorption. The formation of the hydrogen bond between the water molecules prevents them to be placed on the most favorable position to interact with the Cs cation, but the interaction energy by molecule increases with the number of adsorbed molecules. For the one monolayer case (i. e. eight water molecules), the interaction energy is 5,89 eV, and the interaction energy by molecule (0,72eV) still increases. The larger part of the interaction is now due to the water-water interaction as the larger molecular density allows the formation of an hydrogen bond network that includes all the molecules (Figure III-6B). The water surface interaction is only 2.71 eV, (i.e. 0,33 eV par molecule). For coverage larger than one monolayer (see S.I.), water molecules are oriented to interact preferentially with other water molecules.

### **III.2.3.3 Iodine species desorption**

#### **III.2.3.3.1 Reaction without oxidant**

Release of iodine gaseous molecules from CsI surface was studied for the most stable surface. We have considered the formation of different iodine molecules such as I<sub>2</sub>, HI and IOH.

Starting from clean CsI surface, we first study the iodine release without any oxidizing agent. When one I<sub>2</sub> molecule from the surface is extracted, the surface is reduced while the iodides are oxidized. This reaction is very endothermic ( $\Delta_r E = 7.40$  eV), which, thermodynamically, is non-possible. From a chemical point of view, the Cs atoms are too electropositive to be reduced. To oxidize the iodide, the presence of a strong oxidant is mandatory.

In a second step, we have investigated the participation of water molecules and the possible formation of HI in an acid-base reaction or the formation of IOH in a redox reaction. In the first case, the water molecule is dissociated on the surface: one proton is bonded to one iodide on the surface while the OH is attached to cesium one. This step is endothermic ( $\Delta_r E = 3.54$  eV). Removing HI molecule from the surface is also endothermic ( $\Delta_r E = 0.50$  eV). The final displacement of the OH group into the vacancy is exothermic ( $\Delta_r E = -0.30$  eV). The departure of

the HI molecule is very endothermic ( $\Delta_r E = 4.04$  eV) and not possible from a thermodynamic point of view.

The second case: i.e. the formation of IOH leaving one hydride on the surface draws same conclusion as the previous case, it is not possible. The water dissociation is 4.20 eV (Figure III-7) and inhibits the IOH formation.

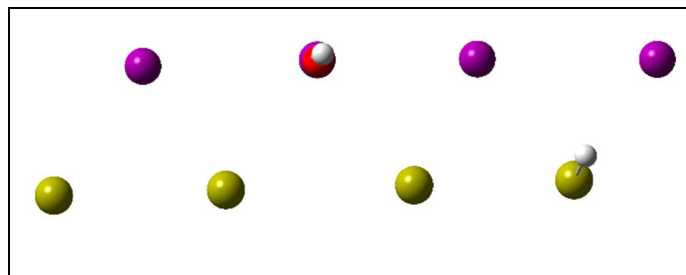


**Figure III-7. Formation of IOH on the surface starting by dissociating one water molecule.**

Simply removing iodine species from surface is not favored. As the formation of  $I_{2(g)}$  is observed experimentally<sup>20</sup> other processes involving the participation of oxidant molecules are required, as it's mandatory to oxidize the surface before removing iodine. In the accidental conditions, the gas phase is composed of a large excess of water. The radiation produced by the radioactive material may dissociate the water and produce  $OH^\circ$  radical which is very oxidizing.

### III.2.3.3.2 Reaction with one $OH^\circ$ radical

We have followed reaction pathways leading to formation of  $I_{2(g)}$  or  $IOH_{(g)}$  using one  $OH^\circ$  as oxidizing agent. A first mechanism leading to the formation of  $IOH_{(g)}$  is studied. The adsorption of one  $OH^\circ$  radical on the surface is followed by the displacement of one iodine to form one IOH group. The addition of the  $OH^\circ$  is exothermic ( $\Delta E = -0.88$  eV) but the desorption of the IOH species is endothermic ( $\Delta E = 2.35$  eV) and not probable. From a chemical point of view, the oxidation state of iodine in the IOH is +I. Since it is -I in the CsI solid, the IOH formation is a two electrons oxidation reaction and is then non possible if only one  $OH^\circ$  is involved in the mechanism. The departure of  $I_2$  from surface is, after one  $OH^\circ$  addition, also endothermic ( $\Delta E = 4.18$  eV (step 'd' to 'e' in Figure III-8) for the most endothermic step and ( $\Delta E = 2.50$  eV for the total reaction) due to similar chemical reasons. The second electron released by the  $I_2$  formation must be localized on the surface which is not favorable.

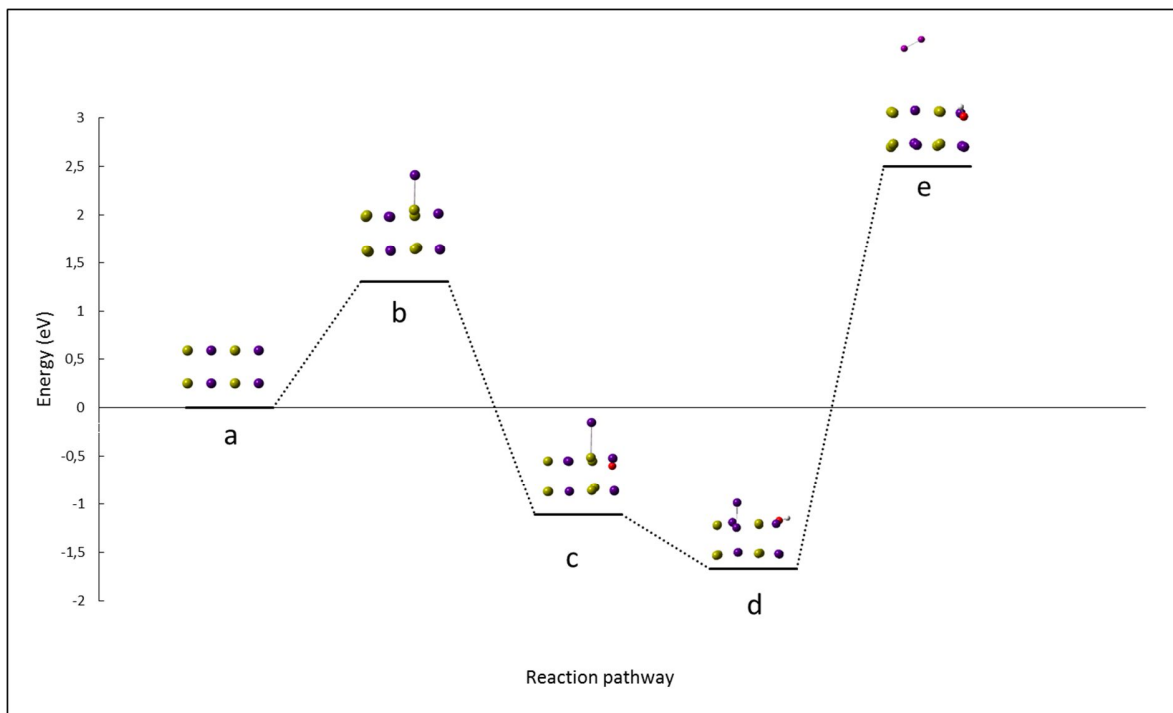


**Figure III-8: Reaction pathway including one OH group before releasing I<sub>2</sub>. (I purple, Cs, yellow, O red, H, grey).**

### III.2.3.3.3 Reaction with two OH° radicals

It is mandatory to introduce a second OH° in the reaction mechanism to accommodate the second electron. From the thermodynamic point of view, the I<sub>2</sub> formation reaction is, as expected, very exothermic  $\Delta_r E = -3.17 \text{ eV}$  and thermodynamically favored. The possible limitation for the I<sub>2(g)</sub> production will only be kinetics. Various reaction mechanisms have been investigated but we will focus on the reaction paths with the lowest endothermic steps: (a). The first two steps of the reaction are similar to the previous one. The first step is the displacement of one iodide on top of a cesium cation. This step is an endothermic step with an activation energy of 1.3 eV. The transition state geometry is very similar to the final geometry. In order to avoid the reduction of the surface, the second step must be the adsorption of the OH° radical. This is an exothermic step ( $\Delta E = -2.41 \text{ eV}$ ). This type of elementary step is non-activated and its rate will be limited by either OH° formation or OH° diffusion at the CsI-gas interface layer.

The addition of the second radical (see Figure III-9: First reaction pathway including two OH groups. (I purple, Cs, yellow, O red, H, grey). intermediate d' in which second OH° on the top of Cs) is exothermic ( $\Delta_r E = -1.05 \text{ eV}$ ). The following step is the formation of I<sub>2</sub> on the surface. The

diiodine molecule formed is in interaction with nearing OH (step e'); this reaction step is activated. Transition state was characterized and shown in Figure III-10. The activation barrier for this step is 0.41 eV. The next step is the displacement of I<sub>2</sub> on the surface which breaks the bond between OH and the I<sub>2</sub> (f'). The activation barrier is 0.72 eV (Figure III-11)

The I<sub>2</sub> Removing step (f' to g') requires 1.2 eV. The activation energy is also 1.2 eV as the I<sub>2</sub> adsorption on the surface is not activated. Last step (g' to h') is the displacement of the OH on the surface to fill the vacancy created by the displacement of the second iodine.

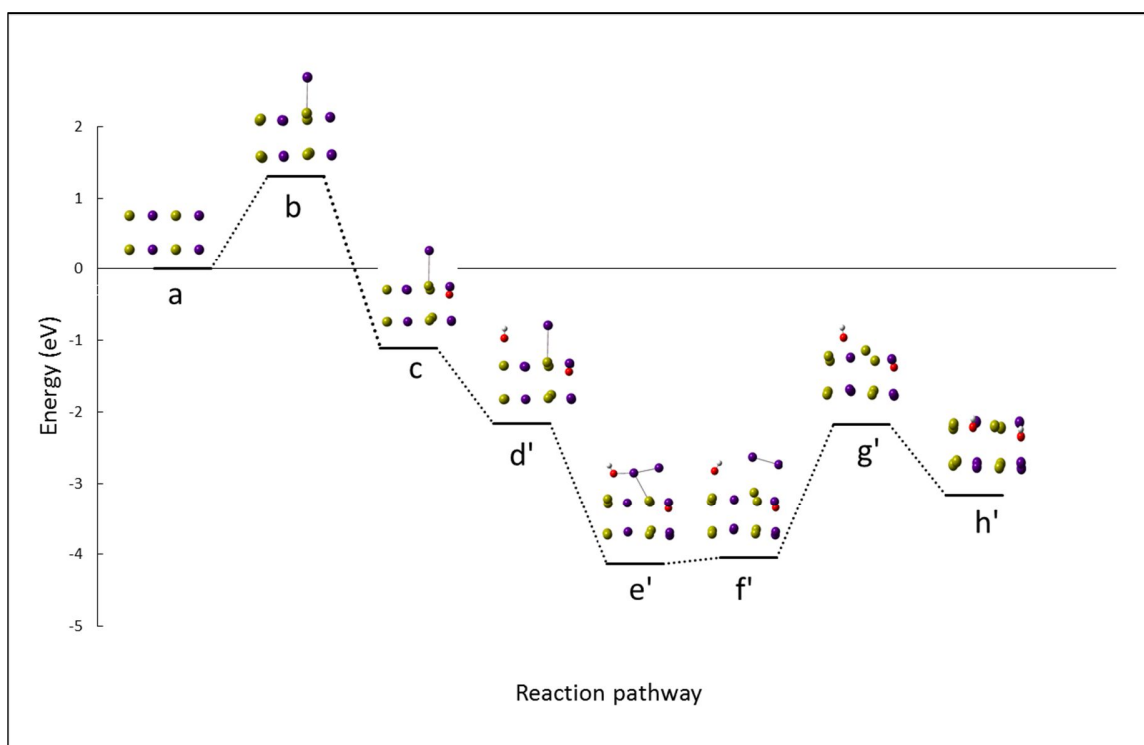


**Figure III-9: First reaction pathway including two OH groups. (I purple, Cs, yellow, O red, H, grey).**

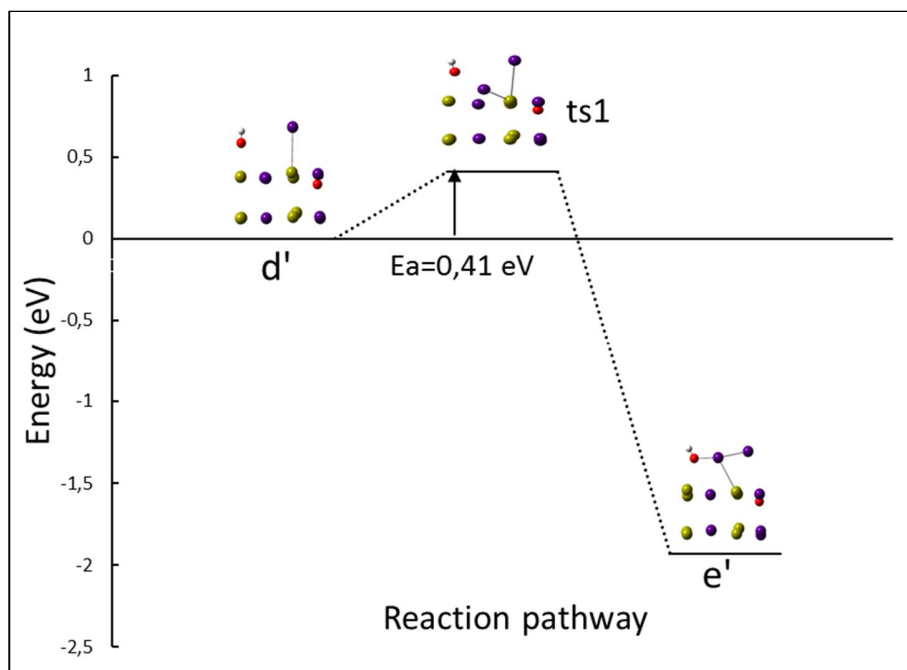


**Figure III-10: Activation energy for step d' to e' .(I purple, Cs, yellow, O red, H, grey).**

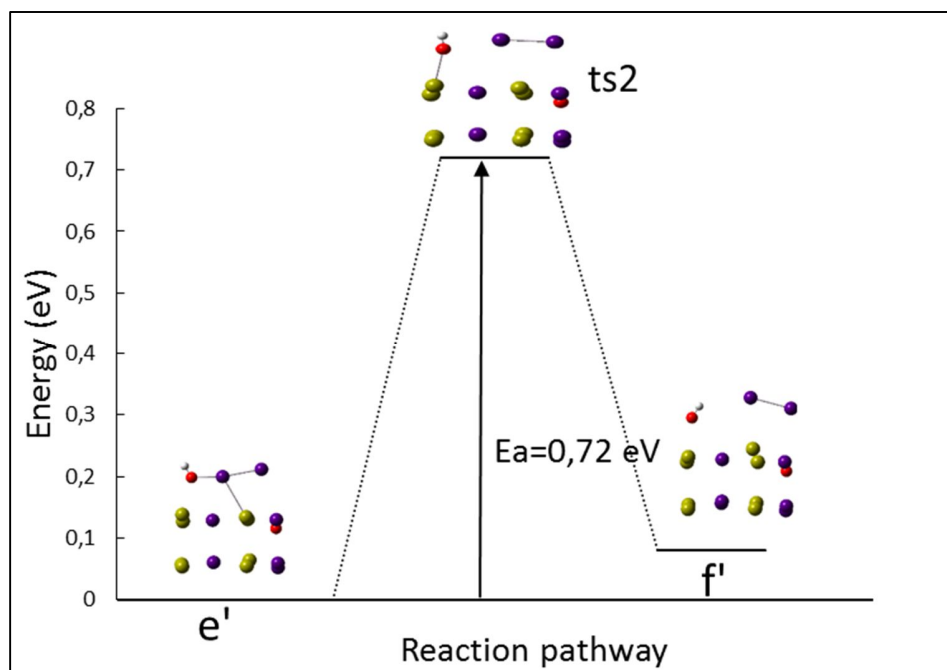


**Figure III-11: Activation energy for step e' to f' .(I: purple, Cs: yellow, O: red and H: grey).**

In order to avoid the first step of the previous mechanism, which is associated to the highest activation energy, it is possible to adsorb two  $\text{OH}^\circ$  radicals directly on the bare surface. The whole reaction path is presented on Figure 12. The surface is oxidized and the displacement of



the I atom (either as  $I^\circ$  or  $I^+$ ) is an exothermic step. The activation energy for the formation of one IOH species is only 0.42 eV (Figure III-13: Activation energy for step b'' to c''). (I purple, Cs, yellow, O red, H, grey). The iodide oxidation before its displacement reduces its negative charge and its strong electrostatic interactions with the  $Cs^+$  network. The  $I_2$  formation is only slightly activated ( $\Delta E = 0.77$  eV) (see Figure III-14: Activation energy for step c'' to d''). (I purple, Cs, yellow, O red, H, grey). Following this reaction pathway, the highest activation energy is 1.20 eV for the  $I_{2(g)}$  release as for the alternative mechanism.

An alternative pathway leads to the formation of IOH after the second step (c''). The IOH can be released to the gas phase. The activation energy is 0.70 eV. This value is almost equal to the  $I_2$  formation activation energy on the surface. As a consequence, the two molecules should be formed at a similar rate. However due to the presence of  $OH^\circ$  in the gas phase, further oxidation reactions are expected and the two species may lead to the same products as IOH is not a stable molecule, just an intermediate product.

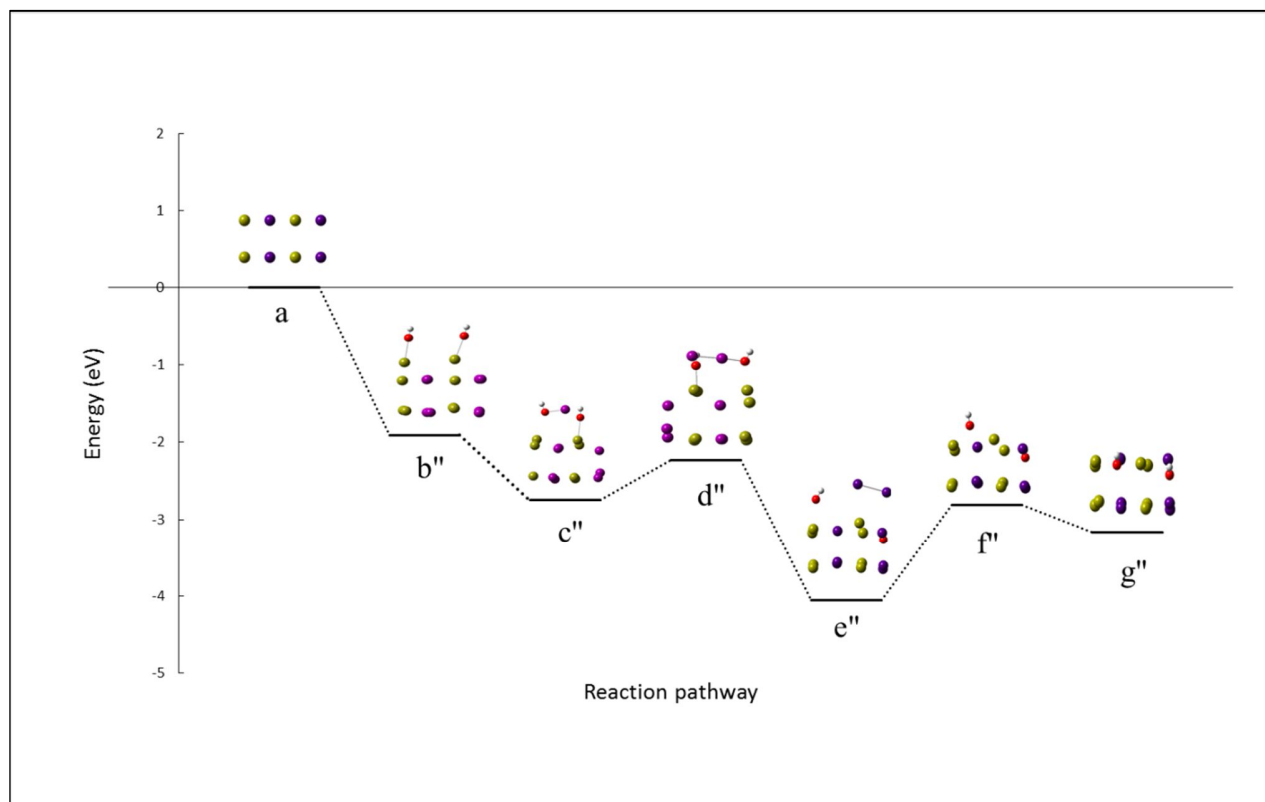


**Figure III-12: Second reaction pathway including two OH groups. (I purple, Cs, yellow, O red, H, grey).**

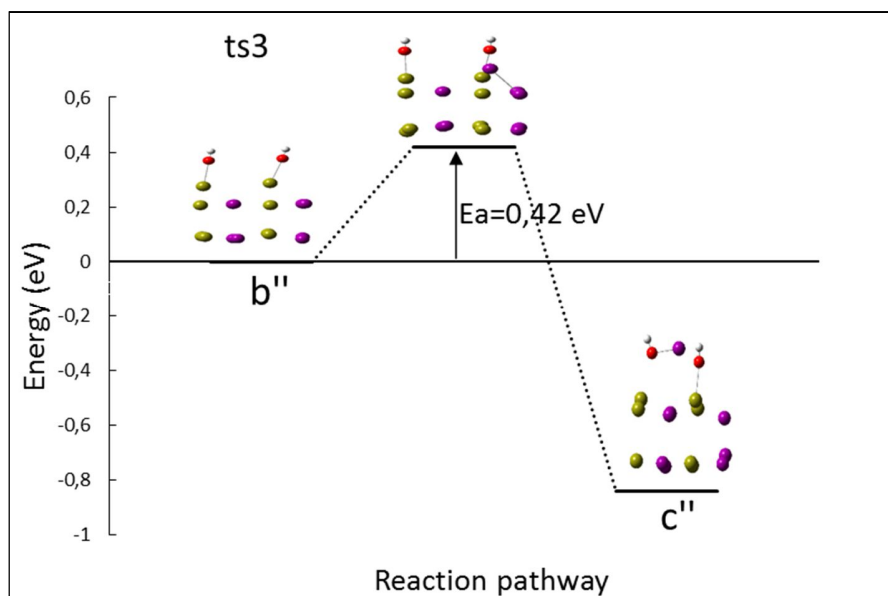


Figure III-13: Activation energy for step  $b''$  to  $c''$ . (I purple, Cs, yellow, O red, H, grey).

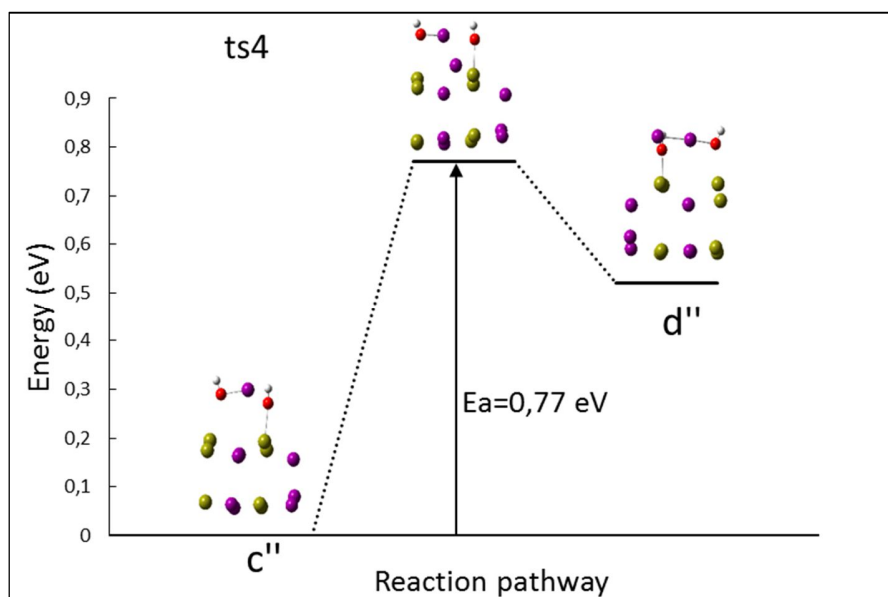


Figure III-14: Activation energy for step  $c''$  to  $d''$ . (I purple, Cs, yellow, O red, H, grey).

### III.2.4 Conclusion

In this work, we have studied the chemistry of CsI nanoparticles in dry and moist atmospheres. To the best of our knowledge, it is the first time that the chemistry of CsI is investigated at the DFT level. The CsI aerosol deposited on inner walls may be an important source of  $I_2(g)$  production in case of severe nuclear accident and its chemistry is of great importance to make

some accurate simulations of radioactive iodine outside releases, called iodine source term. The Wulff construction of the particle shape based on low index surface energies is a rhombic dodecahedron with the (011) surface.

The water adsorption on this surface is a molecular process and the adsorption energy is 0.51 eV. The adsorption of the first water molecule is relatively weak. The main interaction is a hydrogen bond between the water and an iodide. A monolayer of water may be adsorbed at low temperature (about room temperature) due to the formation of hydrogen bond network, but the water molecules desorb at higher temperature. This result indicated that the hygroscopic character of CsI is not due to the direct interaction between the water and the surface but may be mainly due to the very high solubility of the salt and the large  $\text{Cs}^+$  and  $\text{I}^-$  solvation energies.

As the dissociation of water on the surface is not favored, it is not possible to produce HI or IOH from the particle only in presence of water molecules. The rapid formation of gaseous molecular iodine from CsI particle has been evidenced experimentally under radiolysis but the direct formation of  $\text{I}_2$  (without radiolysis) at the surface is very endothermic and not possible at temperature around 100 °C, representative of the nuclear containment temperature in severe accident conditions. Similar to the reaction mechanisms proposed to explain the  $\text{Cl}_2$  formation from  $\text{NaCl}$ <sup>47-51</sup>, it is necessary to introduce a strong oxidant (in our case mostly the OH radical) to explain the formation of  $\text{I}_2$ . The proposed reaction mechanism includes only low activation energy ( $E_{\text{act}} = 1,2$  eV) elementary steps. In this condition, the reaction rate will be limited either by the OH formation or by its diffusion. OH formation depends on dose rates whereas diffusion is linked to thermal effect. Anyway oxidation process is quite fast, in few hours CsI deposited onto stainless steel coupons is completely oxidized.

## III.3 Supplementary data corresponding to the paper

### III.3.1 KPOINTS as function of energy

Tests were done to find the best mesh size. We performed calculations for different mesh sizes at same cutoff energy (300 eV). **Table III-3** shows the variation of total energy depending on the mesh size. It can be shown in the table that the energy is the same in all systems except in 3x3x3 mesh, it means that this mesh is not enough to describe the system. In our calculations we have used the lowest possible cell (5x5x5) to save time.

**Table III-3. Total energy as function of Mesh size.**

Mesh size	Total energy (eV)
3x3x3	-5,419
5x5x5	-5,438
7x7x7	-5,438
9x9x9	-5,438
11x11x11	-5,438

### III.3.2 Lattice constant and bulk volume

Plot of the energy versus the volume of unit cell is presented in **Figure III-15** in order to compare the optimized value of the bulk constant with the experimental one.

The lattice parameter is calculated at the equilibrium volume as  $a = (V_{\text{equilibrium}})^{1/3}$ . The calculated value then is 4.665 Å while the experimental one is 4.567 Å. Our calculated value is greater than the experimental one by 2.1%

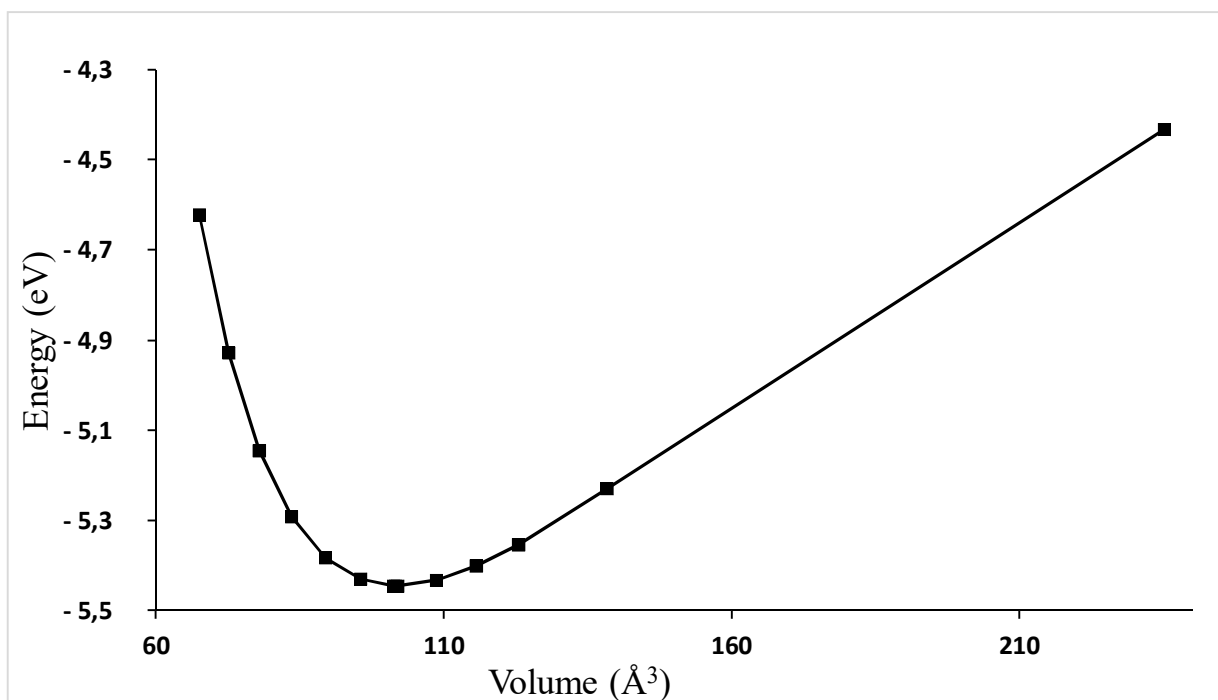
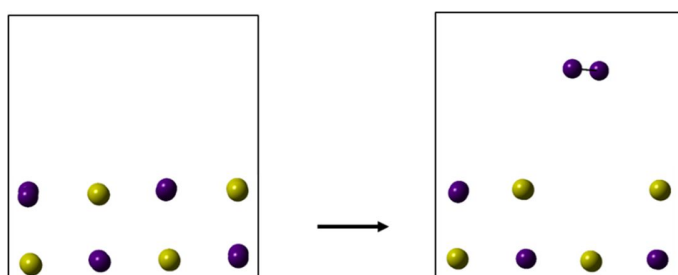


Figure III-15. Plot of the energy versus the lattice parameter of the unit cell.

### III.3.3 Formation of I<sub>2</sub> starting by optimized and experimental lattice constant

To see the effect of the 2.1% difference between our optimized cell volume and the experimental one, we calculated energy of one reaction using different cell volumes. The reaction considered is the formation of I<sub>2</sub> from the surface without any oxidant. Schematic presentation of this reaction and the corresponding energies for both cases are presented in the following figure:



Energy using experimental lattice constant (eV):	-162.78	-155.38
Energy using our optimized lattice constant (eV):	-162.98	-155.53

The reaction energies for the former and latter cases are 7.40 eV and 7.45 eV, respectively. Therefore, the difference in reaction energy is about 0.7%. Based on this result, we have used the experimental value in all our calculations.

### III.3.4 Formation of I<sub>2</sub> on a doubled cell in two directions

To study the effect of the cell size on the energy, we calculated the reaction energy of I<sub>2</sub> formation from a doubled cell in two directions (x and y).

Energy of formation of I<sub>2</sub> from our first cell used is 7.40 eV.

Energy of formation of I<sub>2</sub> from the doubled cell in a and b directions (**Figure III-16**) is 7.53 eV.

Then the difference is 0.13 eV, which means that the cell size has only a small effect on the reaction energy. The size of the cell doesn't affect iodine formation and so the reduction on the defect coverage does not favor I<sub>2</sub> formation.

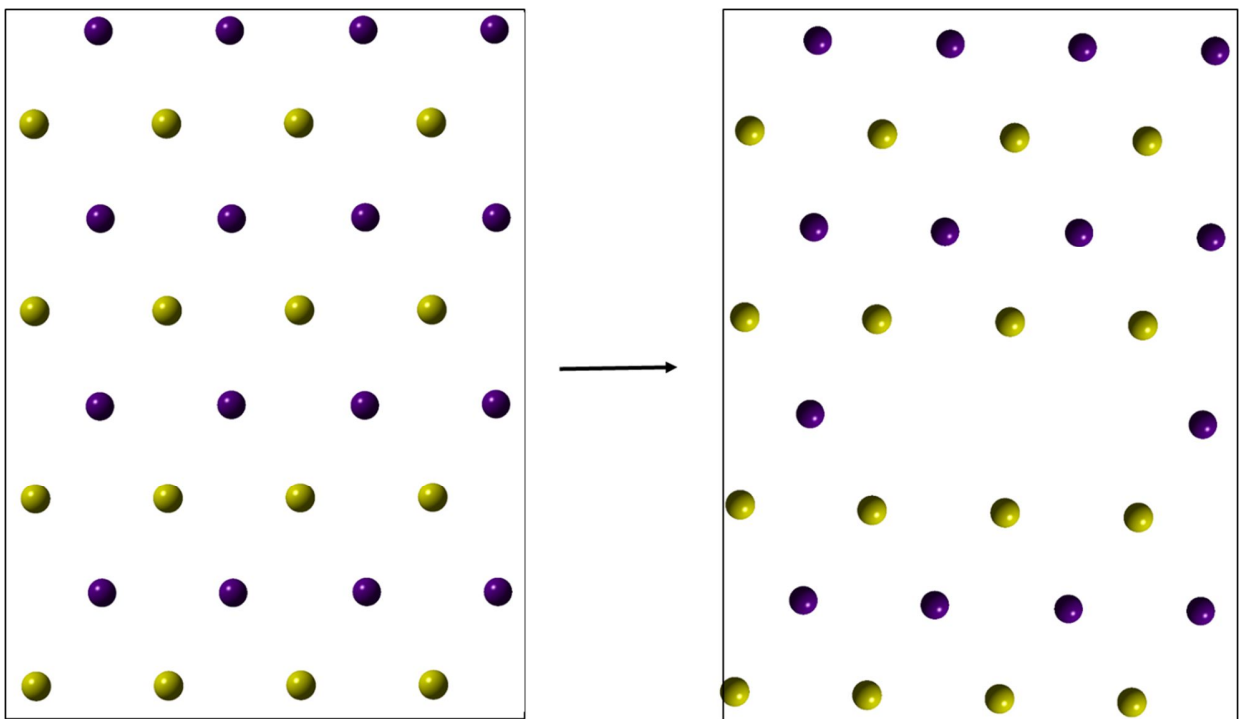


**Figure III-16. Top view of the doubled cell before and after removing I<sub>2</sub>.**

### III.3.5 Adsorption of one monolayer of water using different geometries

To study the most stable adsorption geometries of one water monolayer, we ran molecular dynamics (MD) at 350 K. In MD, we follow atoms trajectories on the surface, in which most stable geometries will have the lowest energies. We performed about 1.4 picoseconds of dynamics which permits to draw the evolution of energy. For some minima on the energy profile, we calculate the adsorption energy and compare it to the most stable adsorption geometry obtained. **Figure III-17** shows the evolution of energy with some minima and their corresponding geometries. **Table III-4** presents the adsorption (ads), water-water (ww) and surface-water (sw) interaction energies. We notice that all interaction energies are quite similar between the different geometries.

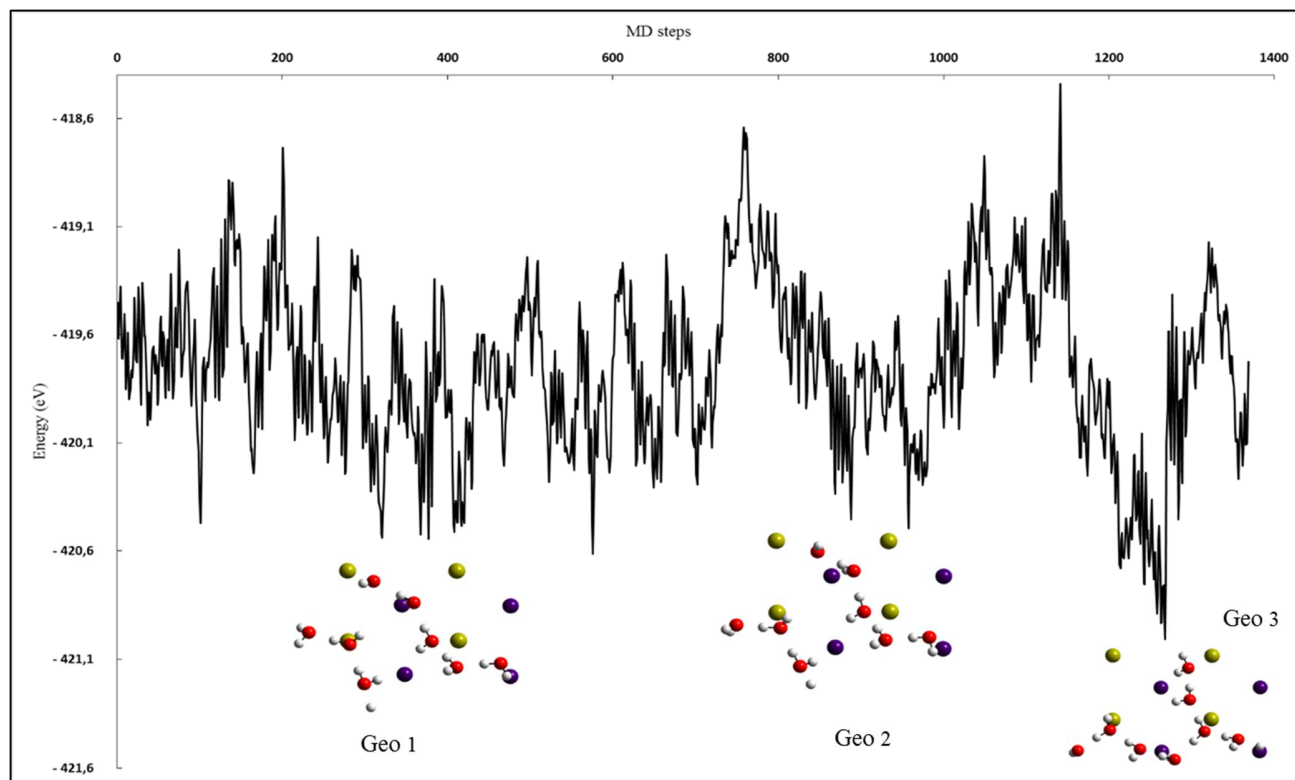


**Figure III-17. Evolution of energy during the MD and the corresponding geometries for some minima.**

**Table III-4. Interaction energies between the surface and one water monolayer.**

	Geo 1	Geo 2	Geo 3
$E_{ads}(eV)$	-5.62	-5.69	-5.89
$E_{ww}(eV)$	-2.86	-2.91	-3.18
$E_{sw}(eV)$	-2.76	-2.78	-2.71

### III.3.6 Effect of temperature and pressure on the adsorption of one water monolayer

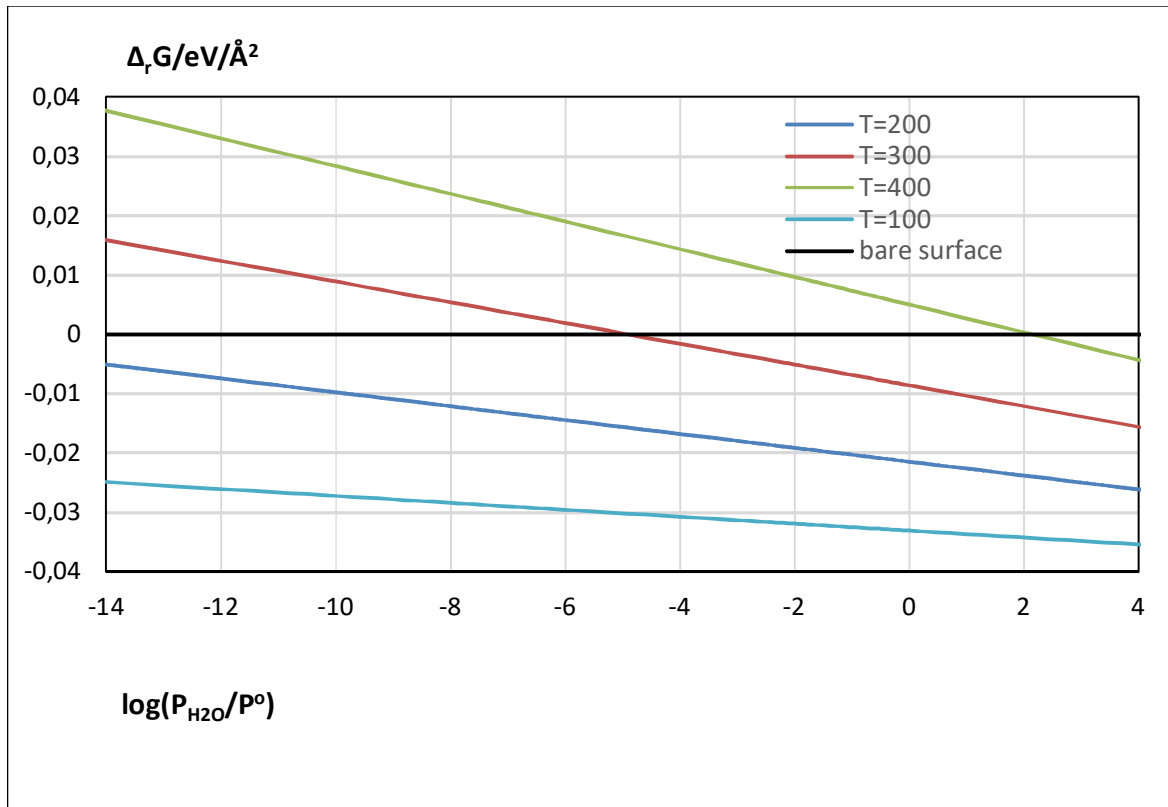


**Figure III-18. Gibbs free energy plot for one monolayer adsorption of H<sub>2</sub>O on CsI surface at different temperatures.**

In order to study the effect of temperature and pressure on the adsorption of one water monolayer, Gibbs free energy plot were obtained starting by the adsorption energy of one monolayer of water on CsI surface. The plots shows that the one monolayer of water can be



adsorbed at low temperatures ( i.e. lower than 200 K) at low pressure also, while at room temperature (300 K), only at partial pressure higher than  $10^{-5}$  bar needed. Almost similar results for the adsorption of one water molecule has been obtained and discussed in the paper.

### III.3.7 Adsorption of more than one water monolayer on (011)

#### CsI surface

In the paper, it was mentioned than once we add more water, the water-water interactions will be more important than the surface-water ones, and also that the water molecules start to form hexagonal network on the surface. To see clearly this fact, we studied the adsorption of more than one water monolayer i.e. ten water molecules. Top view of the corresponding geometry is presented in **Figure III-19**, in which we see the hexagonal network which appears as expected.

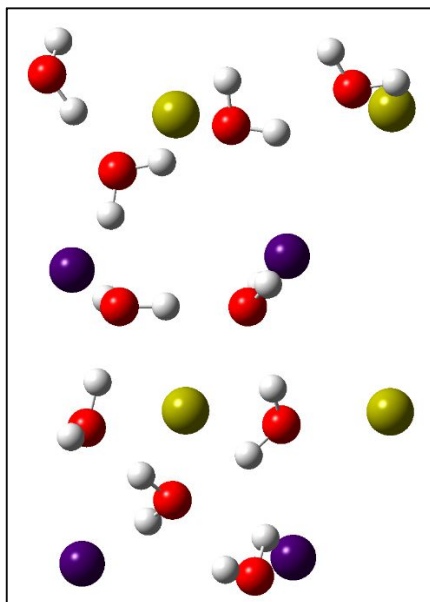


**Figure III-19. Top view of adsorption of 1.25 monolayer of water.**

The calculated adsorption energy of this geometry is 7.28 eV in which the w-w and w-s interactions are respectively 3.44 and 3.84 eV. W-s energy participates with about 53% of the total adsorption energy while it is 56% for one monolayer layer case. These results confirm our conclusion in the paper that the w-s interactions will be lower if the number of the adsorbed molecules are larger.

### III.4 Reactivity of defected surfaces

Beside reactivity on flat perfect surfaces, it is important to study the reactivity on surfaces with defects. In periodic DFT calculations, these defects can be generated by removing part of the upper layer, or by creating surfaces with larger Miller indexes as the 012 surface to generate step surfaces. A cell doubled in y-direction is presented in **Figure III-20**. In some calculations we use single cell, however, in other calculations we need to use double cell to have more atoms on the surface. The size of the used cell is  $18.267 \times 10.212 \times 38.486 \text{ \AA}^3$ , which contains 48 atoms of each element. The upper 24 atoms were fixed while the lower ones were relaxed.

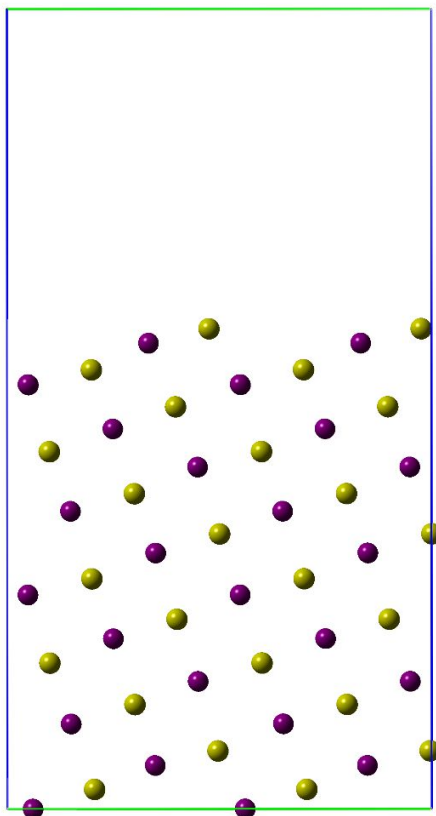


**Figure III-20.** Side view of the (012) stepped surfaces. The cell represented is doubled in the y direction.

## III.4.1 Oxidation by one OH°

### III.4.1.1 Formation of IOH

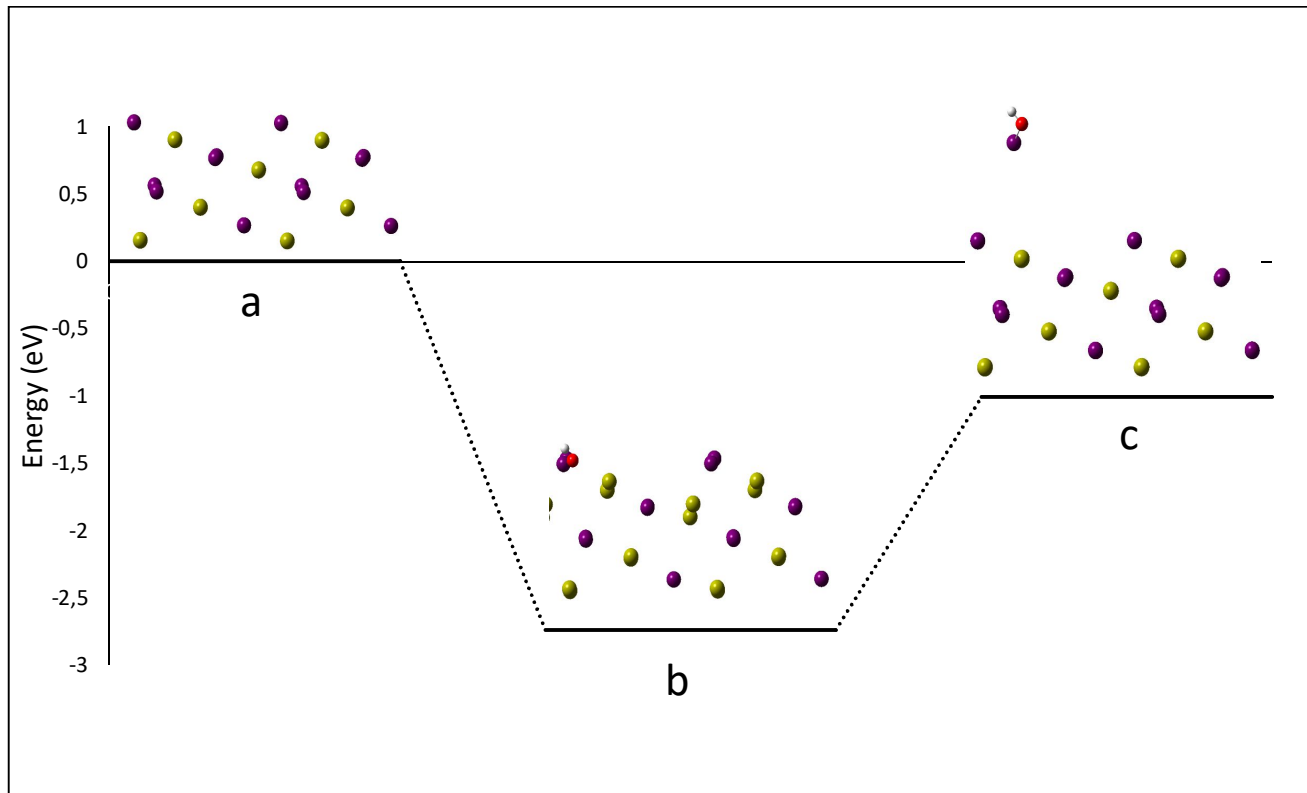


**Figure III-21. Formation of IOH after oxidizing the surface with one OH°.**

As for CsI perfect surface, we start studying the reactivity by oxidizing the surface by one OH°. In the first step, one OH interacts with I on the surface (step 'b' in **Figure III-21**). As for the perfect surface, this adsorption is exothermic ( $E_{\text{ads}} = -2.74$  eV). Finally, we remove the formed IOH into the gas phase. This process is endothermic and requires 1.74 eV. It can be concluded that the formation of IOH after oxidizing the surface by one OH is not very favorable.

### III.4.1.2 Formation of I<sub>2</sub>

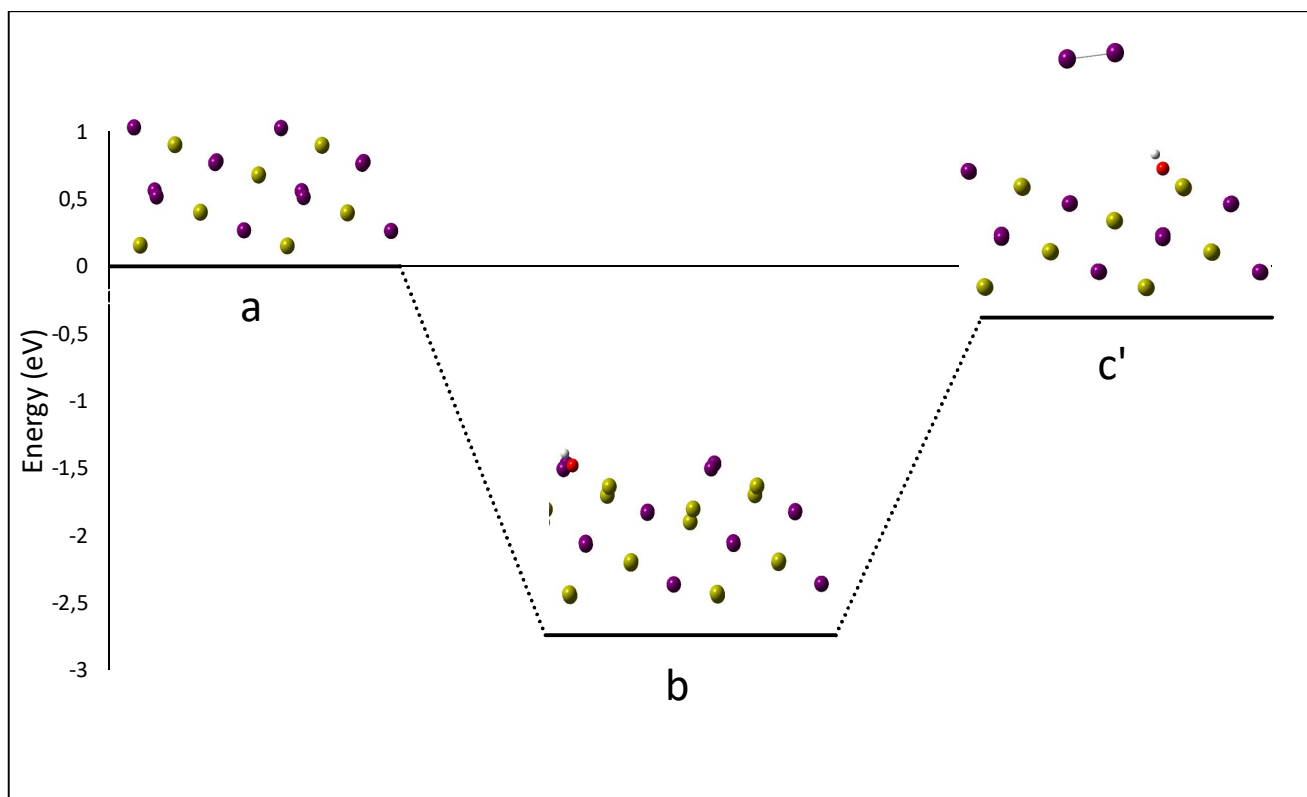


**Figure III-22: Formation of I<sub>2</sub> after oxidizing the surface with one OH°.**

Formation of I<sub>2</sub> from defected surface was studied also after the addition of an OH° on the surface. In the second step we remove I<sub>2</sub> to the gas phase (from 'b' to 'c' in **Figure III-22**). This step is very endothermic and requires 2.36 eV, which means that I<sub>2</sub> formation is also not probable.

### III.4.2 Oxidation by two OH°

knowing that formation of gaseous iodine species from the surface after oxidation by only one OH° is not efficient, we extend the study by oxidizing the surface with two OH radical before removing IOH or I<sub>2</sub>.

### III.4.2.1 Formation of IOH

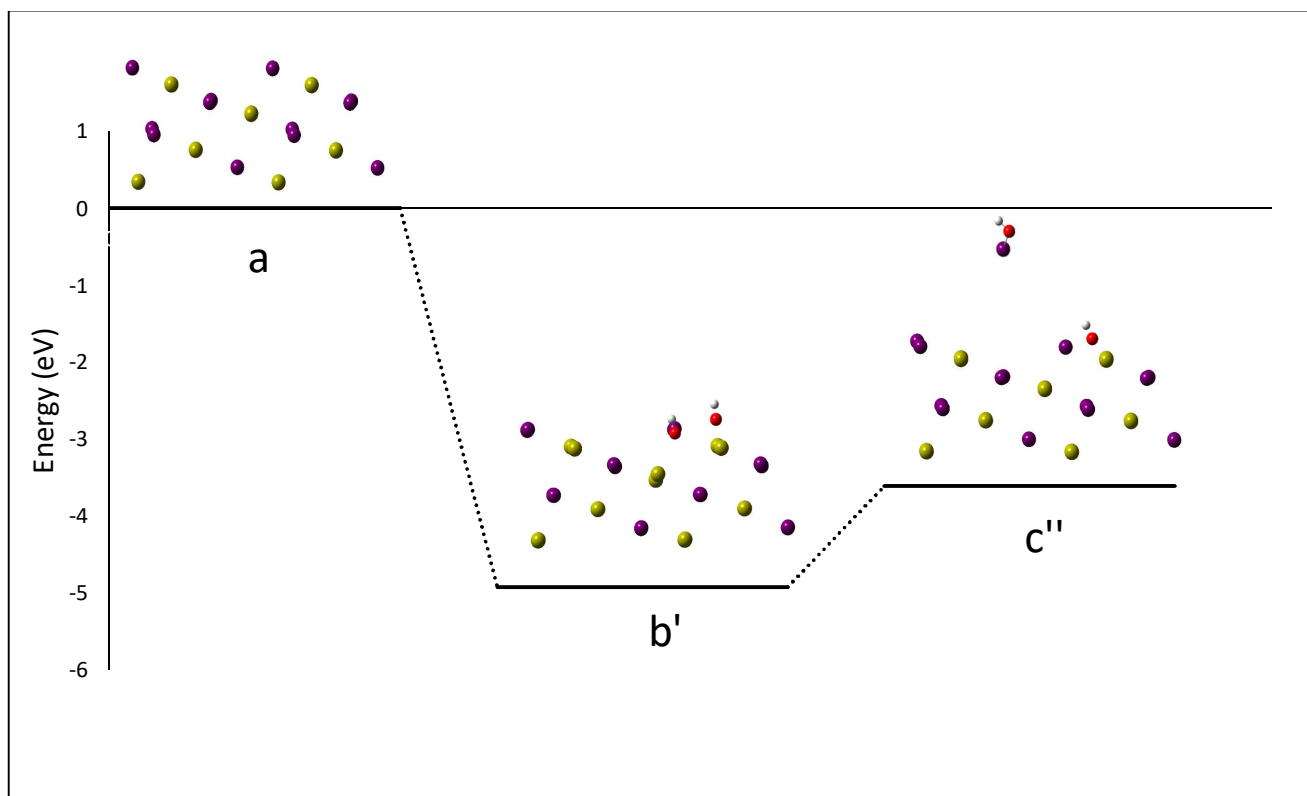


**Figure III-23: Formation of IOH after oxidizing the surface with two OH°.**

In the first step (“b” in Figure III-23), we added two OH° on the surface. The first one interacts with I and the another interacts with cesium. These steps are exothermic with total reaction energy close to -5.0 eV ( $\Delta rE = -4.93$  eV). In the following step, IOH is formed from the surface and the second OH° moves to the vacancy formed by the released iodine. This step is endothermic (1.06 eV) and associated to activation energy is also 1.06 eV. We see now that removing IOH in presence of two OH° is easier than that with only one OH° which requires 1.74 eV (see section III.4.1.1).

### III.4.2.2 Formation of I<sub>2</sub>

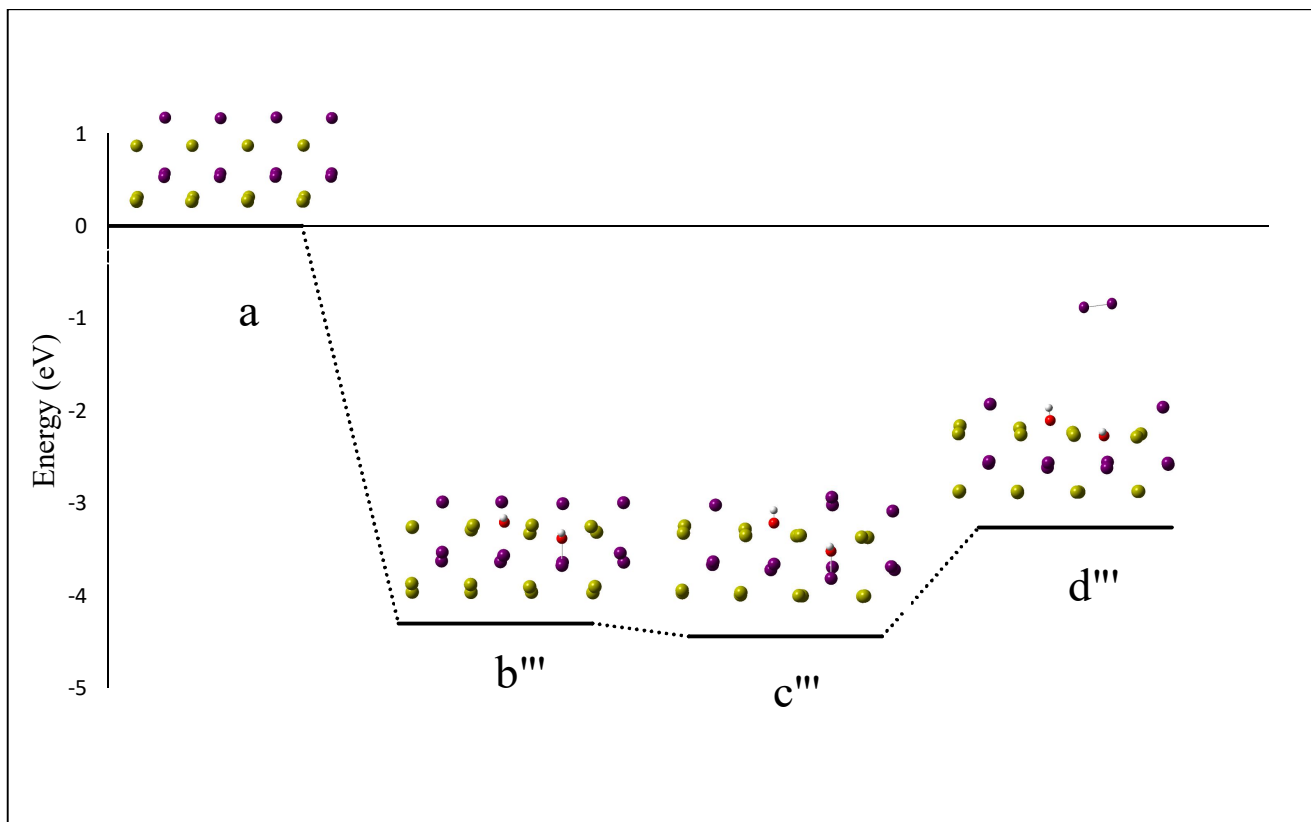


**Figure III-24: Formation of I<sub>2</sub> after oxidizing the surface with two OH°.**

In this part we study the surface oxidation by two OH° groups before formation of I<sub>2</sub>. Figure III-24 shows the corresponding reaction pathway. In the first step, we oxidize the surface by two OH°, this reaction is exothermic with total reaction energy  $\Delta E = -4.3$  eV (in this step the OH° interacts with Cs while in the previous part was interacting with iodine in which the reaction energy -4.93 eV). However, we form I<sub>2</sub> in the following step with activation energy of 0.5 eV, the transition state is shown in Figure III-25. In the last step, I<sub>2</sub> is formed with reaction energy of  $\Delta E = 1.18$  eV. Since the I<sub>2</sub> adsorption on the vacancy is non-activated, the I<sub>2</sub>(g) released activation energy is 1.18 eV.

As for the perfect surface, neither the formation of I<sub>2</sub> nor IOH is favored on the defects and both molecules will be formed due to OH radical reaction.

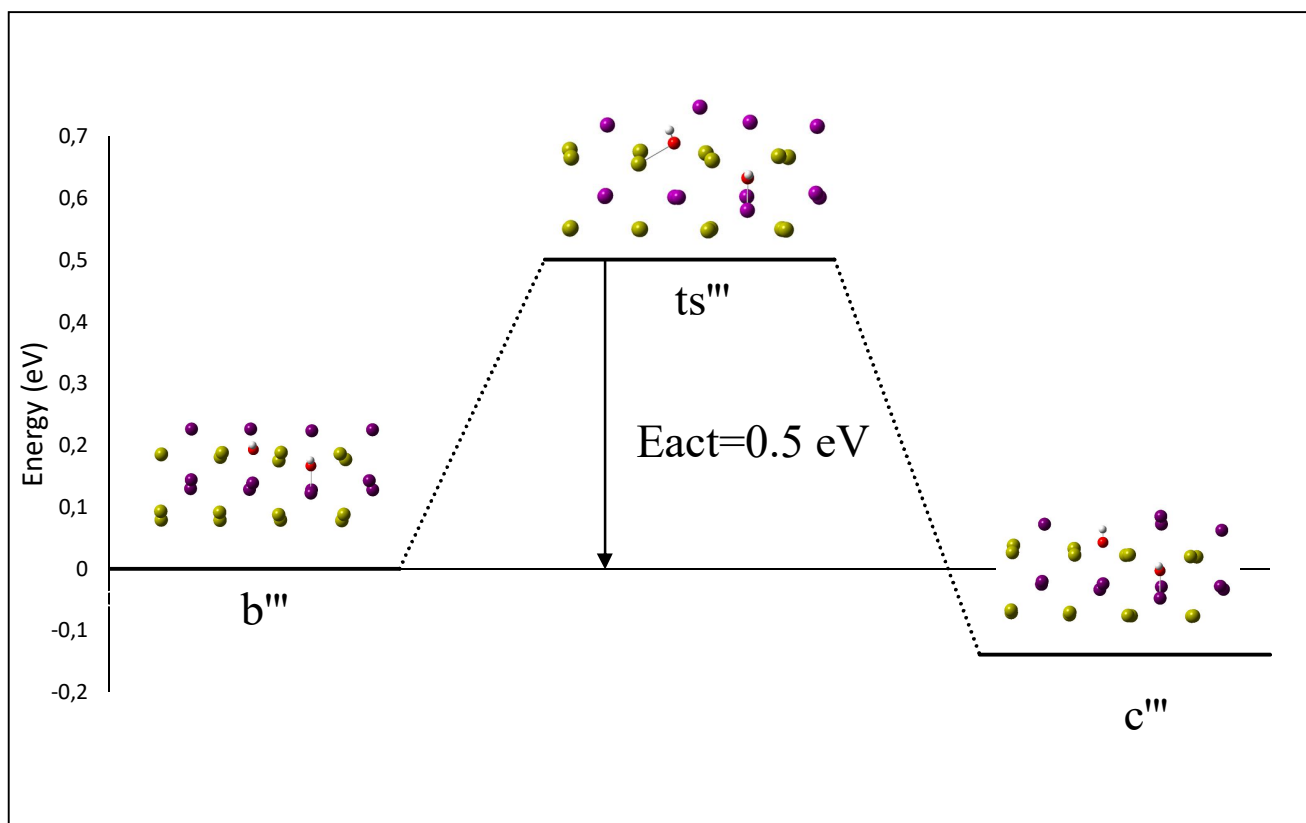


**Figure III-25: Activation energy for the formation of I<sub>2</sub> on the surface after oxidizing it two times.**

## III.5 Conclusion

In this chapter, chemistry of CsI, under aerosol form, has been studied in dry and moist atmospheres. The nanocrystal shape of this particle is rhombic dodecahedron, deduced from the Wulff construction. Water adsorbs on the surface associatively with a corresponding energy 0.51 eV. The main interaction is via H-I bond. Thermodynamic analysis shows that water may be adsorbed at low temperatures (up to roughly room temperature).

Formation of gaseous iodine species (I<sub>2</sub>, IOH and HI) is studied on perfect surface as well as on surfaces including defects. The results show that in both cases, the formation of iodine species without oxidants is very endothermic. Moreover, same conclusion is drawn after oxidizing the surface by adding only one-electron oxidizing species such as OH<sup>•</sup>.

From a chemical point of view, it is mandatory to oxidize the surface twice before removing iodine species. So, we assume that the surface was oxidized by two OH° at the beginning of each proposed reaction pathways. In this case, formation of IOH requires respectively 0.70 eV and 1.06 eV for ideal and with defects CsI surfaces; while for the I<sub>2</sub> formation, the activation energy amounts respectively to 1.2 and 1.18 eV. Then the defects will favor the formation of I<sub>2</sub> and not the formation of IOH.

## III.6 References

- (1) Tietze, S.; Foreman, M.; Ekberg, C.; Kaerkelae, T.; Auvinen, A.; Tapper, U.; Jokiniemi, J. *Adsorption and Revaporisation Studies of Thin Iodine Oxide and CsI Aerosol Deposits from Containment Surface Materials in LWRs*; Nordisk Kernesikkerhedsforskning, 2013.
- (2) Vikis, A. C.; MacFarlane, R. Reaction of Iodine with Ozone in the Gas Phase. *J. Phys. Chem.* **1985**, *89* (5), 812–815.
- (3) Holm, J.; Glänneskog, H.; Ekberg, C.; Kärkelä, T.; Auvinen, A.; Nordisk Kernesikkerhedsforskning. *Experimental Study on Iodine Chemistry (EXSI) - Containment Experiments with Methyl Iodide.*; 2010.
- (4) J.Colombani, C.Pascal, L.Martinet, C.Duffieux, O.Leroy. AER-CsI STEM/EPICUR Tests Synthesis Report. Juillet 2015.
- (5) Beahm E.C., Weber C.F., Kress T.S., Par-ker G.W. *Iodine Chemical Forms in LWR Severe Accidents*; NUREG/CR-5732 ORNL/TM-11861; US Nuclear Regulatory Commission, 1992.
- (6) Burns, P. C.; Ewing, R. C.; Navrotsky, A. Nuclear Fuel in a Reactor Accident. *Science* **2012**, *335* (6073), 1184–1188.
- (7) Buessler, K.; Aoyama, M.; Fukasawa, M. Impacts of the Fukushima Nuclear Power Plants on Marine Radioactivity. *Environ. Sci. Technol.* **2011**, *45* (23), 9931–9935.
- (8) Kaneyasu, N.; Ohashi, H.; Suzuki, F.; Okuda, T.; Ikemori, F. Sulfate Aerosol as a Potential Transport Medium of Radiocesium from the Fukushima Nuclear Accident. *Environ. Sci. Technol.* **2012**, *46* (11), 5720–5726.
- (9) Badawi, M.; Xerri, B.; Canneaux, S.; Cantrel, L.; Louis, F. Molecular Structures and Thermodynamic Properties of 12 Gaseous Cesium-Containing Species of Nuclear Safety Interest: Cs<sub>2</sub>, CsH, CsO, Cs<sub>2</sub>O, CsX, and Cs<sub>2</sub>X<sub>2</sub> (X=OH, Cl, Br, and I). *J. Nucl. Mater.* **2012**, *420* (1–3), 452–462.
- (10) Paquette, J.; Torgerson, D. F.; Wren, J. C.; Wren, D. J. Volatility of Fission Products during Reactor Accidents. *J. Nucl. Mater.* **1985**, *130*, 129–138.



- (11) Lin, C. C.; Wang, C. F.; Sun, Y. C.; Chao, J. H.; Tseng, C. L. Radiation Effects on Gaseous Iodine at Very Low Concentrations &lt;/P&gt; &lt;/P&gt; *J. Radioanal. Nucl. Chem.* **2006**, *268* (2), 419–424.
- (12) Kissane, M. P.; Mitrakos, D.; Housiadas, C.; Sabroux, J. C. Investigation of Thermo-Catalytic Decomposition of Metal-Iodide Aerosols due to Passage through Hydrogen Recombiners. *Nucl. Eng. Des.* **2009**, *239* (12), 3003–3013.
- (13) Nagai, H.; Terada, H.; Katata, G.; Yamazawa, H. Preliminary Estimation of Release Amounts of <sup>131</sup>I and <sup>137</sup>Cs Accidentally Discharged from the Fukushima Daiichi Nuclear Power Plant into the Atmosphere. *J. Nucl. Sci. Technol.* **2011**, *48* (7), 1129–1134.
- (14) OECD NEA/CSNI/R. State-of-the Art Report on Iodine Chemistry. 2007.
- (15) Soffer, L.; Burson, S. B.; Ferrell, C. M.; Lee, R. Y.; Ridgely, J. N. Accident Source Terms for Light-Water Nuclear Power Plants. *NUREG-1465* **1995**, 6.
- (16) Sudolská, M.; Cantrel, L.; Černušák, I. Microhydration of Caesium Compounds: Cs, CsOH, CsI and Cs<sub>2</sub>I<sub>2</sub> Complexes with One to Three H<sub>2</sub>O Molecules of Nuclear Safety Interest. *J. Mol. Model.* **2014**, *20* (4).
- (17) Chatelard, P.; Reinke, N.; Arndt, S.; Belon, S.; Cantrel, L.; Carenini, L.; Chevalier-Jabet, K.; Cousin, F.; Eckel, J.; Jacq, F.; et al. ASTEC V2 Severe Accident Integral Code Main Features, Current V2.0 Modelling Status, Perspectives. *Nucl. Eng. Des.* **2014**, *272*, 119–135.
- (18) Šulková, K.; Cantrel, L.; Louis, F. Gas-Phase Reactivity of Cesium-Containing Species by Quantum Chemistry. *J. Phys. Chem. A* **2015**, *119* (35), 9373–9384.
- (19) NEA/CSNI/R(2016)5. International Iodine Workshop Full Proceedings. *Incl. Append.* **2016**, 1.
- (20) Colombani, J.; Pascal, C.; Monchalain, N.; Martinet, L.; Gomez, C. Experimental Study of Organic Iodide Volatilization from Painted Surfaces Present in the Containment during a Severe Accident. In *Proceedings of the 6th European Review Meeting on Severe Accident Research, Avignon, 2-4 October, France*; 2013.
- (21) Finlayson-Pitts, B. J. The Tropospheric Chemistry of Sea Salt: A Molecular-Level View of the Chemistry of NaCl and NaBr. *Chem. Rev.* **2003**, *103* (12), 4801–4822.
- (22) Yang, Y.; Meng, S.; Wang, E. G. Water Adsorption on a NaCl (001) Surface: A Density Functional Theory Study. *Phys. Rev. B* **2006**, *74* (24).
- (23) Hafner, J. *Ab-Initio* Simulations of Materials Using VASP: Density-Functional Theory and beyond. *J. Comput. Chem.* **2008**, *29* (13), 2044–2078.
- (24) Kresse, G.; Furthmüller, J. Efficiency of *Ab-Initio* Total Energy Calculations for Metals and Semiconductors Using a Plane-Wave Basis Set. *Comput. Mater. Sci.* **1996**, *6* (1), 15–50.
- (25) Kresse, G.; Joubert, D. From Ultrasoft Pseudopotentials to the Projector Augmented-Wave Method. *Phys. Rev. B* **1999**, *59* (3), 1758–1775.
- (26) John P. Perdew, Kieron Burke, Matthias Ernzerhof. Generalized Gradient Approximation Made Simple.pdf. *Phys. Rev. Lett.* 1996, pp 3865–3868.

- (27) Hendrik J. Monkhorst and James D. Pack. Special Points for Brillouin-Zone Integrations.pdf. *Physical Review B*. 1989, p 3616.
- (28) Kebede, G. G.; Spångberg, D.; Mitev, P. D.; Broqvist, P.; Hermansson, K. Comparing van Der Waals DFT Methods for Water on NaCl(001) and MgO(001). *J. Chem. Phys.* **2017**, *146* (6), 064703.
- (29) Tkatchenko, A.; Scheffler, M. Accurate Molecular Van Der Waals Interactions from Ground-State Electron Density and Free-Atom Reference Data. *Phys. Rev. Lett.* **2009**, *102* (7), 073005.
- (30) Bučko, T.; Lebègue, S.; Hafner, J.; Ángyán, J. G. Improved Density Dependent Correction for the Description of London Dispersion Forces. *J. Chem. Theory Comput.* **2013**, *9* (10), 4293–4299.
- (31) Bučko, T.; Lebègue, S.; Ángyán, J. G.; Hafner, J. Extending the Applicability of the Tkatchenko-Scheffler Dispersion Correction via Iterative Hirshfeld Partitioning. *J. Chem. Phys.* **2014**, *141* (3), 034114.
- (32) Hendrik J. Monkhorst and James D. Pack. Special Points for Brillouin-Zone Integrations. *Physical Review B*. June 15, 1976.
- (33) Satpathy, S. Electron Energy Bands and Cohesive Properties of CsCl, CsBr, and CsI. *Phys. Rev. B* **1986**, *33* (12), 8706.
- (34) Reuter, K.; Scheffler, M. Composition and Structure of the RuO<sub>2</sub> (110) Surface in an O<sub>2</sub> and CO Environment: Implications for the Catalytic Formation of CO<sub>2</sub>. *Phys. Rev. B* **2003**, *68* (4).
- (35) Geysmans, P.; Finocchi, F.; Goniakowski, J.; Hacquart, R.; Jupille, J. Combination of (100), (110) and (111) Facets in MgO Crystals Shapes from Dry to Wet Environment. *Phys. Chem. Chem. Phys.* **2009**, *11* (13), 2228.
- (36) Henkelman, G.; Uberuaga, B. P.; Jónsson, H. A Climbing Image Nudged Elastic Band Method for Finding Saddle Points and Minimum Energy Paths. *J. Chem. Phys.* **2000**, *113* (22), 9901.
- (37) Henkelman, G.; Jónsson, H. Improved Tangent Estimate in the Nudged Elastic Band Method for Finding Minimum Energy Paths and Saddle Points. *J. Chem. Phys.* **2000**, *113* (22), 9978–9985.
- (38) Wulff, G. XXV. Zur Frage Der Geschwindigkeit Des Wachstums Und Der Auflösung Der Krystallflächen. *Z. Für Krist. - Cryst. Mater.* **2015**, *34* (1–6), 449–530.
- (39) Zucker, R. V.; Chatain, D.; Dahmen, U.; Hagège, S.; Carter, W. C. New Software Tools for the Calculation and Display of Isolated and Attached Interfacial-Energy Minimizing Particle Shapes. *J. Mater. Sci.* **2012**, *47* (24), 8290–8302.
- (40) Meyer, H.; Entel, P.; Hafner, J. Physisorption of Water on Salt Surfaces. *Surf. Sci.* **2001**, *488* (1–2), 177–192.
- (41) Cabrera-Sanfelix, P.; Holloway, S.; Darling, G. R. Monolayer Adsorption of Water on NaCl(100). *Appl. Surf. Sci.* **2007**, *254* (1), 87–91.

- (42) Riggs, C. A.; Tompson, R. V.; Ghosh, T. K.; Loyalka, S. K.; Viswanath, D. S. Water Adsorption Isotherms for Charged and Uncharged Cesium Iodide Aerosol Particles. *Nucl. Technol.* **2007**, *157* (1), 74–86.
- (43) Foster, M. C.; Ewing, G. E. Adsorption of Water on the NaCl(001) Surface. II. An Infrared Study at Ambient Temperatures. *J. Chem. Phys.* **2000**, *112* (15), 6817–6826.
- (44) National Research Council (U.S.); Washburn, E. W.; West, C. J. *International Critical Tables of Numerical Data, Physics, Chemistry and Technology*; Pub. for the National research council by the McGraw-Hill Book Company, Inc.: New York, 1926.
- (45) Xu, L.; Lio, A.; Hu, J.; Ogletree, D. F.; Salmeron, M. Wetting and Capillary Phenomena of Water on Mica. *J. Phys. Chem. B* **1998**, *102* (3), 540–548.
- (46) Goldman, N.; Fellers, R. S.; Brown, M. G.; Braly, L. B.; Keoshian, C. J.; Leforestier, C.; Saykally, R. J. Spectroscopic Determination of the Water Dimer Intermolecular Potential-Energy Surface. *J. Chem. Phys.* **2002**, *116* (23), 10148.
- (47) Finlayson-Pitts, B. J.; Ezell, M. J.; Pitts, J. N. Formation of Chemically Active Chlorine Compounds by Reactions of Atmospheric NaCl Particles with Gaseous N<sub>2</sub>O<sub>5</sub> and ClONO<sub>2</sub>. *Nature* **1989**, *337*, 241–244.
- (48) Ravishankara, A. R. Heterogeneous and Multiphase Chemistry in the Troposphere. *Science* **1997**, *276* (5315), 1058–1065.
- (49) Behnke, W.; Zetzsch, C. Heterogeneous Photochemical Formation of Cl Atoms from NaCl Aerosol, NO<sub>x</sub> and Ozone. *J. Aerosol Sci.* **1990**, *21*, S229–S232.
- (50) Finlayson-Pitts, B. J. Reaction of NO<sub>2</sub> with NaCl and Atmospheric Implications of NOCl Formation. *Nature* **1983**, *306* (5944), 676–677.
- (51) Karlsson, R.; Ljungström, E. A Laboratory Study of the Interaction of NH<sub>3</sub> and NO<sub>2</sub> with Sea Salt Particles. *Water, Air, Soil Pollut.* *103* (1–4), 55–70.



# **Chapter IV: Chapter 4: Reactivity of Silver Iodide (AgI)**

## IV.1 Introduction

Silver iodide (AgI) is an inorganic compound, which is used widely in cloud seeding and also in manufacturing photosensitive materials. Beside these applications, AgI is one of the possible iodide aerosols produced after a severe accident in a nuclear power plant. Unlike the CsI compounds AgI is almost insoluble which may induce a different behavior.

Large number of studies investigate theoretically and experimentally the electronic structure and properties of silver halides<sup>1-8</sup>. Gordienko et al.<sup>1</sup> performed theoretical study, using linear response method, on lattice dynamics of three silver halides including AgI. Two phase of AgI has been studied which are  $\gamma$ - (a zinc blende structure<sup>6</sup>) and  $\beta$ -phases (wurtzite structures). Catti<sup>5</sup> performed theoretical study in order to understand the phase transitions of AgI. A transition from the blende to tetragonal antilitharge structure is observed at room temperature and pressure of 0.3 GPa. A second transition to a wurtzite structure occurs when pressure increases to 0.4 GPa, while inverse transformation from wurtzite to zinc blende occurs at normal pressure and temperature of 420 K. Hull et al.<sup>7</sup> observed a transformation to AgI rocksalt (KOH type) at higher pressure (11.3 GPa). On the other hand, Waldbaum<sup>9</sup> deduced experimentally that  $\beta$ -AgI structure is the most stable one at RT and 1 atm. Experimental work<sup>10</sup>, in 1964, compared the adsorption of water vapor on AgI prepared either by direct reaction (between metallic silver and iodine) or by precipitation (starting by AgNO<sub>3</sub> and NH<sub>4</sub>I) at 30 °C. The results show huge amount of water molecules adsorbed on AgI prepared by precipitation which contains hygroscopic impurities, and only with small amounts adsorbed on the AgI prepared by direct reaction without any hygroscopic impurities demonstrating the importance of the AgI purity on its properties as well as low chemical affinity of H<sub>2</sub>O with pure AgI. In the RCS in case of nuclear severe accident, AgI is probably formed at high temperature (around 1000 °C) by reactions between metallic and/or oxidized silver particles and iodine atoms and/or HI. It means that nuclear AgI aerosol should be close to pure AgI.

Shevkunov<sup>8</sup> used classical molecular dynamics to study the behavior of steam filled in flat split in  $\beta$ -AgI crystal. Crystal surface model on one side contains Ag<sup>+</sup> cations while the other one contains I<sup>-</sup> anions. Interaction of water molecules with the surfaces differs between the two terminations. On the former, the cohesion between water molecules and crystal surface takes place by interaction between hydrogen atoms and iodine anions located in the second layer,

whereas in the latter one, it takes place by interaction between oxygen atoms and silver cations in the second layer also. It means that water molecules are held on the surface by interaction with the second layer of the substrate not the first one. This result is relatively unexpected. Higher level calculations are needed to confirm this point. In this chapter, theoretical calculations have been carried out to investigate the mechanism of iodine formation from AgI surfaces. In the first part, we studied the stability of the surface in dry atmosphere and determined the shape of the aerosol nanoparticles. In a second part, we first studied the role of water and next mechanisms that may be responsible for the release of Iodine in gaseous phase, taking into account the possible role of oxidizing agent formed under radiation.

## IV.2 Theoretical parameters of AgI

Calculation method in this part is the same as the previous one, as well as the efficiency criteria. The electron configurations [Kr] 4d<sup>10</sup> 5s<sup>1</sup>, [Kr] 4d<sup>10</sup> 5s<sup>2</sup> 5p<sup>5</sup>, [He] 2s<sup>2</sup> 2p<sup>4</sup> and 1s<sup>1</sup> were used for silver, iodine, oxygen and hydrogen respectively. Test Calculations were done by varying cut-off energy from 200 to 600 eV and the k-points mesh from 1× 1× 1 to 11x11x11 following Monkhorst-Pack32 schemes to define calculation parameters (cf SI). From these evaluations, all the bulk and surface calculations were performed with a 450 eV cut-off energy, a 5x5x5 kpoint mesh for bulk calculations, and 5x5x1 one for all surface calculations.

AgI crystal has a hexagonal structure which belongs to the P63mc S space group, with four atoms in the unit cell (see Figure IV-1). The volume of the cell is 137.2 Å<sup>3</sup> (cell size is 4.59 Å \*4.59 Å \*7.52 Å while  $\alpha$ ,  $\beta$  and  $\gamma$  are 90°, 90° and 120°, respectively).

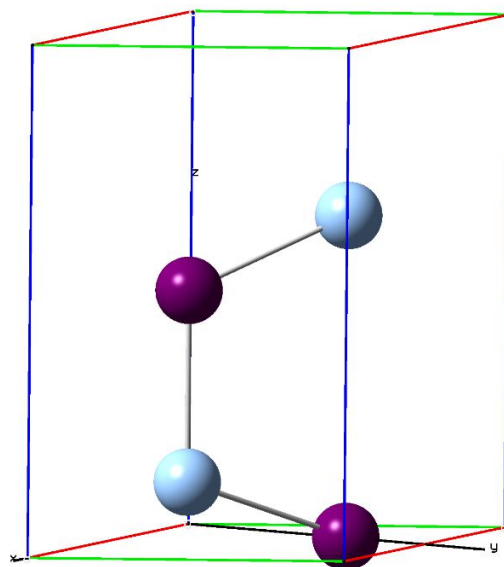


**Figure IV-1: Unit cell of AgI crystal (Ag and I are respectively colored in bright blue and purple).**

A supercell composed of eight AgI layers was used for our calculations. The four outermost layers were allowed to relax to take into account the surface formation, while the rest layers were kept fixed to mimic bulk constraints. We added 15 Å of vacuum between two consecutive slabs to avoid interactions between them. Unit cell of AgI crystal (Ag and I are respectively colored in bright blue and purple).

### **IV.3 Surface energy**

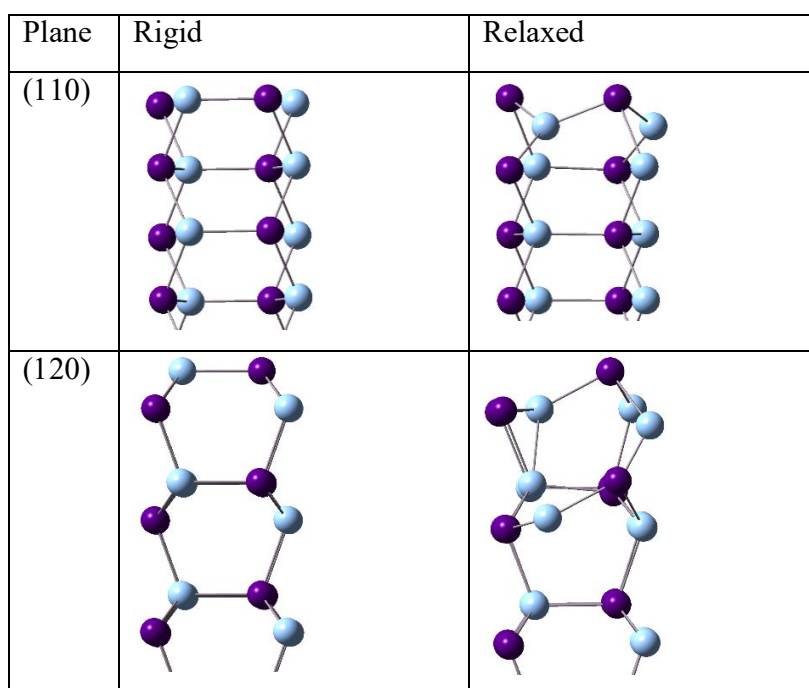
According to the calculated surface energies (Table IV-1) the most stable low index planes for AgI are (100), (110), (120) and (001). All these surfaces are non-polar surfaces and end up with the two types of ions  $\text{Ag}^+$  and  $\text{I}^-$ . After relaxation, we noticed large reconstruction in some planes (110, 120 and 100) for atoms on the surface unlike the CsI case where we didn't notice any relaxation on the surface.



**Table IV-1: Surface energy of the exposed surfaces.**

	(110)	(120)	(100)	(001)
<b>Rigid</b> $\gamma(\text{mJ.m}^{-2})$	300	307	286	416
<b>Relaxed</b> $\gamma(\text{mJ.m}^{-2})$	109	119	114	413
<b>Relaxation Percentage (%)</b>	64	61	60	1

Figure IV-2 shows side view of the studied surfaces before and after relaxation. All surfaces were modeled by orthorhombic cell except for (001) surface which was studied in a hexagonal ( $\gamma=120^\circ$ ) cell. The non-polar, (110), (100) and (001) surfaces contain four atoms (two silver and two iodine atoms) while the (120) has six atoms on the surface.



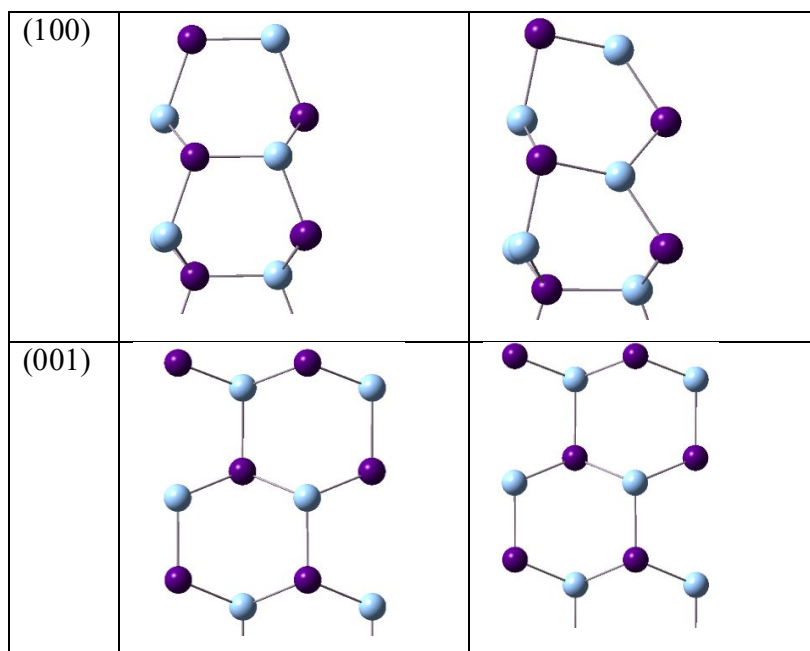


Figure IV-2. Side view of the low index surfaces of AgI. (Ag and I are respectively colored in bright blue and purple).

Table IV-2. Atomic displacements after relaxation in Å.

Direction	Label	x	y	z
(110)	Ag1	-0.29	0.53	-0.65
	Ag2	-0.29	0.53	-0.65
	I1	0.03	-0.11	-0.34
	I2	0.03	0.11	-0.34
(120)	Ag1	-0.41	-0.31	0.76
	Ag2	0.04	0.28	-0.19
	Ag3	0.66	-0.30	0.56
	I1	0.04	0.02	-0.32
	I2	0.01	0.13	-0.19
	I3	0.17	0.02	-0.32
(100)	Ag1	0.23	-0.45	0.93
	I1	-0.11	-0.09	-0.43

The (110) surface was modeled in a 1x1 cell (7.514 Å x 7.96397 Å x 57.59 Å). Surface relaxation analysis (cf. Table IV-2) shows that silver atoms relax inward by 0.65 Å whereas iodine atoms relax outward by 0.34 Å. Less important relaxations appeared in x and y directions. The cell size used to model the (120) surface are: 12.165 Å x 7.51 Å x 41.07 Å. Like the (110) case, two silver atoms relax inwardly by almost half angstrom whereas two iodine atoms relax outwardly by 0.32 Å. More important relaxation in x and y directions for silver atoms than in the (110) case. The (100) and (001) surfaces are respectively modeled in cells of 9.196 Å x 7.514 Å x 40.332 Å and 9.195 Å x 4.598 Å x 50.055 Å. For (100), upper silver atom relaxes inwardly by about one angstrom while the iodine atom relaxes inwardly by 0.43 Å. In (001), all surface atoms relax outward by the same distance 0.3 Å and with almost no relaxation in x and y directions.

For these surfaces we calculate the surface energy in similar way as for the CsI crystal. In Table IV-1, the energies of the rigid and relaxed surfaces are reported, and the relative relaxation energy percentages. Surface energy of the relaxed planes range in the following order: (110) < (100) < (120) < (001). (110), (100) and (120) are stable surfaces of AgI. These surfaces show high relaxation energy percentage (~ 60%), which is in agreement with our previous discussion that reported great surface relaxation for these planes.

Nanocrystal shape of AgI will be formed mainly from (110), (120) and (100) planes which are of lower energy, while (001) has very high surface energy which means its existence is not very probable. Figure IV-3 presents the shape of the particle according to Wulff model, (110) and (100) are the main planes. (001) plane has the highest energy while it exists in the particle shape, this

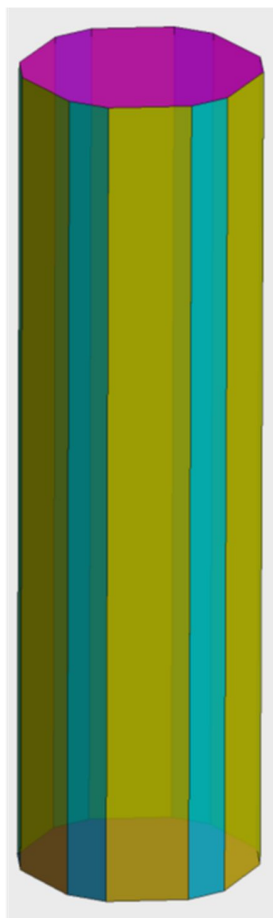


**Figure IV-3. Wulff shape of the AgI particle (110, 100 and 001 are respectively colored in yellow, blue and violet, while 120 plane doesn't exist).**

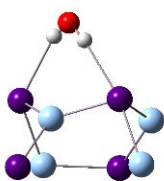
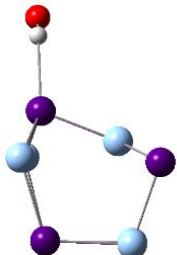
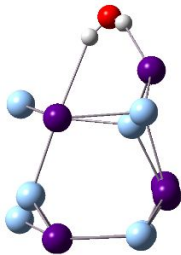
## **IV.4 Water adsorption on AgI surfaces.**

To study surface reactivity, we started by adsorbing one water molecule on the surfaces. Molecular and dissociative adsorption modes were tested on the three stable surfaces of AgI. For each adsorption mode, different starting geometries were tested to get the most favored optimized geometry. In the second step, we have added water molecules successively until we reach one monolayer of water on top of the surfaces. We present in this part the geometries for one molecule, half and one monolayer of water with their corresponding adsorption and interaction energies.

#### IV.4.1 Associative adsorption of one water molecule on AgI surfaces

Starting by molecular adsorption of one water molecule on the surface, we tested different interaction types. For the first one, hydrogen atom of the water molecule interacts with iodine ion (H-I) on the surface while, in the second case, we study the interaction between oxygen atom of the water molecule with one silver ion (O-Ag) from the surface. H-I interaction has been studied by sitting the water molecule almost normal to the surface with an H-I distance around 2.9 Å for all surfaces with H atom pointing toward I<sup>-</sup> ion on the surface. For the O-Ag interaction, the water molecule is parallel to the surface with an O-Ag distance of about 2.6 Å, the O atom being in top position of Ag<sup>+</sup> ion. Geometrical parameters of the optimized water molecule are very similar to the gas phase ones (H-O-H angle about 105° and H-O bond about 0.98 Å). Hydrogen bonded water molecule adsorption on the surfaces does not induce important relaxation in the upper layer of AgI crystal. While in the other case, interacting Ag<sup>+</sup> ion moved up around 0.5 Å in the three surfaces reflecting the high flexibility of the surfaces already noted on the bare surfaces.

Adsorption energy for the H-I interaction is about 0.1 eV for the three surfaces (Figure IV-4) while they are higher than 0.2 eV for the second orientation. It means that the main interaction is O-Ag<sup>+</sup>.

Surface direction	(110)	(100)	(120)
H-I interaction (in eV)	 <p style="text-align: center;"><b>0.10</b></p>	 <p style="text-align: center;"><b>0.12</b></p>	 <p style="text-align: center;"><b>0.10</b></p>

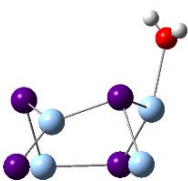
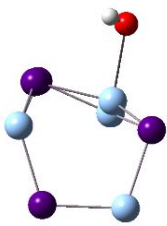
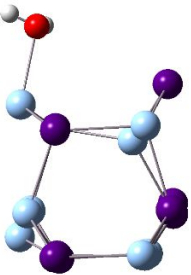
<b>O-Ag interaction (in eV)</b>			
	<b>0.32</b>	<b>0.24</b>	<b>0.20</b>

Figure IV-4. Molecular adsorption geometries and energies of one water molecule on the stable surfaces of AgI (Ag, I, H and O are respectively colored in bright blue, purple, red and white).

#### IV.4.2 Dissociative adsorption of one water molecule on AgI surfaces

Dissociative adsorption has been also studied for the three surfaces. Before optimization, one proton placed about 1.6 Å on top of I while the OH group set on top of Ag at distance around 2.6 Å. After optimization, the calculated adsorption energy is almost about -3.0 eV, see Figure IV-5, for all surfaces which indicated an highly endothermic adsorption that is non-favored. So dissociation of water on AgI stable surfaces is not probable.

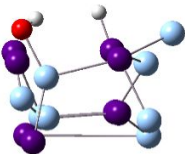
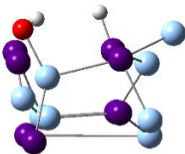
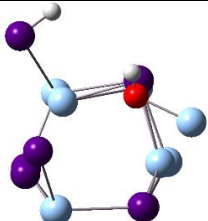
<b>Surface direction</b>	<b>(110)</b>	<b>(100)</b>	<b>(120)</b>
<b>Energy of dissociative adsorption (in eV)</b>	 <b>-3.21</b>	 <b>-2.79</b>	 <b>-2.83</b>

Figure IV-5. Dissociative adsorption geometries and energies of one water molecule on the stable surfaces of AgI (Ag, I, H and O are respectively colored in bright blue, purple, red and white).

### IV.4.3 Temperature and pressure dependence on the associative adsorption of water on AgI surfaces

In order to study the effect of temperature and pressure on the adsorption of water on AgI surfaces, we have calculated Gibbs free energy using as input the adsorption energy of one water molecule on (110) surface in the case of Ag-O interaction ( $E_{\text{ads}} = 0.32$  eV). The stability plot, including the thermodynamic correction (cf Chapter III.2.2.2), plot is shown in. Figure IV-6, adsorption can happen only at very low temperature (200 K curve) while it is not possible at room temperature and standard pressure. These results demonstrate that no water will be adsorbed on the AgI surface at temperature pressure representatives of the containment in severe accident conditions.

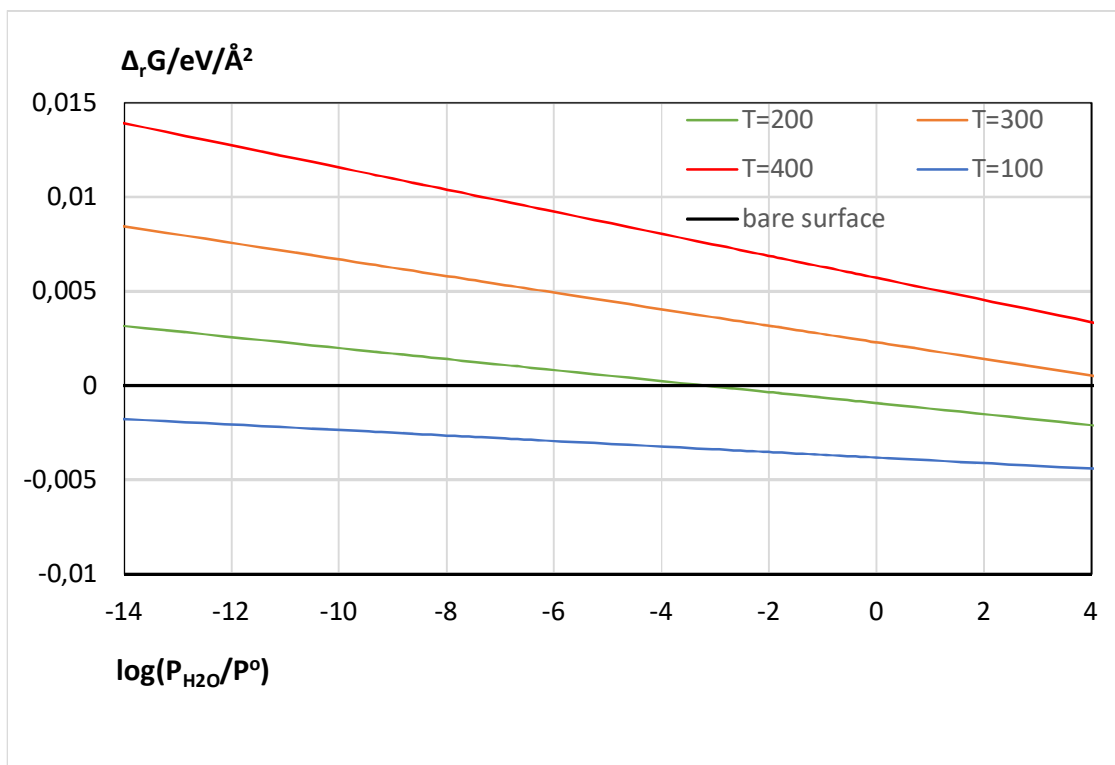


Figure IV-6. Gibbs free energy plot for associative adsorption of water on AgI (110) surface.

#### IV.4.4 Half and one monolayer adsorption of water on AgI surfaces

##### surfaces

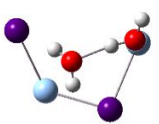
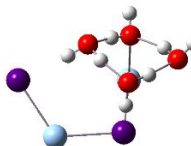
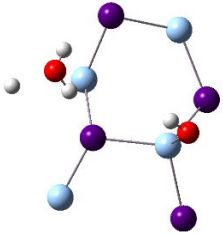
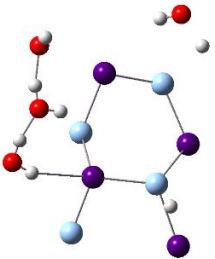
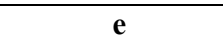
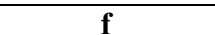
Water molecules were added successively on each AgI surfaces to reach half and one monolayer. All the configurations are presented in Figure IV-7. The adsorption interaction energies were calculated according to the following equation:

$$E_{\text{ads}} = E_{(\text{AgI} + n \text{H}_2\text{O})} - n \times E_{\text{H}_2\text{O}} - E_{\text{AgI}}$$

Whereas  $E_{(\text{AgI} + \text{H}_2\text{O})}$ ,  $n \times E_{\text{H}_2\text{O}}$ ,  $E_{\text{AgI}}$  are the energies of the adsorption cell, 'n' separate water molecules in gas phase and energy of AgI substrate respectively. Moreover, water-water and surface-water interactions were calculated according to the following formulas respectively:

$$E_{\text{w}_w} = E_{\text{water polymer}} - n \times E_{(\text{H}_2\text{O})_{\text{gas}}}$$

$$E_{\text{s}_w} = E_{\text{ads}} - E_{\text{ww}}$$

	Half monolayer	One monolayer
(110)	<p>a</p> 	<p>b</p> 
(100)	<p>c</p> 	<p>d</p> 
(120)	<p>e</p> 	<p>f</p> 



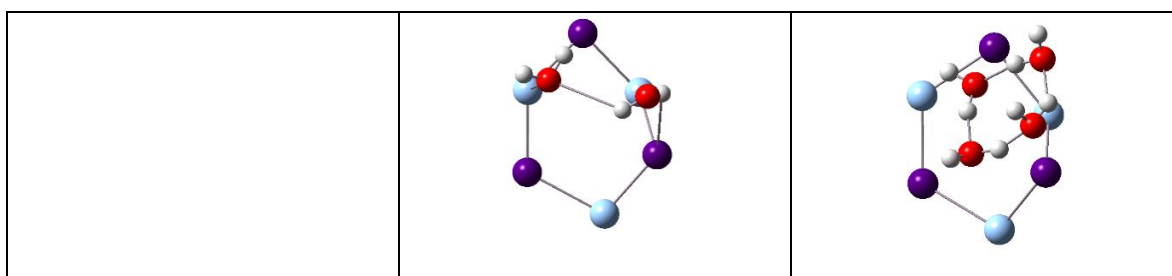


**Figure IV-7. Adsorption of half and one monolayer of water on the stable surfaces of AgI (Ag, I, H and O are respectively colored in bright blue, purple, red and white).**

Surface	Half monolayer (2 H <sub>2</sub> O)			One monolayer (4 H <sub>2</sub> O)		
	(110)	(100)	(120)	(110)	(100)	(120)
<b>E<sub>ads</sub>(eV)</b>	0.60	0.71	0.41	1.74	2.09	1.50
<b>E<sub>w-w</sub>(eV)</b>	0.25	0.22	0.18	1.36	1.37	1.33
<b>E<sub>s-w</sub>(eV)</b>	0.35	0.49	0.23	0.38	0.72	0.17

**Table IV-3. Adsorption and interaction energies for half and one monolayer coverage on the stable surfaces of AgI.**

**Table IV-3** contains the calculated energies for half and one monolayer adsorption on water for the stable surfaces of AgI with the corresponding geometries in **Figure IV-7**.

Starting by the half monolayer case, we have two water molecules on the surface which interact together and with the surface in the same time. Adsorption on (100) is the most favored one ( $\Delta rE = 0.71$  eV) and followed by (110) and (120) with interaction energies equal to 0.60 and 0.41 eV, respectively. Water-water interaction energy is almost the same for the three surfaces with energy close to 0.20 eV; the differences appear to be due to the surface-water interaction contribution.

On the other hand, adding more water molecules on the surface will favor the water-water interaction instead of the surface-water part. This fact appears in the water-water interaction which is the dominant part of the interaction energy. The (100) surface has the lowest interaction energy (2.09 eV, i.e. larger adsorption energy) with a water-water energy of 1.37 eV and a surface water one of 0.72 eV, which means that interactions between water molecules are the most important one. Same conclusion can be drawn for all other surfaces since the energies are comparable with (100) surface. Orientation of water molecules presented in **Figure IV-7** (d, b

and f) shows that each proton of a water molecule is directed toward oxygen of the neighboring one with distance about 1.8 Å which is the typical distance between interacting water molecules.

#### **IV.4.5 Conclusion concerning adsorption of water on AgI surfaces**

From all our previous results it can be concluded that interactions between water molecule and AgI surfaces are very weak. Adding more water molecules on the surface will enhance interaction between water molecules itself instead of interaction with the surface ( $E_{w-w}$  is about 40% of the  $E_{ads}$  for the half-monolayer case while it's about 80% of  $E_{ads}$  in the one monolayer adsorption). So we can say that *chemistry of AgI crystal happen in severe accident conditions on the bare surface without any water molecules.*

### **IV.5 Reactivity of AgI**

In the second part of our study, we investigate the possible formation of volatile iodine species from the stable surfaces of AgI. As for the CsI case, the formation of different species, i.e. AgI, HI, IOH and I<sub>2</sub> were taken into account in our studies. In this part, we will restrict this study on AgI (110) surface since all stable surfaces are similar and lead to similar chemistry processes. We will discuss the formation of chemical species from clean surface and later by oxidizing it (irradiation conditions) separately to draw a general conclusion at the end.

#### **IV.5.1 Reactivity without oxidant**

##### **IV.5.1.1 Formation of AgI and I<sub>2</sub> molecules from clean surface**

Starting from bare surfaces, AgI molecule is released from the surface directly to the gas phase. In this process, the iodine atoms on the surface are oxidized while the silver atoms are reduced. As expected, this reaction is very endothermic ( $\Delta_r E = 2.38$  eV in **Figure IV-8**) which is not probable thermodynamically. For I<sub>2</sub>, a similar result is obtained with no possibility to form directly I<sub>2(g)</sub> ( $\Delta_r E = 3.5$  eV presented in **Figure IV-9**).

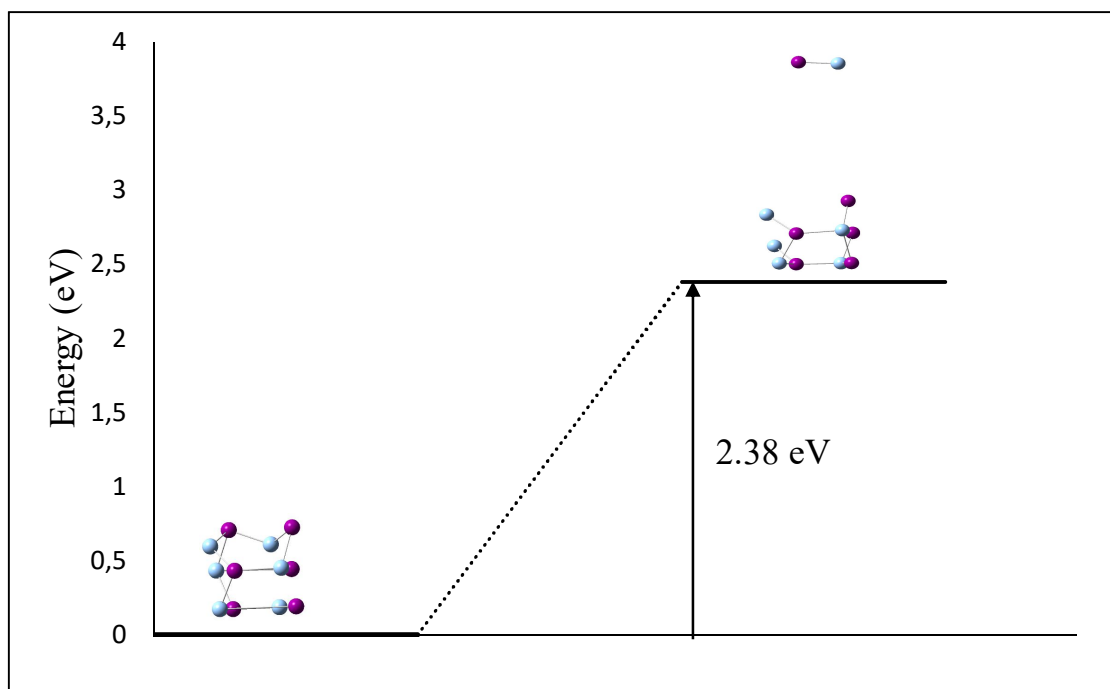


**Figure IV-8. Formation of AgI molecule from clean AgI(110) surface (Ag and I are respectively colored in bright blue and purple).**

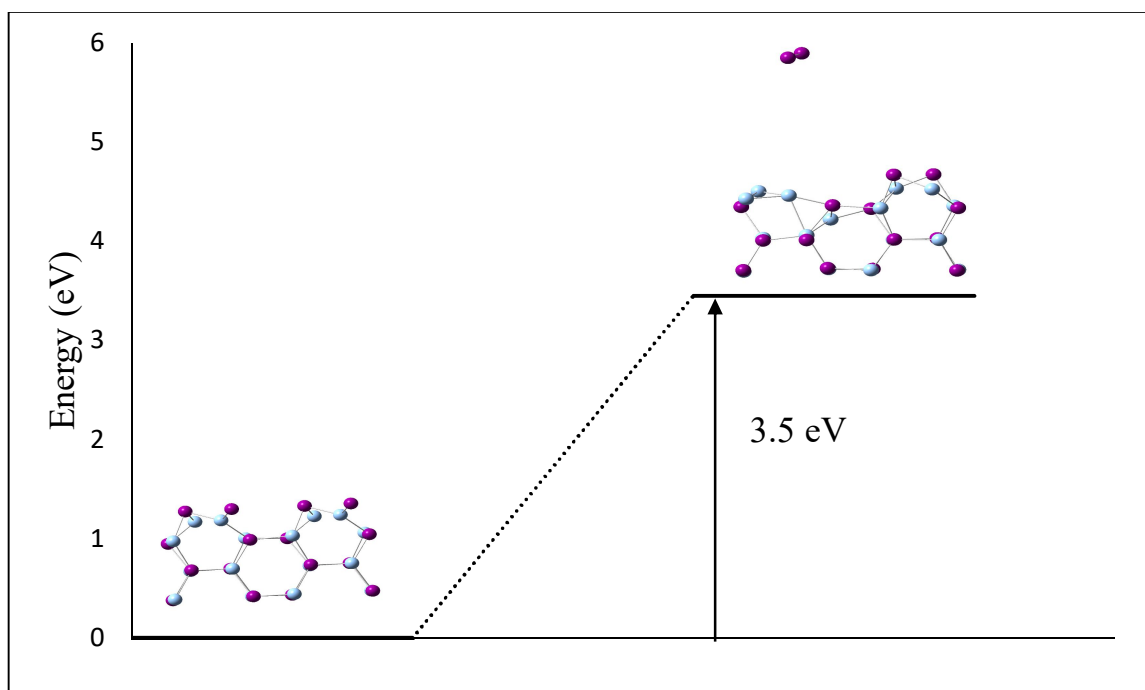


**Figure IV-9. Formation of I<sub>2</sub> molecule from clean AgI(110) surface (Ag and I are respectively colored in bright blue and purple).**

### IV.5.1.2 Formation of HI after dissociating water molecule on the surface

In second step, we studied the participation of one water molecule in the mechanism that could lead to HI formation by acid-base reaction. From the dissociated water molecule, one hydrogen interacts with iodide on the surface at a distance of 1.63 Å while the OH group on top of silver atom is located at 2.16 Å. Dissociation of water in this way on the surface is very endothermic ( $\Delta_r E = 3.0$  eV as shown in Figure IV-10) while the formation of HI molecule in the second step is exothermic reaction ( $\Delta_r E = -0.38$  eV). Thermodynamically, this reaction is not possible due to the first step (water dissociation).

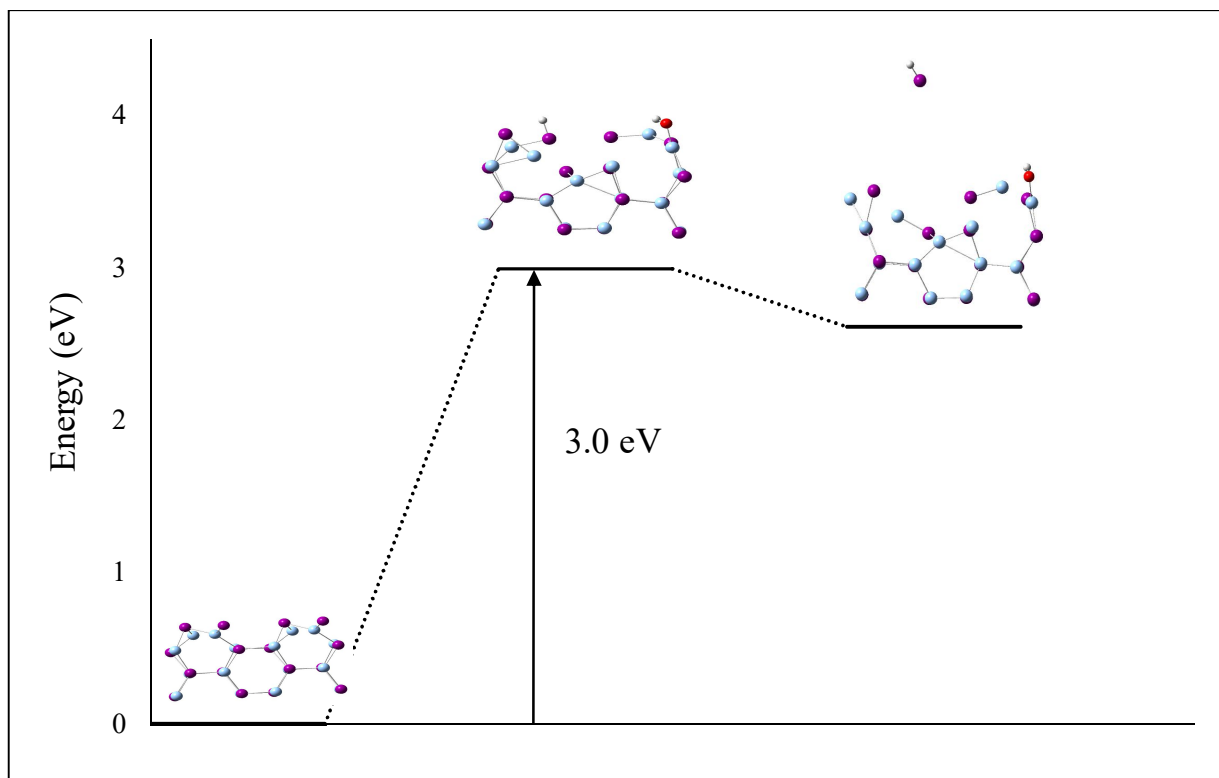


**Figure IV-10. Formation of HI molecule after dissociation of one water molecule on AgI(110) surface (Ag, I, H and O are respectively colored in bright blue, purple, red and white).**

### IV.5.2 Reactivity with oxidants

In absence of oxidants, we have showed that formation of iodine species from the surface is not favored. Thus we will oxidize the surface one and two times in order to have a possible reaction

pathway without high endothermic steps. From a chemical point of view, it's mandatory to oxidize the surface before removing I<sub>2</sub>. One of the possible oxidants that may exist after a severe accident is the OH° radicals, produced from water radiolysis.

#### IV.5.2.1 Formation of I<sub>2</sub> after oxidizing the surface with one OH° radical

Starting with a clean surface, one OH° radical adsorbed on top of Ag atom at 2.07 Å is used to oxidize it. After that, I<sub>2</sub> is formed from the surface and released into the gas phase. Addition of OH° group on the surface is exothermic ( $\Delta_r E = -1.52 \text{ eV}$  as shown in Figure IV-11) while the departure of I<sub>2</sub> is a very endothermic step which requires 2.20 eV, for the same reasons as CsI (when we remove I<sub>2</sub> we leave two electrons on the surface which requires two OH°). Then the departure of I<sub>2</sub> in presence of one OH° is not probable since its mandatory to oxidize the surface twice during the reaction.

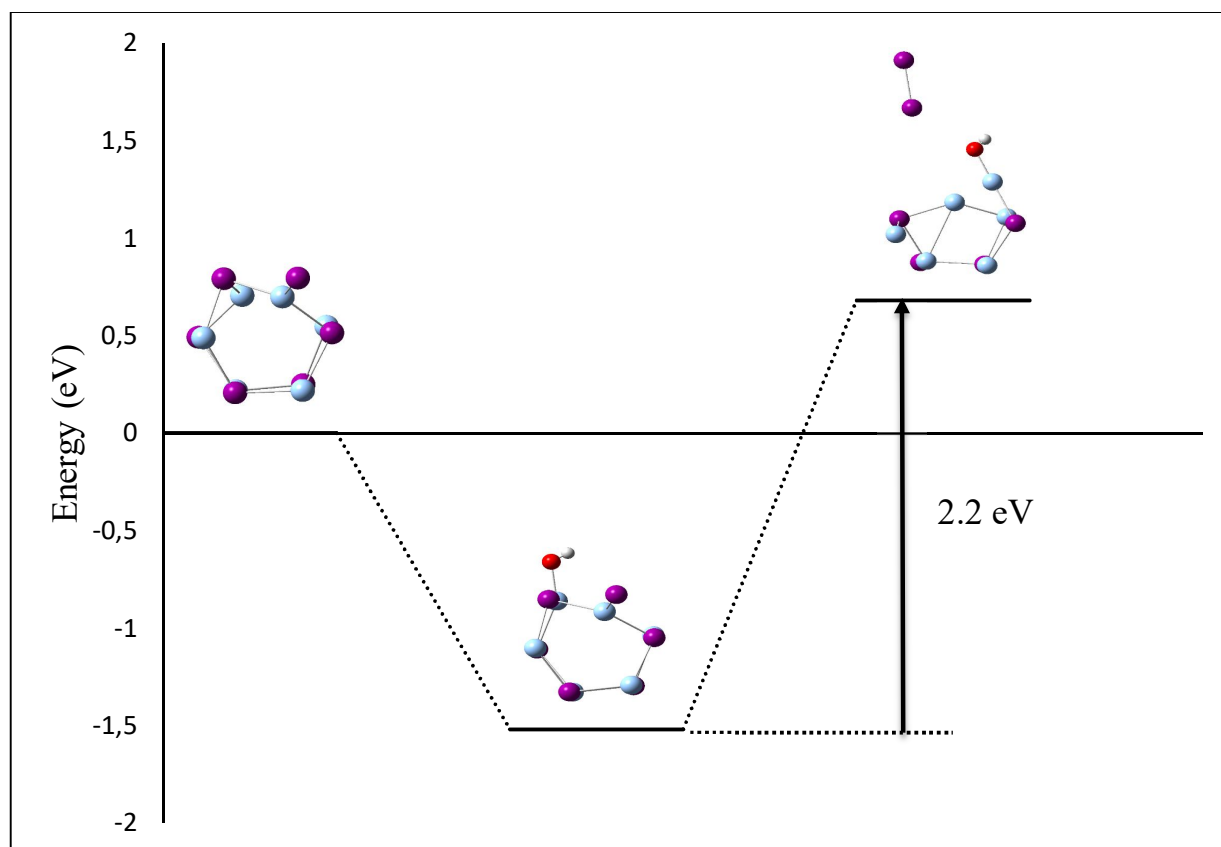


Figure IV-11. Formation of I<sub>2</sub> molecule after oxidizing the AgI(110) surface by one OH° (Ag, I, H and O are respectively colored in bright blue, purple, red and white).

## **IV.5.2.2 Formation of IOH and I<sub>2</sub> after oxidizing the surface with two OH° radicals**

### **IV.5.2.2.1 Formation of I<sub>2</sub>**

In this section, reaction pathways including two OH are investigated to avoid the Ag<sup>+</sup> oxidation on the surface. Different mechanisms have been examined to find the one with the lowest endothermic steps.

Figure IV-12 shows the identified pathway in which we oxidize the surface twice in a first step (A to B pictures) which is exothermic ( $\Delta E = -2.83$  eV). The second step corresponds to the displacement of one iodine from the surface to form IOH on top of Ag atom (B to C pictures).

Transition state of this step, shown in Figure IV-13, was found by Nudged Elastic Band theory (NEB) already described. The activation energy is 0.45 eV. The next step is to form I<sub>2</sub> on the surface. I<sub>2</sub> interacts in one side with OH and on the other side with Ag atom on the surface (geometry D). Activation energy of this step is 0.39 eV while the transition state of this step is described in Figure IV-14. Next step is the displacement of I<sub>2</sub> on the surface such that it breaks the bond with Ag and positioned almost perpendicularly to the surface (geometry E). The activation energy of for step D to E is 0.15 eV as shown in Figure IV-15.

The I<sub>2</sub> departure from the surface (E to F) requires activation energy of 0.43 eV in which its adsorption on the surface is not activated. Finally, F to G corresponds to the displacement of OH from top of the surface in order to fill the vacancy created by the missing iodine.

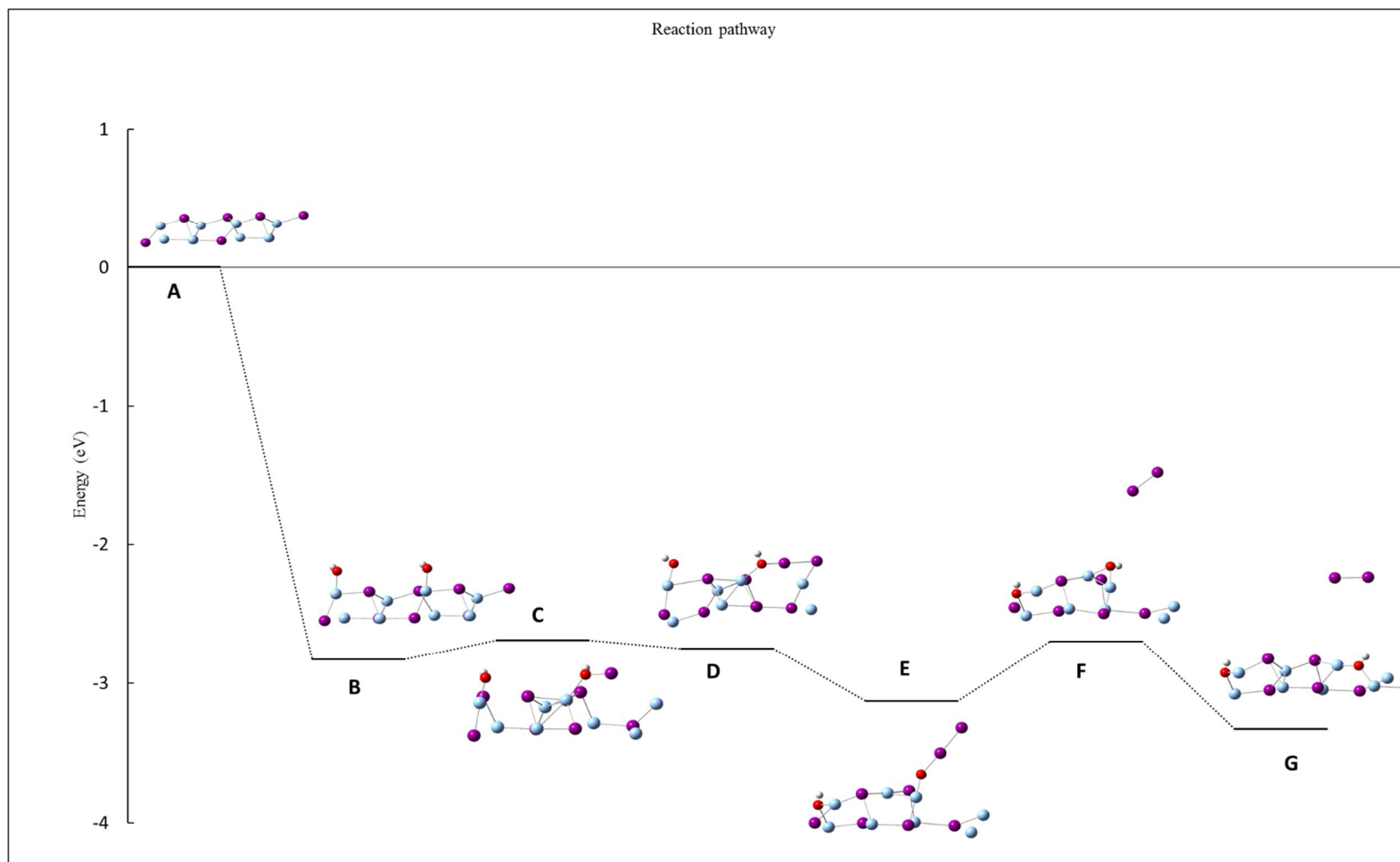


**Figure IV-12. Reaction pathway leading to the formation of I<sub>2</sub> including oxidizing the surface twice with two OH<sup>o</sup> (Ag, I, H and O are respectively colored in bright blue, purple, red and white).**





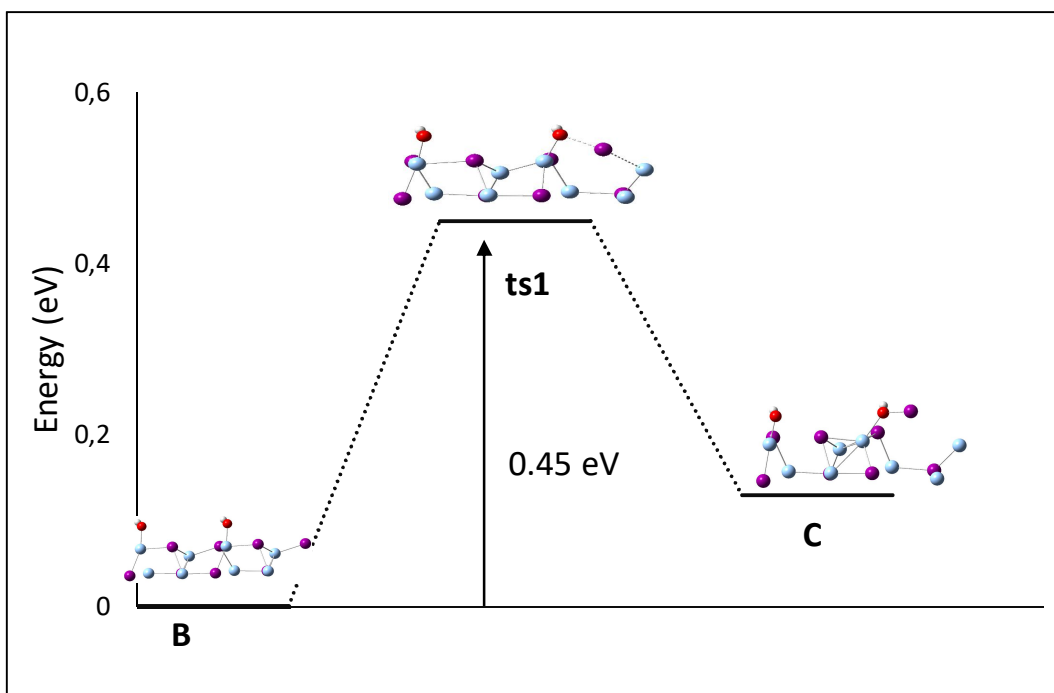


Figure IV-13. Transition state for B to C steps (Ag, I, H and O are respectively colored in bright blue, purple, red and white).

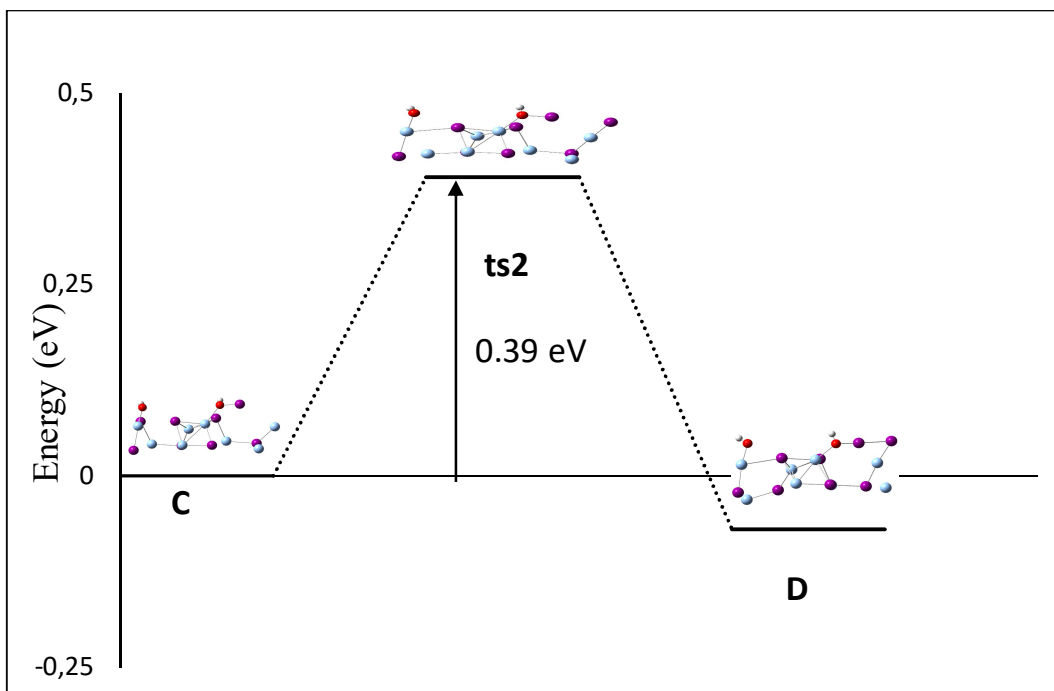
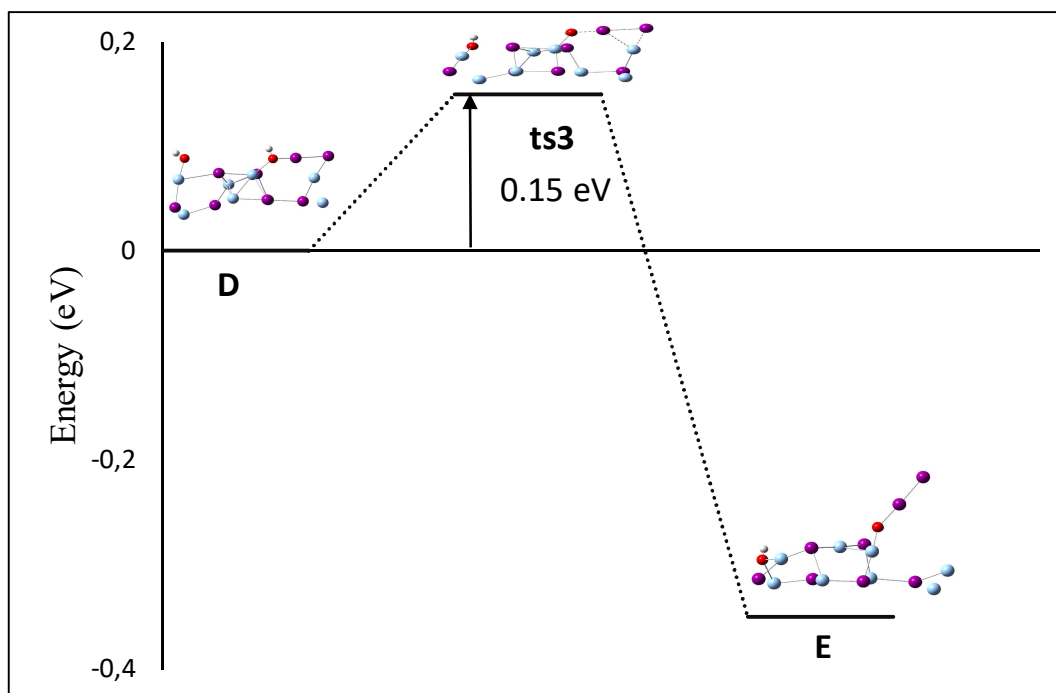


Figure IV-14. Transition state for step C to D (Ag, I, H and O are respectively colored in bright blue, purple, red and white).



**Figure IV-15: Transition state for step D to E (Ag, I, H and O are respectively colored in bright blue, purple, red and white).**

#### **IV.5.2.2.2 Formation of IOH**

The formation of IOH after oxidizing the surface twice has also been considered. The reaction pathway is presented in Figure IV-16 in which the first two steps are the same as the previous case (Figure IV-12). Formation of IOH, in step D', such that the molecule desorbed from the surface by breaking the bond with the iodine on the surface. Activation energy of this step is 0.21 eV while the transition state geometry is very similar to the final step (D'). Finally, as before, the second OH<sup>o</sup> on the surface takes the place of the displaced iodine. Then the activation energy for the formation of IOH is 0.45eV.

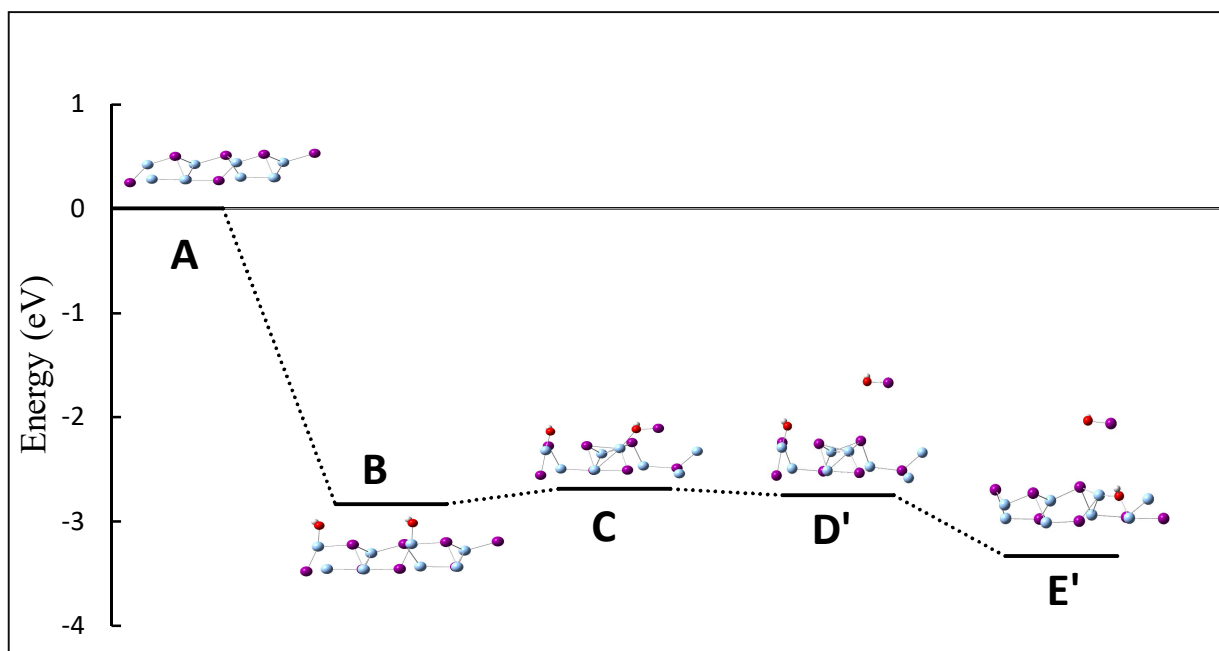


**Figure IV-16.** Reaction pathway leading to the formation of IOH including oxidizing the surface twice with two  $\text{OH}^\circ$  (Ag, I, H and O are respectively colored in bright blue, purple, red and white).

## IV.6 Conclusion

In the present chapter, we studied the chemistry of AgI nanocrystal in dry and moist atmospheres with the same organization and methods as for CsI. The Wulff construction of AgI particles, based on the relaxed energies of the low indices surfaces (100), (110) and (120) surfaces, has been established.

Water adsorbed associatively on the surface by interaction mainly between oxygen and silver on the surface with adsorption energy of 0.32, 0.24, 0.20 eV for respectively (110), (100) and (120) planes. Adsorption of half and one monolayer of water tends to show that water-water interactions are more important than water-surface interactions and it highlights that interactions between water layer and surface are very weak. Water can only be adsorbed at very low temperature. It can be noticed the formation of hydrogen bonds network between the adsorbed water molecules which tend to stabilize water layer on the surface.

Release of iodine species from AgI (110) surface was studied. Formation of  $\text{I}_2$  and AgI is not directly possible. Moreover, dissociating of water molecule on surface is very endothermic, thus HI formation is also not favored from a thermochemistry point of view. On the other hand,

formation of I<sub>2</sub> after oxidizing the surface once by OH° requires high energy ( $\Delta E = 2.20$  eV). Finally, oxidation mechanism involving the participation of two OH° seems to be the easier pathway. The activation energy for the formation of I<sub>2(g)</sub> and IOH is similar (0.45 eV). It worth noticing that formation of IOH from AgI requires lower activation energy than that from CsI surfaces (0.45 eV and 1.06 eV for ideal and with defects, respectively). IOH is well known to be an intermediate state in iodine chemistry, with a +I oxidation state and under irradiation it may react to form iodine oxides which nucleate into fine particles.

In absence of experimental data, we can expect that deposited AgI aerosol onto the containment inner walls should be oxidized as the same way that CsI, at least for the gas phase mechanism. In the STEM2 OECD project (2016-2019), a test of AgI under irradiation is planned to check this assessment but qualification tests are needed to make and label AgI aerosol with <sup>131</sup>I in order to monitor online release of gaseous iodine.

## IV.7 Bibliography:

- (1) Gordienko, A. B.; Kravchenko, N. G.; Sedelnikov, A. N. Ab Initio Calculations of the Lattice Dynamics of Silver Halides. *Russ. Phys. J.* **2010**, *53* (7), 692–697.
- (2) Vogel, D.; Krüger, P.; Pollmann, J. Ab Initio Electronic Structure of Silver Halides Calculated with Self-Interaction and Relaxation-Corrected Pseudopotentials. *Phys. Rev. B* **1998**, *58* (7), 3865.
- (3) Wilson, D. J.; Sokol, A. A.; French, S. A.; Catlow, C. R. A. Defect Structures in Silver Chloride. *J. Phys. Condens. Matter* **2004**, *16* (27), S2827–S2838.
- (4) Gordienko, A. B.; Zhuravlev, Y. N.; Poplavnoi, A. S. Electronic Structure of AgCl, AgBr, and AgI. *Phys. Status Solidi B* **1991**, *168* (1), 149–156.
- (5) Catti, M. First-Principles Landau Potential for the Rocksalt to KOH to TII-Type Phase Transitions of AgI. *Phys. Rev. B* **2006**, *74* (17).
- (6) Catti, M. Kinetic Mechanisms of the Pressure-Driven Phase Transitions of AgI. *Phys. Rev. B* **2005**, *72* (6).
- (7) Hull, S.; Keen, D. A. Pressure-Induced Phase Transitions in AgCl, AgBr, and AgI. *Phys. Rev. B* **1999**, *59* (2), 750.
- (8) Shevkunov, S. V. Structure of Water in Microscopic Fractures of a Silver Iodide Crystal. *Russ. J. Phys. Chem. A* **2014**, *88* (2), 313–319.
- (9) Waldbaum, D. R. Structural and Thermodynamic Properties of Silver Iodide, Massachusetts Institute of Technology, 1960.

(10) M. L. Corrin, Harry W. Edwards and John A. Nelson. The Surface Chemistry of Condensation Nuclei: 2. The Preparation of Silver Iodide Free of Hygroscopic Impurities and Its Interaction with Water Vapor. *Journal of the atmospheric sciences*. University of Arizona, Tucson, Ariz 1964, pp 565–567.



## **Chapter V: Reactivity in liquid phase**

## V.1 Introduction

CsI aerosols is well known to have a hygroscopic nature (while AgI is almost insoluble in water), so that part of its reactivity may be linked to aqueous reactivity phase. Thus it is important to study its reactivity in liquid phase and its dissolution in order to determine the potential relative contribution of the liquid/gas reactivities responsible of the I<sub>2</sub> release. Molecular dynamics calculations were performed to study the interaction of the CsI surface with water. This study will provide us some information about the activation energy needed to dissolve iodide in liquid phase, characterizing by some interesting steps at all stages of the dynamics.

Three different methods can be used to perform this study: either implicit solvent or explicit solvent. For explicit solvent, we can use both classical or *ab initio* methods. In the next parts, the three methods are discussed, and finally *ab initio* molecular dynamics was used to perform some computations.

## V.2 Classical molecular dynamics

Classical molecular dynamics had been performed at the beginning to model our system due to its advantages (very fast, large numbers of molecules can be included). These calculations were carried out using General Utility Lattice Program (GULP)<sup>1</sup>. In this classical approach, potentials constructed by using empirical parameters are used to describe, with the same accuracy, the solid and liquid phase. Once the parameters are set, various statistical ensembles can be used in this model. Test calculations were done on a primitive cell containing one Cs and one I atom.

Due to the lack of parameters for Cs and I ions in the literature, we try to develop a new set of parameters but we did not succeed to build a coherent set of parameter for the two phases. The main issue is due to the geometry of the solid phase in which the I/I electrostatic repulsion is not screened by Cs<sup>+</sup> cations. In a second try, we tried to use interaction parameters like those for NaCl<sup>2</sup>, but again it doesn't work.



### V.3 Implicit solvent model

Another approach has been applied which can be quite fast and well known to model the solid-liquid interfaces (ref need not so common with vasp). Implicit solvent methods in VASP was deeply investigated by Mathew et al.<sup>3</sup>. They have demonstrated the importance of considering the solvent and ions effects on the calculation of adsorption and activation energy. In this method, the solvent molecules were considered as a continuous medium. A cell consists of 8 layers contenting 64 atoms were used (its size 9.134Å x12.917Å x60.599Å).

This method also was not able to represent our system due to the very low electronic density between the ions in the solid CsI. As a consequence, the implicit model introduces implicit solvent between the ions in the solid phase leading to, after optimization, a dissolution of the solid in the calculation cell and a dispersion of the Cs/I ions the whole cell (see Figure V-1).

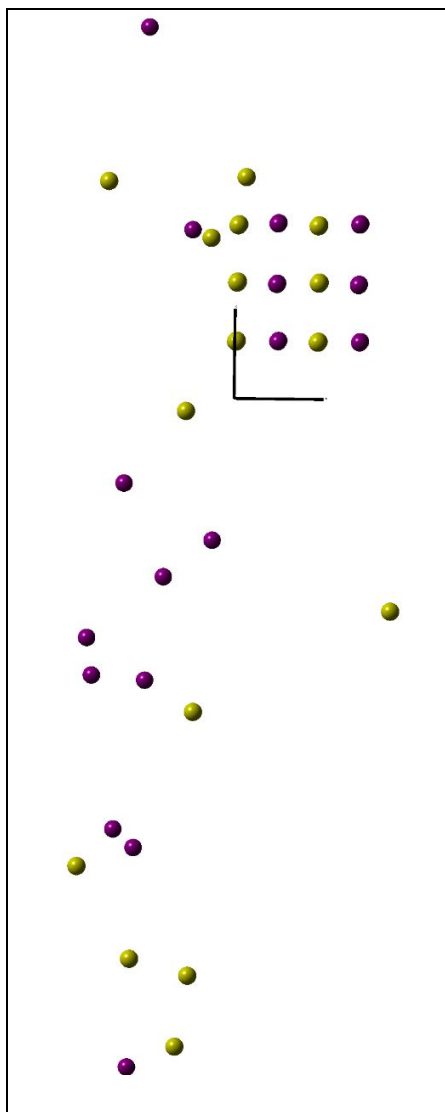


**Figure V-1: The geometry of the cell after optimisation (Cs and I are respectively colored in green and purple).**

## **v.4 Ab initio molecular dynamics**

After testing various methods with no success, we concluded that an ab initio method is required even if it involves very large CPU time. In the present chapter, ab initio calculation were performed with the VASP program

Molecular dynamic simulations were realized with the projector augmented wave potentials (PAW)<sup>4</sup>. The functional of these potentials are implemented in the code VASP<sup>5</sup>. The equations

of motion resolved numerically using Verlet algorithm<sup>6</sup> which solves Newton's equation of motion using time step of 1 fs.

Initial configuration is composed with a given number of atoms in a cell, while the water molecules were distributed randomly on the top of the surface with a density about  $1 \text{ g/cm}^3$ . The cell of our study is presented in Figure V-2, in which we have a  $6 \text{ \AA}$  layer of water on the surface corresponding to 23 water molecules.

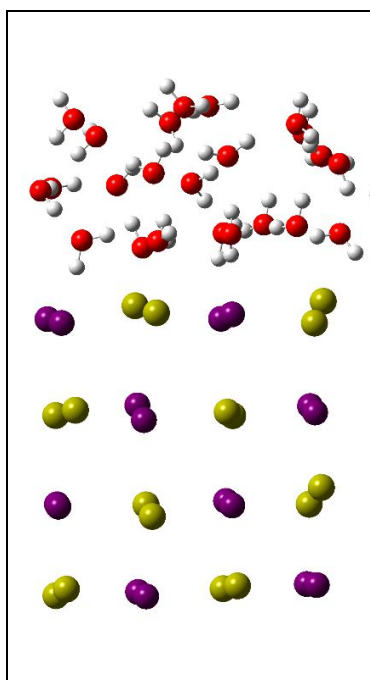


**Figure V-2. Used system in MD, one layer of water on the top of the surface (Cs, I, O and H are respectively colored in green, purple, red and white).**

A first dynamics were performed during 50 ps at temperature of 350 K in the frame of canonical ensemble (NVT). First 5 ps of the dynamics have been used to thermalize the system at the specified temperature. Note that we tested the effect of thermostat by doing calculation by micro canonical ensemble (NVE). The obtained results in both ensembles (NVT and NVE) are very similar as function of the geometry during the simulation. Therefore, we chose to do our analysis on the NVT system.

### V.4.1 Free energy diagram and dynamics evolution

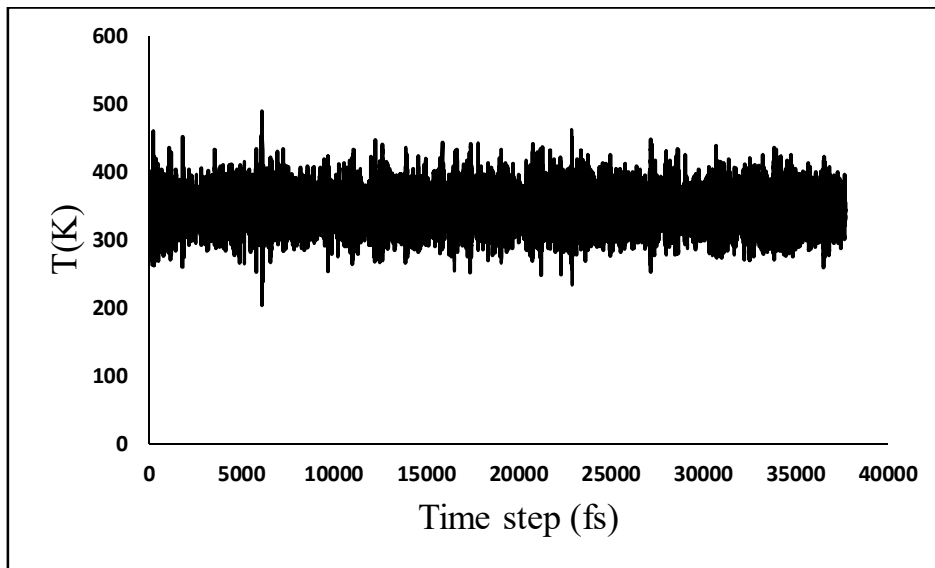


Figure V-3. Variation of temperature during the dynamics.

In NVT dynamics, temperature is always oscillating around the target value (350 K), as shown in Figure V-3.

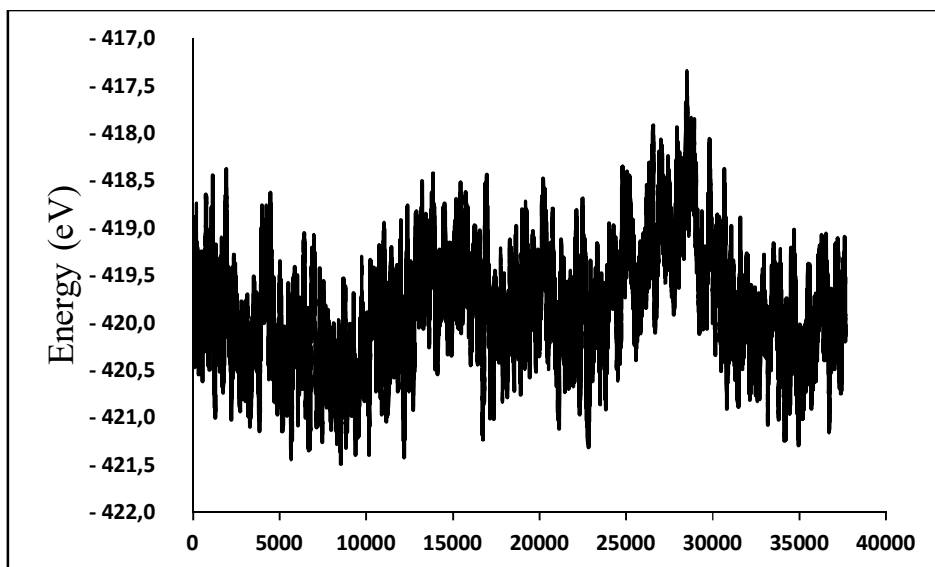


Figure V-4. Variation of energy during the dynamics.

Figure V-4 presents the variation of energy during the dynamics. The energy is oscillating and showing different stages, with the first 5000 steps dedicated to thermalize the system.

Geometries of the system after 5 and 15 picoseconds are presented in Figure V-5. At 5 ps, the energy (electronic or total) is -419.51 eV. We see that the water molecules are still far from the surface. After 15 ps, the water molecules start approaching the surface with one water molecule almost located on the surface and disorder appears on the crystal surface. The energy of this step is lower than the previous one ( $\Delta E = -0.89$  eV). The formation of water/ion interaction compensates the decrease of the ion/ion ones

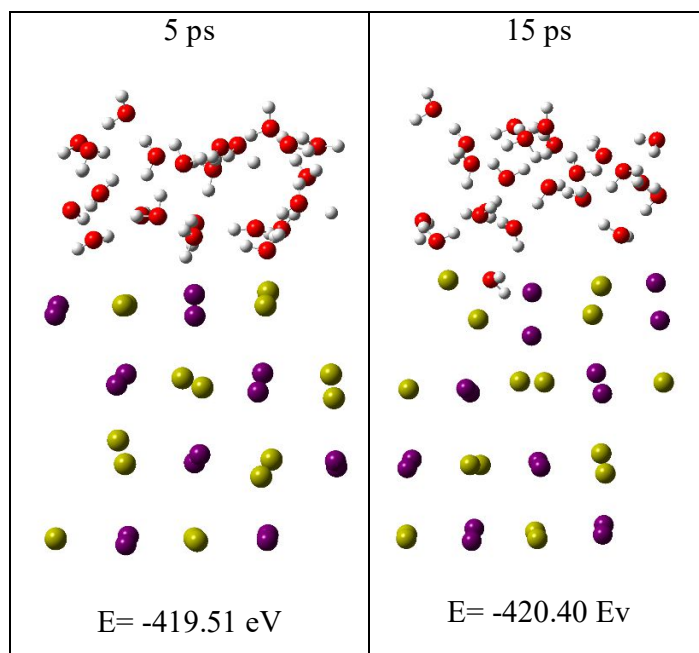


Figure V-5: geometry of the system after 5 and 15 picoseconds.

After this stage, water molecules start to diffuse under the first layer of the surface. Figure V-6 shows the geometry after 28 ps (highest energy in the diagram, Figure V-4), in which we notice that the surface is in direct contact with the water molecules and some defects are created in the surface.

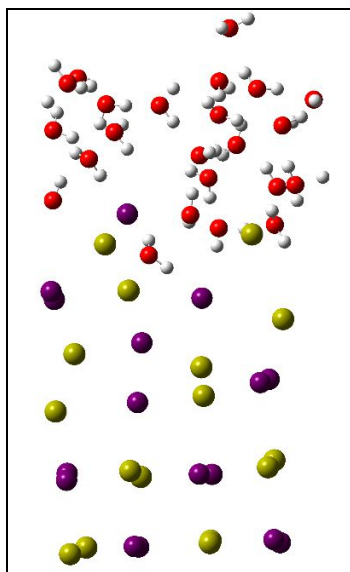


Figure V-6. Geometry of the highest energy point.

Once one defect is created (i.e. when one water molecule diffuses below an ion), more water molecules are inserted in the solid, screening the electrostatic interaction and destabilizing the crystal surface layer. Later on the surface is dislocated with the ion transfer towards the liquid phase (Figure V-7).

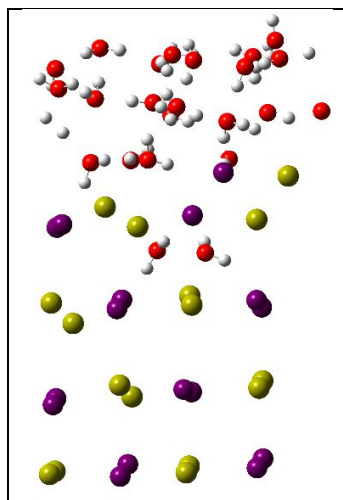


Figure V-7. Geometry of the final point of the dynamics.

#### V.4.2 Pair correlation function and coordination number

In this part, we will examine the local order in the direct space by considering the pair correlation functions and the associated coordination numbers.

### V.4.2.1 One layer of water on the top of the surface

Radial distribution function (RDF) and its integration (represents the coordination number during the simulation) were calculated for the previous system (Figure V-2) at 350K. Figure V-8 shows the RDF and its integration after 10 ps between one iodine ion on the surface and the oxygen ions. The position of the first peak in  $g(r)$  corresponds to the average bonding distance between the iodine ion and the surrounding oxygen atoms. This average distance measured to be 3.6 Å. Therefore, the distance between the specified iodine ion and the surrounding water molecules is about 2.6 Å (we subtract the distance of the O-H bond which is about 1 Å) in which the coordination number is 1.5.

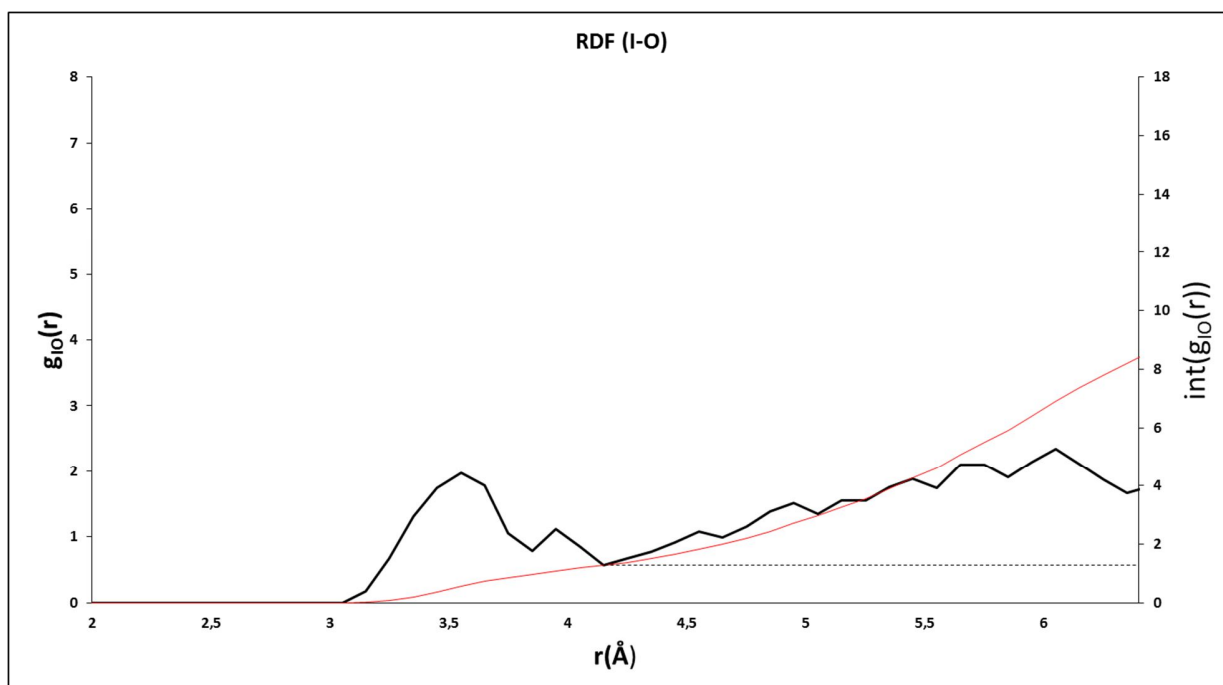


**Figure V-8: Radial distribution function,  $g(r)$ , between one I on the surface and O at 350 K at 10ps (black line) and its integration (red line).**

However, same analysis were made after 35 ps of simulation (starting time of the RDF calculation). Figure V-9 shows the RDF and its integration between the iodide anion moved above the surface and oxygen atoms. The average bonding distance between the iodine ion and the surrounding oxygen atoms measured to be same as the previous case (3.6 Å). However, the coordination number increase up to 3 which means that three water molecules are interacting with this iodine ion. This step is the beginning of the iodide solvation process. This indicates

that without adding any energy, we succeed in dissolving the surface of CsI particle by interacting with water molecules.

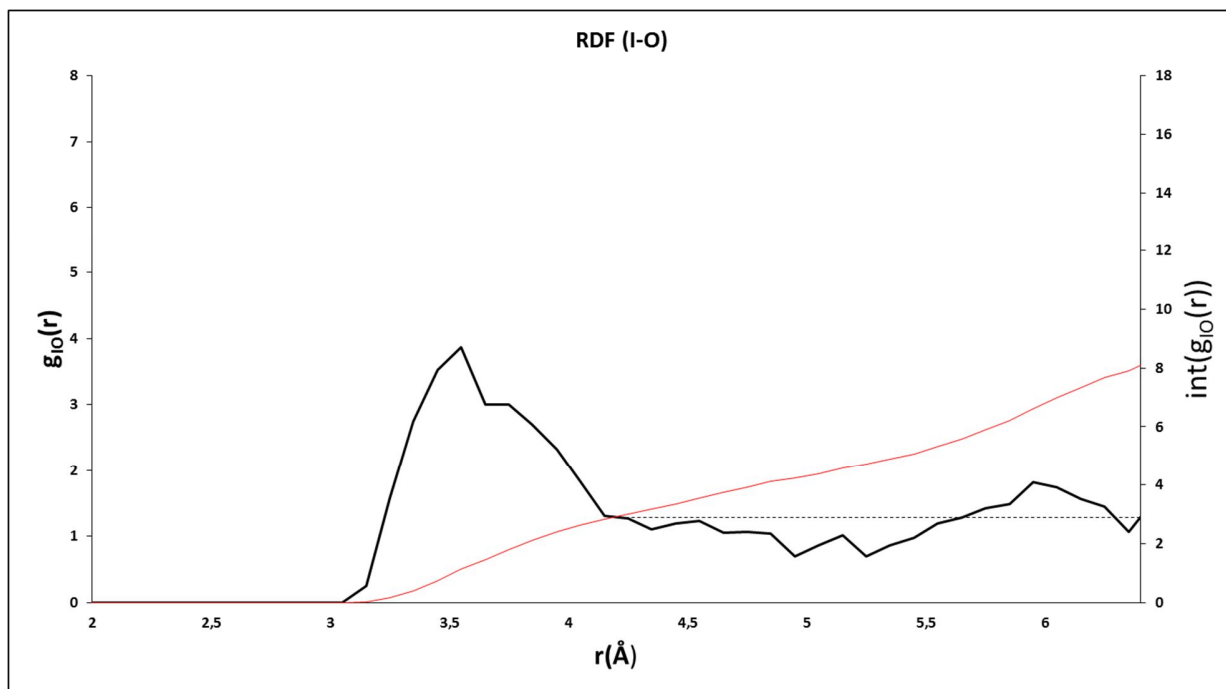


**Figure V-9: Radial distribution function,  $g(r)$ , between one I on the surface and O at 350 K after 35 ps (black line) and its integration (red line).**

#### **V.4.2.2 Starting by one iodine in liquid phase**

To assure our conclusion, we performed a dynamics starting by one I<sup>-</sup> in the liquid layer. Figure V-10 shows the correlation function between the considered iodide ion and the oxygen atoms which presents the water molecules at 350K and its integration.



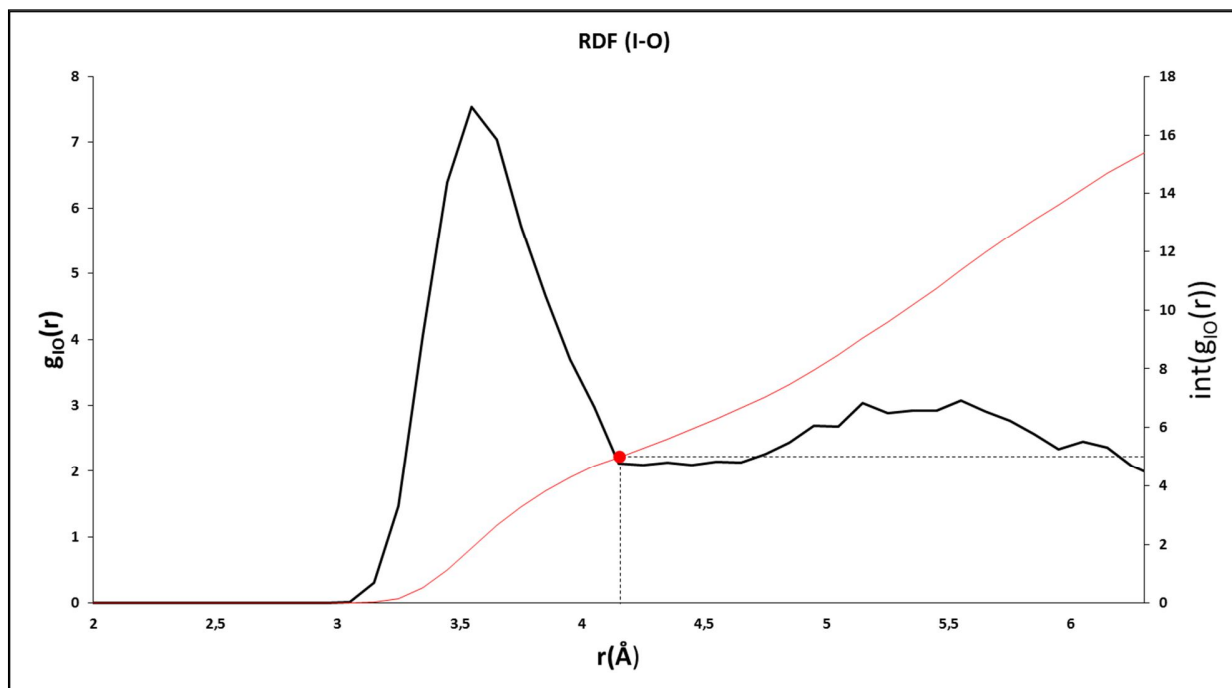


**Figure V-10. Radial distribution function,  $g(r)$ , between I and O at 350 K over 50 ps (black line) and its integration (red line).**

The average bonding distance between the iodine ion and the surrounding oxygen atoms measured to be the same (3.6 Å), while the coordination number is 5. However, a second solvation layer can be detected between 5 and 5.5 Å. The total coordination number is around 12. From this analysis we can conclude that we observed a dissolution of the particle surface after few ps.

### V.4.3 Diffusion coefficient of water

Diffusivity of water has also been determined. The calculated diffusion coefficient for water on top of the surface is  $2 \times 10^{-5} \text{ cm}^2/\text{s}$  which is in good agreement with the experimental value ( $2.3 \times 10^{-5} \text{ cm}^2/\text{s}$ )<sup>7</sup>.

After that, water molecules after 30 ps can diffuse inside the vacancies and move inside the first layer. The calculated diffusion coefficient for the bulk diffusion is  $4.6 \times 10^{-5} \text{ cm}^2/\text{s}$ , value higher than the experimental one. This increase of diffusion coefficient is expected since the water molecules motion is greater because vacancies have been created in the first surface layers.

#### **V.4.4 Iodide reactivity in liquid phase**

Iodide dissolved in liquid phase can be oxidized into molecular iodine in solution under irradiation. The first step is a OH radical reacting with I<sup>-</sup> to form atomic iodine, I<sup>°</sup> which can later recombine with another I<sup>°</sup> to product I<sub>2</sub>. As molecular iodine is quite volatile, I<sub>2</sub> in the liquid phase can be transferred towards the gas phase with a kinetics depending on interface area between liquid and gas and some mass transfer parameters.

This iodide oxidation under radiation is well referenced in the literature, for further details it can be referred to Burns et al.<sup>8</sup> and <sup>9,10</sup>

### **V.5 Conclusion**

In this chapter, we examined the reactivity of CsI aerosols in liquid phase. The results show fast solvation of the surface in water (after 40 ps). However, we notice from the dynamics that once we have some vacancy on the surface, everything will be in liquid phase and we will not have any defined surface anymore.

The classical mechanism proposed for the dissolution of an ionic solid in water is decomposed in three main step: Displacement of an ion pair above the surface; solvation of the ion pair and finally separation of the pair due to the individual solvation of the ions (ref need). The CsI behavior seems peculiar. Indeed, the formation of the ion pair does not seem mandatory (Fig XX). Ions are moved one by one in the liquid. This can be due to the crystal geometry in which the I/I interaction are not screened by the Cs<sup>+</sup> cation. A small displacement of the I<sup>-</sup> above the surface allows the insertion of one water molecule between the iodide and reduce the electrostatic repulsion. Once the first vacancy is created in few ps at room temperature, water molecules diffuse into the vacancy and between the ions. These molecules force more ion into the liquid phase. The process is such irreversible as soon as a defect is created. We observed the dissolution of the surface in the 3 MD performed during the study (NVE or NVT) which indicate that the process is easy and that the activation energy must be very small. Its estimation will be done using constraint MD.

Associate to a large solubility of the Cs and I ions, previous process may explain the hygroscopic behavior of the solid. However, due to the weak interaction between the CsI surfaces and isolated water molecules, the dissolution can only occur if the humidity is large enough to allow the

formation of a thin water layer (some angstroms) on the surface. In these conditions, the liquid phase process can contribute to the gaseous molecular iodine formation observed experimentally.

## V.6 References:

- (1) Gale, J. D. GULP: A Computer Program for the Symmetry-Adapted Simulation of Solids. *J. Chem. Soc. Faraday Trans.* **1997**, *93* (4), 629–637.
- (2) Sangster, M. J. L.; Atwood, R. M. Interionic Potentials for Alkali Halides. II. Completely Crystal Independent Specification of Born-Mayer Potentials. *J. Phys. C Solid State Phys.* **1978**, *11* (8), 1541.
- (3) Mathew, K.; Hennig, R. Implicit Solvent Models in VASP; 2015.
- (4) Kresse, G.; Joubert, D. From Ultrasoft Pseudopotentials to the Projector Augmented-Wave Method. *Phys. Rev. B* **1999**, *59* (3), 1758.
- (5) Hafner, J. *Ab-Initio* Simulations of Materials Using VASP: Density-Functional Theory and beyond. *J. Comput. Chem.* **2008**, *29* (13), 2044–2078.
- (6) Verlet, L. Computer “Experiments” on Classical Fluids. I. Thermodynamical Properties of Lennard-Jones Molecules. *Phys. Rev.* **1967**, *159* (1), 98–103.
- (7) Price, W. S.; Ide, H.; Arata, Y. Solution Dynamics in Aqueous Monohydric Alcohol Systems. *J. Phys. Chem. A* **2003**, *107* (24), 4784–4789.
- (8) W G Burns, M C Kent, W R Marsh and H E Sims. The Radiolysis of Aqueous Solutions of Caesium Iodide and Caesium Iodate. March 1990.
- (9) Sellers, R. M. *Reaction Kinetics of Iodine Compounds in Aqueous Solution*; CEGB-TPRD/B--0688/R85; Central Electricity Generating Board, 1985.
- (10) Sawai, T.; Shinozaki, Y.; Meshitsuka, G. The Radiolysis of Aqueous Solutions of Potassium Iodide. *Bull. Chem. Soc. Jpn.* **1966**, *39* (5), 951–955.



# **Chapter VI: General conclusion and perspectives**



# General conclusion and perspectives

During the nuclear reactor life, complementary safety systems were implemented in order to prevent/mitigate the consequences of a severe accident. Beside all the existing safety systems and management guides, some LOCA were happened like Three Mile Island in 1979, Tchernobyl in 1986 and recently Fukushima in 2011, in which significant amounts of radioactive elements released to the environment. Therefore, studies relative to evaluate the potential releases are of prime importance to estimate radiological consequences and define just after the accident some possible suitable counter-measurements for population.

One of the main issues is the radioactive releases into the environment. Radionuclides may release via some leakages in the nuclear containment building in significant amounts to the environment. Radioactive iodine is of interest due to its radiological consequences on the human being at short and middle term. Iodine containing aerosols (like CsI and AgI) may reach the containment and can be oxidized in moist atmosphere leading to formation of gaseous iodine I<sub>2</sub>. Recent experimental works (OECD/STEM project) have exhibited the formation of volatile iodine species from CsI aerosols deposited on coupons under an irradiation phase (30 hours). The results show fast and large amounts of molecular iodine released. From that, understanding the mechanism leading to this volatile iodine formation is of importance to be capable to extrapolate these data to a large range of conditions as well as other types of metallic iodide aerosol. The aim of this PhD work is to identify theoretically possible reaction pathways leading to the I<sub>2(g)</sub> formation starting by CsI and AgI aerosols which can be formed in the reactor coolant system.

These Theoretical studies were performed using VASP package in using DFT with a periodic approach. VASP is the reference software, well known to model some condensed chemical systems at atomic level. The wave function is developed as a set of plane waves and the electron-ion interactions are described using the PAW method.

First part of the study was made on the bulk properties of CsI crystal. The calculated lattice constant is 4.665 Å which is in good agreement with the experimental value (4.567 Å). However, stability studies were performed on low indices surfaces. The stability order was (011) > (210) > (211) > (111) > (001), (011), the most stable one, is composed of alternating I and Cs ions. Wulff shape of CsI depending on the calculated surface energies at 0 K were constructed, which shows

only (011) surface due to the large difference in surface energies with the other planes. Different water adsorption modes were studied on the most stable surface (i.e. (011)). Dissociative adsorption was shown to be very endothermic ( $E_{\text{ads}} = -3.54$  eV) and thus not possible. However, two different orientation of the water on the surface were tested. Water molecule in the most favored case oriented such that OH group is located on the top of Cs and H atom interacts with I, the corresponding adsorption energy is equal to 0.51 eV. Moreover, Gibbs free energy were plotted to consider the effect of temperature on the adsorption. It can be concluded that adsorption can happen only at low T (less than 200 K), far away from severe accident conditions. Going further the adsorption of more than one water molecule were taken into account. The calculations show that once we increase the number of water molecules, the interaction is lower with the surface whereas the water molecules strongly interact between themselves.

The second part of this study was to identify reaction pathway leading to the formation of volatile iodine species. At first, formation of  $I_2$  from clean CsI surface were considered. This reaction is very endothermic ( $\Delta_r E = 7.40$  eV). Also the formation of IOH and IH with the participation of one water molecule was shown to be endothermic. However, participation of an oxidant was taken into account.  $OH^\circ$  radical seems to be a good oxidant which can be formed by radiolysis of water. Oxidation of the surface by one  $OH^\circ$  radical is an exothermic step ( $\Delta E = -0.88$  eV). Formation of IOH after this step is endothermic ( $\Delta E = 2.35$  eV), also the formation of  $I_2$  ( $\Delta E = 4.18$  eV). After these endothermic steps, the participation of two  $OH^\circ$  radicals in the mechanism is needed. Activation energy of all the steps were calculated. The activation energy for the formation of  $I_2$  and IOH are respectively 1.2 eV and 0.70 eV. Reactivity on the defected surfaces were studied. As for the flat surface case, formation of  $I_2$  and IOH is not possible without the participation of two  $OH^\circ$  radicals. The activation energy for the formation of  $I_2$  and IOH are respectively 1.18 eV and 1.06 eV. We conclude that the defects will favor the formation of  $I_{2(g)}$ .

Same studied were performed on the AgI crystal, not soluble at the opposite of CsI. Surface energy calculations show the following stability order for the low indices surfaces: (110) > (100) > (120) > (001). (110), (100) and (120) are stable surfaces of AgI which have quiet similar surface energies. Wulff shape show (110), (100) and (001) planes constituting the surface particle ; (001) plane exists even its not stable surface but only to close the crystallographic shape of the



particle. Dissociative adsorption of water on the stable surfaces was very endothermic while the associative process is exothermic such as the water molecule oriented in a way to enhance the O-Ag interaction. The plot of Gibbs free energy shows that adsorption can happen only at low temperature, lower than 293 K. Adding more water molecules will enhance the interactions between water molecules instead of the surface, which is the same as the conclusion drawn on CsI surface. Formation of iodine species were studied as in the case of CsI i.e. with and without the presence of oxidants. Formation of AgI and I<sub>2</sub> molecules from flat surface is very endothermic ( $\Delta_r E = 2.38$  eV and 3.5 eV, respectively) thus not possible without oxidants. However, dissociation of one water molecule on the surface is endothermic too ( $\Delta_r E = 3.0$  eV), this means that the formation of HI is also not probable. The departure of I<sub>2</sub> after oxidizing the surface once is very endothermic ( $\Delta_r E = -2.20$  eV), which is not probable as in CsI case. In the last step, AgI surface were oxidized twice by two hydroxyl radicals. The activation energy for the formation of I<sub>2</sub> and IOH is 0.45 eV for both cases. We notice that the formation of IOH from AgI requires lower activation energy than that from CsI surfaces (defected 1.06 eV and flat 0.70 eV).

In the last part, ab initio molecular dynamic simulations were performed on the CsI particle since its well known to be hygroscopic (unlike AgI) and its reactivity linked to aqueous phase reactivity, so its interesting to study it in liquid phase. The calculations were performed during 50 ps around 350K in the frame of canonical ensemble (NVT). The results showed that CsI aerosols solves quickly in water and once we creat a vacancy on the surface, everything will be in the liquid phase.

To sump up the results, the oxidation of CsI can result from two possible pathways: i) a formation of a water layer stabilised by water interactions and next CsI will be solved in this water layer. I<sup>-</sup> formed can react with OH in solution to form I<sub>2(g)</sub> which will be transferred towards the gas phase ii) a direct pathway in gas phase involving two OH<sup>°</sup> with possible release of I<sub>2(g)</sub> and IOH<sub>(g)</sub> with some calculated energetic barriers around 1.0 eV. The oxidation of AgI can only happen with the oxidation by two OH<sup>°</sup>. The energetic barrier is lower than for CsI for IOH formation, it can be expected that IOH<sub>(g)</sub> will be quickly oxidised into I<sub>2</sub> in gas phase.

In 2018 in the frame of the follow-up of STEM project, a test with AgI aerosol under irradiation will be performed and it will be possible to consolidate these pathways with regards to the experimental result, noticeably if some I<sub>2(g)</sub> formation is observed.

